UNIVERSITA' DEGLI STUDI DI UDINE

Dottorato di ricerca in tecnologie chimiche ed energetiche
XXVII CICLO

Tesi di Dottorato

DETERMINATION OF THE THERMODYNAMIC PARAMETERS OF INTERACTION BETWEEN THE COMPONENTS OF HETEROGENEOUS ZIEGLER NATTA PRE-CATALYST

Dott. Cristian GRAZIOLI

Prof. Carla DE LEITENBURG	REFEREE
Prof. Barbara MILANI	REFEREE
Prof. Pietro MASTRORILLI	REFEREE
Prof. Alessandro TROVARELLI	SUPERVISOR
Prof. Marilena TOLAZZI	CO-SUPERVISOR
Prof. Andrea MELCHIOR	CO-SUPERVISOR
Prof. Alfredo SOLDATI	DIRECTOR OF Ph.D. PROGRAM

2015

UNIVERSITA' DEGLI STUDI DI UDINE

Dottorato di ricerca in tecnologie chimiche ed energetiche
XXVII CICLO

Tesi di Dottorato

DETERMINATION OF THE THERMODYNAMIC PARAMETERS OF INTERACTION BETWEEN THE COMPONENTS OF HETEROGENEOUS ZIEGLER NATTA PRE-CATALYST

Dott. Cristian GRAZIOLI

Prof. Carla DE LEITENBURG	REFEREE
Prof. Barbara MILANI	REFEREE
Prof. Pietro MASTRORILLI	REFEREE
Prof. Alessandro TROVARELLI	SUPERVISOR
Prof. Marilena TOLAZZI	CO-SUPERVISOR
Prof. Andrea MELCHIOR	CO-SUPERVISOR
Prof. Alfredo SOLDATI	DIRECTOR OF Ph..D. PROGRAM

2015

The work described in this thesis is part of the Research Program of the Dutch Polymer Institute (DPI), Eindhoven, the Netherlands, project nr. #754.

SUMMARY

This Ph.D. project is part of a cooperation between the universities of Udine, Turin, Naples and Antwerp and aims at elucidating the still obscure nature of the catalytic core of the heterogeneous high yield Ziegler-Natta catalysts (HY-ZNC or ZN) for α-olefin polymerization. The Ziegler-Natta catalysts, discovered in the early 1950s by Karl Ziegler and Giulio Natta, allowed the synthesis of new materials such as polyethylene (PE) and polypropylene (PP) and opened the age of industrial olefin polymerization. Even though a lot of knowledge has been acquired since the discovery of the catalytic system, the extensive experimental study of the active core of Ziegler-Natta catalysts is particularly complicated because of the extreme reactivity of such systems towards water, with which the components of the catalytic system immediately react in an irreversible way. Therefore, the structure of active catalytic site(s) and the relationships between the constituents of the active catalyst are not well known yet and a computational approach has been preferred over an experimental one.

In particular, the aim of the experimental studies presented in this work of Ph.D. thesis is to determine the thermodynamic parameters of the interactions between the constituents of the heterogeneous High Yield Ziegler-Natta Catalysts (HY-ZNC) and to use the experimental results as a benchmark for DFT calculations performed by researchers of the University of Naples. HY-ZNC are constituted of a solid magnesium chloride support on which titanium tetrachloride, source of catalytic metal, and internal donors (IDs), small organic molecules used as catalysis enhancers, are adsorbed; the pre-catalyst so obtained is then activated by adding alkyl-aluminum compounds.

Techniques such as UV-Vis spectrophotometry and calorimetry were used to determine Gibbs free energy (ΔG_{ads}) and enthalpy (ΔH_{ads}) of adsorption, while analytical techniques such as Karl-Fischer titrations and BET determinations were used for characterization purposes.

The binary systems $TiCl_4$-$MgCl_2$ and IDs-$MgCl_2$ were first studied. Ethyl benzoate (EB) and *ortho*-diethylphthalate (DEP) were chosen as models for monodentate and bidentate ligands because both benzoates and phthalates are commonly used in industrial formulations and have an aromatic ring thanks to which their concentration can be easily monitored through UV-Vis

spectrophotometry. Eventually the study has been extended to the ternary system DEP-$MgCl_2$-$TiCl_4$ by means of adsorption of DEP on co-milled $MgCl_2$-$TiCl_4$ samples.

The experimental data referring to a process from solution to surface were compared to the data resulting from DFT calculations (adsorption from gas phase) by adding terms which take into account the condensation and mixing processes (thus the different phases of reactants) according to the equation below:

$$\Delta X_{ads(g \rightarrow surf)} = \Delta X_{ads(sol \rightarrow surf)} + \Delta X_{cond(g \rightarrow l)} + \Delta X_{mix(l \rightarrow sol)}$$

where X is a generic thermodynamic function.

Specific results can be summarized as follows: both magnesium chloride and titanium tetrachloride are extremely reactive towards water, therefore its presence inside the titration apparatus, even in traces, strongly affects the experimental results, in particular the calorimetric ones. Water must be removed as much as possible from the titration apparatus using chemical methods (addition of $SiCl_4$ as a water scavenger inside the system) and working inside a dry-box; procedures to remove water and reduce its effect on titrations were expressly developed.

The adsorption of $TiCl_4$ was studied on several different samples of $MgCl_2$. Loading (n_{tot}) of fresh samples of $MgCl_2$ remained quite constant (n_{tot}=0.15±0.02 mmol g^{-1}) independently from the sample and the surface area preparation procedure, but decreased in aged batches. The binding of $TiCl_4$ was found to be weak, with a correspondent Gibbs free energy of -16.8±0.7 kJ mol^{-1} and a weakly exothermic adsorption reaction (ΔH_{ads}=-12.4± 1.8 kJ mol^{-1}). Experimental data were analyzed using various adsorption models, the Langmuir one resulting the best.

The loading of donors was lower than $TiCl_4$ but, among donors, higher in case of small EB (n_{totDEP}=0.068±0.004 mmol g^{-1}, n_{totEB}=0.113±0.008 mmol g^{-1}). Donors bind $MgCl_2$ more strongly than $TiCl_4$; Gibbs binding free energies of both IDs were found to be essentially the same, with EB and DEP values of -29.1± 0.8 kJ mol^{-1} and -29.7±2.9 kJ mol^{-1} respectively. On the other hand, the adsorption enthalpies were found to be different, with a more exothermic process associated to the adsorption of DEP (ΔH_{ads} =-61.2±2.1) kJ mol^{-1}) compared to EB (ΔH_{ads}=-27.5± 2.3 kJ mol^{-1}). In conclusion, for binary systems Gibbs free energies of adsorption of $TiCl_4$ and donors from solution to surface follow the order $TiCl_4$>EB~DEP, while the trend is different for the enthalpy of the process according to the sequence $TiCl_4$>EB>DEP. After correction for gas phase, Gibbs free

energies and enthalpies of adsorption become more negative (e.g. $\Delta G_{adsTiCl4(g\rightarrow surf)}$ =-39.1 kJ mol^{-1}, $\Delta H_{adsTiCl4(g\rightarrow surf)}$ =-47.6 kJ mol^{-1}), but the energetic trends do not change.

The presence of titanium on magnesium chloride surface (ternary system) has a little effect on the Gibbs free energy of adsorption, which results slightly lower than the energy detected in the binary system DEP–$MgCl_2$ (ΔG_{ads} =-25.6±1.1 kJ mol^{-1}, $\Delta\Delta G_{ads\ trenary7binary}$ = 4.1 kJ mol^{-1}). The adsorption of DEP on co-milled $MgCl_2$-$TiCl_4$ samples, however, was significantly different compared to the binary system (ΔH_{ads} =-83±3 kJ mol^{-1}, $\Delta\Delta H_{ads}$ ~22 kJ mol^{-1}).

Abbreviations

BET	Brunauer–Emmett–Teller theory
Cyc	Cyclohexane
DD	Direct determination
DEP	*ortho*-diethylphthalate
DPI	Dutch Polymer Institute
DRIFT	Diffuse reflectance infrared Fourier transform
EB	Ethyl benzoate
ED(s)	External donor(s)
GB	Glove Box
Hept	*n*-heptane
HPM	Hydrogen peroxide method
ID(s)	Internal donor(s)
IR	Infrared spectroscopy
KF	Karl –Fischer
LB(s)	Lewis Base(s)
MAO	Methylaluminoxane
MS	Molecular sieves
NMR	Nuclear magnetic resonance
PP	Polypropylene
PE	Polyethylene
Py	Pyridine
TCE	Tetrachloroethane
Tol	Toluene
UV-Vis	UV-Visible spectrophotometry

1 Introduction

Ziegler–Natta catalysts were discovered by the chemists Giulio Natta[1,2] and Karl Ziegler[3] in the 1950s and opened the age of industrial polymerization of olefins. Since then a lot of knowledge has been acquired in both the academic and the industrial domain[4,5] and eventually exported to different chemistry and technology research fields; despite the frequent modifications to the original receipt, the improvement of polyolefin productivity (yield, stereoselectivity) is the result of essentially random discoveries. The currently used Ziegler-Natta catalysts consist in a solid support of magnesium chloride ($MgCl_2$) on which titanium tetrachloride ($TiCl_4$) as source of catalytically active metal and small organic molecules named donors, as catalysis enhancer, are adsorbed; this system (called pre-catalyst) is activated trough the addition of an organo-aluminium compound and used for olefins polymerization.

Ziegler-Natta catalysts are stereoselective, which means that they allow the control of tacticity (orientation of lateral substituents) of the polymer when prochiral monomers such as propylene are used as starting material. Such control allowed the production of polymers with a homogeneous sequence of lateral groups, which is of fundamental importance for the mechanical properties of the final polymer and, thus, for its applications.

Owing to the extreme reactivity of the components of these systems towards water, a computational approach has usually been preferred to investigate the structure of the active catalyst. A lot of computational work has been done on these systems from, practically, every point of view[6–12]. On the other hand, works involving experimental determinations have been inadequate and limited to donors, because they can be easily manipulated. Notably, works focusing on the experimental determination of thermodynamic reaction parameters between the constituents of the active catalyst and the solid support of $MgCl_2$ are not even present in literature.

The present work aims at clarifying the persistently obscure heart of high yield Ziegler-Natta catalysts (HY-ZNC) providing a series of experimental thermodynamic data relative to the adsorption of $TiCl_4$ and donors (*ortho*-diethylphthalate, DEP and ethyl benzoate, EB) on physically activated $MgCl_2$. The experimental data relative to the adsorption from gas phase (obtained by adding the contribution of condensation and mixing of adsorbent) are then used as

benchmark for the validation of computational results, thereby contributing to an in-depth study of this field of chemistry.

1.1 Overview on α-olefin polymerization

1.1.1 Brief history

Titanium-based catalysts for the polymerization of olefins were discovered in the 1950s by the German chemists Karl Ziegler[3] and his Italian colleague Giulio Natta[1,2]; such revolutionary discoveries opened a new era in polymer science and technology. In 1953 Ziegler catalysed the polymerization of ethylene at low temperatures and pressures using a mixture of $TiCl_4$ and $Al(C_2H_5)_3$[3]. A few months after Ziegler's discovery, Natta obtained the first crystalline isotactic polypropylene (iPP) using a combination of crystalline α-$TiCl_3$ and $Al(C_2H_5)_3$[1]. A few years later, Natta also carried out a study on the isolation and structure of a new material, the syndiotactic polypropylene[13]. Over the following years, the catalysts were developed through systematic investigations in order to obtain from simple α-olefins materials with a higher molecular weight and tacticity.

Industrial development

The industrial production of polyolefins started in the late 1950s with the use of a mixture of $TiCl_4$ and $AlEt_3$ as a catalytic system[2]. The polymerization process was characterized by a low productivity and stereospecificity (a stereoregularity lower than 40%)[2] and thus efforts were focused on finding a more active and stereospecific catalytic system. Natta and his collaborators discovered that $TiCl_3$ was more stereoselective than $TiCl_4$ and, moreover, only three out of four possible structural modifications of $TiCl_3$ were highly stereoselective. The first modification to the industrial protocol consisted in replacing $TiCl_4$ with $TiCl_3$ (in particular with the violet modification, resulting from the reduction of $TiCl_4$ with H_2 or powdered Al[14]), thereby increasing the stereoregularity of the polymer up to 90%; stereospecificity was further improved by replacing $AlEt_3$ with $AlEt_2Cl$[4,5].

After stereoregularity had been improved, attention and efforts in the industrial domain moved during the 1960s to the development of increasingly high-productive catalytic systems. In

fact, the object of the research was to increase both activity and stereospecificity of the catalysts (up to 95%) by lowering the chlorine and the metal-transition content as much as possible (to 30-50 ppm and 5-10 ppm respectively). Heterogeneous Ziegler-Natta catalysts development was based on the introduction of solid $MgCl_2$ as a support for the catalytically active centre (1970s). In the following decades $MgCl_2$-based catalysts have been constantly improved to enhance yields and stereoselectivity by adding Lewis bases (LBs), also named internal and external donors (IDs and EDs). IDs are added prior to the activation of the catalyst and EDs are added after the activation with an alkyl-aluminium compound. Current heterogeneous catalysts consist in a mixture of $TiCl_4$ and a suitable Lewis base adsorbed on the anhydrous $MgCl_2$ support; the pre-catalyst is activated by addition of aluminium alkyls and (if necessary) another Lewis bases (ED)[15].

Beside heterogeneous catalysts, in the late 1960s[16–18], while Natta's system was being improved, the ethylene polymerization by a homogeneous $Cp_2TiCl_2/AlEt_2Cl$ catalyst was also developed, but activities were well below those of the heterogeneous catalyst and the catalyst was inactive toward propylene. An important step towards the improvement of homogeneous polymerization catalyst was done by Kaminsky, who discovered that an addition of water to $Cp_2ZrCl_2/Al(CH_3)_3$ rendered the system active not only for ethylene, but also for propylene polymerization[19–21]. The increased activity and stereoselectivity was due to the formation of oligomeric methylaluminoxanes (MAO), produced by the reaction of water with $AlMe_3$[20]. Soon MAO became the activator of choice for metal-catalysed olefin polymerization[22,23]. However, while the activity of the heterogeneous system was thus reproduced, the polymerization of propylene was unselective and led to atactic polymers. The problem was resolved by Ewen as well as by Brintzinger and Kaminsky, who obtained highly isotactic polypropylene by using chiral, bridged, stereorigid "ansa-metallocenes"[22,24–26]. Homogeneous catalysts allowed the control of the polymer microstructure (unavailable with heterogeneous catalysis) and structure-reactivity relationships were established to address activity, regiochemistry and stereoselectivity of the polymerization reaction. Finally, the commercial production of stereoblock-copolymers[27,28] was made possible by chain shuttling polymerization [24,26,27,29,30], a dual-catalyst method which makes use of a chain shuttling agent to generate copolymers of alternating tacticity.

In Table 1 the time-line of discoveries about Ziegler-Natta polymerization catalysts is summarized. Usually the evolution of ZN catalysts is discussed in terms of 'generations'. No

standard and well-defined classification of generations has been provided yet, so there is an on-going discussion[31] about the number of existing generations and their characteristics. Therefore, the generations listed below usually overlap, and their starting dates are only approximate.

Year	Progress in olefin polymerization process
1951	Synthesis of crystalline PP (Hogan and Banks) using chromium-NiO catalyst supported on silica alumina.
1953	Karl Ziegler polymerizes ethene to PE with catalyst based on titanium tetrachloride and diethylaluminium chloride (first generation).
1954	Giulio Natta uses Ziegler's catalyst to produce PP. In 1963 Both Ziegler and Natta will be awarded the Nobel Prize for Chemistry.
1957	Commercial production of PP commences in Italy, Germany, and USA. Discovery of metallocene catalyst for olefin polymerization with conventional co-catalyst (Al-alkyls).
1961–1980	PP is used for manufacturing fibers, fabrics, upholstery, nonwoven fabrics and other products on a commercial scale.
1973	Introduction of $TiCl_3$ purple phases (second generation).
1975–1978	Commercialization of olefins obtained by catalysts supported on $MgCl_2$ (third generation) by many companies.
1977–1980	Discovery of high activity metallocene single-site catalysts (SSC), using methylaluminoxane (MAO) as co-catalyst (fourth generation).
1991	Introduction of silica-supported metallocene complexes catalysts activated with aluminium-oxane (fifth generation).
1995–1998	Discovery of non-metallocene SSC based on chelated late transition metals. Synthesis of chiral bridged ansa-metallocenes for homogeneous stereospecific 1-olefin polymerization. Commercialization of PP obtained with SSC.
1997	Commercialization of PP based on Ziegler-Natta catalyst with 1.3-diethers and succinates as donors.
2006	Synthesis of olefin block copolymers.

Table 1: Timeline of discoveries pertinent the olefin polymerization.

1.1.2 Classification of catalysts for olefin polymerization

Catalysts for olefin polymerization are usually divided in two main classes depending on the solubility of the active catalyst[4,5].

Homogeneous catalysts are metal complexes able to dissolve in the organic reaction medium. Homogeneous polymerization catalysts are usually divided in metallocenes of early transition metals or late transition metals with nitrogen ligands.

Metallocenes are mostly cyclopentadienyl complexes of zirconium(IV) and titanium(IV), either sandwich or half-sandwich, discovered shortly after Ziegler's and Natta's reports in the 1950s[16,17,2531], while late transition metal catalysts are nickel(II) and palladium(II) complexes with nitrogen (imine) ligands[32–35]. These homogeneous catalysts give access to polyolefins with a wider choice of properties and are thus likely to be increasingly used for the production of polymers for special-purpose applications, which require properties not easily accessible otherwise.

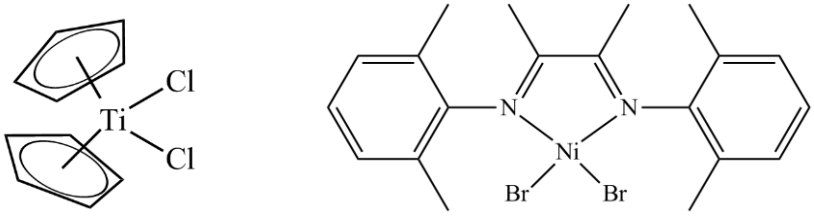

Figure 1: Examples of homogeneous catalysts for polymerization of olefins: titanium-cyclopentadienyl complex (left) and nickel-iminoligand complex (right).

Heterogeneous catalysts may also be divided in two groups based on the active metal: chromium-based catalysts (usually called Phillips catalysts)[36,37] and titanium based catalysts[38–40].

Phillips catalyst is prepared by adsorption of a chromium compound, mostly chromium trioxide, on an amorphous silica support and subsequent reduction by exposure to hydrogen[36,37]. They are used to produce high-density polyethylene (HDPE) with particularly high molar mass and do not polymerize propene. Titanium-based catalysts allow the stereospecific polymerization of propene (*isotactic polypropylene*)[4] and have been constantly improved. Despite the degree of perfection attained, they permit only limited degrees of variability with regard to some relevant polymer properties.

1.1.3 Polymerization pathways

Polymerization is the process with which monomer molecules react together in a chemical reaction to form polymeric chains or three-dimensional networks[41]. The polymerization processes may follow different mechanisms; below a description of the different pathways is reported.

Radical polymerization

Free radical polymerization easily occurs with monomers with unsaturated side groups (such as styrene, acrylate, 1,3-dienes, vinyl chloride, vinyl cyanide), whereas the radical polymerization of simple unsubstituted α-olefins is not possible because their structure do not stabilize radicals efficiently[42]. Organic radical initiators such as benzoyl peroxide or azabisisobutyronitrile (activated by thermolysis and photolysis respectively) are used as initiators[43,44]. During polymerization, the radicals presents in the system disappear rapidly and randomly, yielding a polymer the properties of which (chemical/physical/mechanical) are inadequate for most purposes. Polymers formed by free-radical mechanisms such as polyvinyl chloride are usually atactic and mainly amorphous[4].

Anionic polymerization

In anionic polymerization a strongly nucleophilic anion (e.g. *n*-butylithium or potassium amide[45]) reacts with olefin to form a carbanion, which attacks another monomer, thereby extending the chain. As for free radical polymerization, the monomer has to afford stabilization by resonance (*e.g.* styrene). In anionic polymerization resonance-stabilized anions are quite long-lived in aprotic media and lead to polymerization in which the anionic chain ends continue to grow upon addition of further monomers until they anionic ends are quenched (*e.g.* by protonation).

Cationic polymerization

Cationic polymerization initiation occurs when a Lewis-acid is attached to the vinyl monomer to form the carbocation, which then grows into a polymer chain by subsequent additions of monomers[46]. Only 1,1-disubstitution (*e.g.* isobutene) afford sufficient stabilization of

carbocations. Shorter chains are generally obtained, as protons are released from the cationic chain end and other side reactions are easy.

Insertion polymerization

In the insertion polymerization the polymer grows by successive insertions of olefin into a metal-alkyl bond: a positively charged metal catalyst, which is connected to a chain end bearing a partial negative charge, binds – thus polarizing – a monomer molecule and then adds it to the growing chain[35,46,47]. The coordination sphere of the metal controls the stereochemistry of olefin coordination and insertion, which enhances the stereoregularity of the chain growth. This is the polymerization pathway followed by heterogeneous Ziegler-Natta catalysts; a description of the mechanism is present in section 1.2 "Heterogeneous $MgCl_2$-based ZN-catalysts".

1.1.4 Polyolefins

Polyolefins are thermoplastic polymers constituted of long hydrocarbon chains. Polyethylene (PE) and polypropylene (PP) are two of the most widely used polymers in the world, because of their versatility, easy processability, low cost and recyclability.

Nowadays polyolefins are widely used in almost all fields of life (both everyday life and industrial fields, e.g. aerospace, food and mechanical) and the global demand of these polymers is growing; Table 2 shows the world consumption and the estimated increase of the demand of PE, which is supposed to rise by 4% per year, reaching $9.96 * 10^7$ kg (valued \$164 billion[48]) in 2018.

	2008	2013	2018	Annual growth (% 2008-2013)	Annual growth (% 2013-2018)
PE demand (kg)	$6.74 \cdot 10^7$	$8.18 \cdot 10^7$	$9.96 \cdot 10^7$	3.9	4.0
North America (kg)	$1.53 \cdot 10^7$	$1.60 \cdot 10^7$	$1.81 \cdot 10^7$	0.9	2.5
Western Europe (kg)	$1.39 \cdot 10^7$	$1.29 \cdot 10^7$	$1.38 \cdot 10^7$	-1.5	1.3
Asia/Pacific (kg)	$2.47 \cdot 10^7$	$3.66 \cdot 10^7$	$4.75 \cdot 10^7$	8.1	5.4
Other (kg)	$1.35 \cdot 10^7$	$1.63 \cdot 10^7$	$2.02 \cdot 10^7$	3.8	4.4

Table 2: World polyethylene demand.

Polyethylene and polypropylene are characterized by good mechanical properties and a high resistance to chemicals and environmental factors. Various kinds of PE and PP may be obtained depending on the reaction conditions and the catalyst used[5]. The mechanical properties of polymers depend significantly on variables such as the extent and type of branching, the orientation of lateral substituents and the molecular weight[49,50]. Polyethylene is classified into several different categories based mostly on its density and branching, while classification of PP is usually based on the relative orientations of lateral groups. The comparison among isotactic PP and the commonest types of PE according to density, melting point and cristallinity is shown in Table 3 . None of data reported below must be considered as absolute; specific preparation conditions can result in samples whose properties fall outside the ranges indicated in the table.

	LLDPE	LDPE	HDPE	UHMWPE	iPP
Density (g cm^{-3})	0.90-0.94	0.91-0.94	0.94	0.930-0.935	0.88-0.92
Melting point (°C)	100-125	98-115	125-132	130-136	160-166
Cristallinity (%)	22-55	30-54	55-77	39-75	30-60

Table 3: General features of polyethylene. LLDPE: Linear low density polyethylene; LDPE: low density polyethylene; HDPE: high density polyethylene; UHMWPE: ultra-high molecular density polyethylene; iPP: isotactic polypropylene.

Linear Low Density Polyethylene

Linear low density polyethylene is characterized by significant numbers of short branches[5]. Linear low density polyethylene resins are hazy white materials with slightly waxy surface. Thin films of LLDPE appear quite clear and are highly tear resistant; deformation proceeds by necking. LLDPE is used for plastic bags and sheets, plastic wrap, stretch wrap, pouches, toys, covers, lids, pipes, buckets and containers, covering of cables and flexible pipes.

Low Density Polyethylene

Low density polyethylene is a generally translucent, quite pliable resin which shows a high resilience prepared by free radical polymerization[5]. It has a high degree of short and long chain branching, which means that the chains do not pack into the crystal structure and the intermolecular forces (e.g. instantaneous-dipole induced-dipole attraction) are low. The result is a low tensile strength and an increased ductility. The high degree of branching with long chains gives molten LDPE unique and desirable flow properties. LDPE is widely used for manufacturing containers, dispensing bottles, wash bottles, tubing, plastic bags for electronics and various molded laboratory equipment and bags. Other applications include corrosion-resistant work surfaces, parts that require flexible, very soft and pliable parts and multicomponent materials.

High Density Polyethylene

High-density-polyethylene is a hard opaque material known for its large strength-to-density ratio and produced by chromium/silica[36,37] or Ziegler-Natta catalysts[51]. HDPE has little branching (ensured by an appropriate choice of catalyst and reaction conditions) which makes its intermolecular forces stronger and its tensile strength higher than LDPE's. High-density-polyethylene is resistant to many different solvents and has a wide range of applications such as detergent bottles, butter tubs, garbage containers, chemical-resistant pipes, corrosion protection, fuel tanks, geomembrane for hydraulic applications, natural gas distribution pipe systems and plastic surgery.

Ultra High Molecular Weight Polyethylene

Ultra-high-molecular-weight-polyethylene is PEe with a molecular weight between 3 and 6 million Daltons synthesized by metallocene catalysts[52], highly resistant to corrosive chemicals and abrasion. The very high molecular weight makes it a very tough material, but results in less efficient packing of the chains into the crystal structure as evidenced by densities of less than high density PE. Because of its outstanding toughness and its cut, wear and excellent chemical resistance, UHMWPE is used in a diverse range of applications such as moving parts on weaving machines, bearings, gears, artificial joints, edge protection on ice rinks and many other things. UHMWPE is also used in bulletproof vests and for the construction of articular portions of implants used for hip and knee replacements.

Polypropylene

Polypropylene is a widely used polymer that offers excellent electrical and chemical resistance at higher temperatures. While the properties of PP are similar to those of PE, there are specific differences such as a lower density and higher softening point (PP does not melt below 160 °C)[53].

Polypropylene is obtained through the polymerization of the prochiral molecule of propene. The relative orientation of methyl groups in the final product strongly influences the polymer properties[49,50], therefore PP is usually classified as isotactic, syndiotactic or atactic depending on the orientation of lateral groups[4]. In *isotactic polypropylene* all the substituents on the main chain

are located on the same side of the macromolecule (Figure 2, top), in *syndiotactic polypropylene* the lateral groups on the chain possess an alternate positions (Figure 2, center) while in *atactic polypropylene* the substituents are placed randomly along the chain (Figure 2, down).

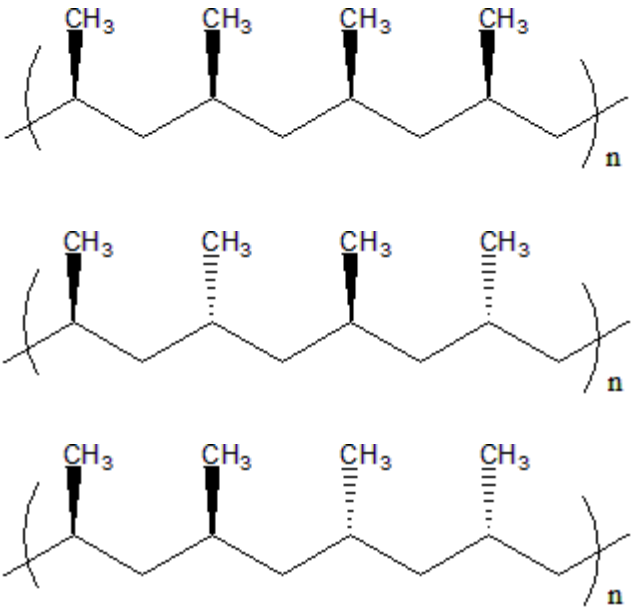

Figure 2: Structures of isotactic (top), syndiotactic (center) and atactic (down) polypropylene.

Most commercial PP is isotactic. Polypropylene is used in the manufacturing of piping systems, bottles, dielectric film, pipes laboratory tools and general long-living plastic items. This material is often chosen for its resistance to corrosion and chemical leaching; it is also heat resistant and can withstand autoclave temperatures, therefore it is used to make plastic items for medical or laboratory use.

1.1.5 Polymerization process

Polymerization by linkage of molecules having different functional groups (e.g. polyurethanes or nylons) are usually catalysed by Brønsted or Lewis acids. The polymer properties mainly depend on factors such as temperature and molar ratios of monomers, and the linkage pattern is dictated by the functional groups. The catalyst has little leverage on the properties of the resulting polymer.

In the case of polyolefins, in addition to the above-mentioned parameters (in particular molar ratios of monomers), the polymer properties and the polymerization pathway drastically depend on the catalyst used[4,554,55]. If the monomer possesses a prochiral carbon atom (e.g. propene) it can be introduced in the growing polymer chain in two different orientations with a process called 1,2 or 2,1 insertion. In 1,2 insertion the monomer binds titanium though C1 carbon atom and the lateral substituent R is close to the growing chain, while in 2,1 insertion olefin bind titanium with C2 carbon atom (Figure 3).

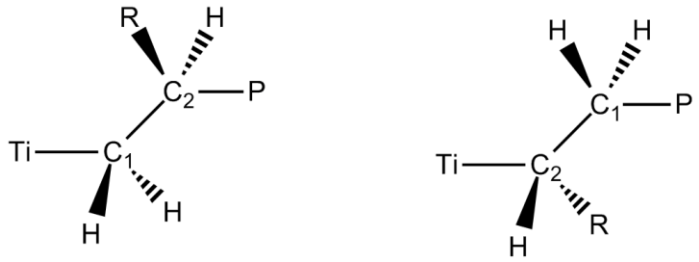

Figure 3: Products of 1,2 (left) and 2,1 (right) insertion of α-olefin. P= growing polymer, Ti=active site, R=lateral substituent.

A polymeric chain is called *regioregular* if the incoming olefin inserts in the active site with the same (or almost the same) insertion mechanism of the other monomers, and the equivalent catalyst is called *regioselective*. Along with the regioregularity of the polymer, the relative orientation of lateral groups (e.g. methyl group in propene) is also important for the final properties. The polymer is called *stereoregular* if the sequence of the configurations of chiral carbons is regular, and the equivalent catalyst is called *stereoregular*. A regioreguar polymer is stereoregular if the prochiral monomer inserts always with the same enantioface (*si* or *re*). From the point of view of the polymer properties the addition of a monomer should be as much regular as possible.

1.2 Heterogeneous $MgCl_2$-based ZN-catalysts

Actually, heterogeneous Ziegler-Natta catalysts are based on a solid support, usually $MgCl_2$, which binds the active catalytic structure to the surface; the active site(s) includes a titanium core and a small organic molecule named “donor” (used as a polymerization enhancer) bound to the

metal or in a close position[4,15]; the growth of the polymer takes place close to the surface of the solid support.

1.2.1 Preparation of heterogeneous ZN-catalyst

The synthesis of Ziegler-Natta catalyst consists in the preparation of a solid matrix of $MgCl_2$ impregnated with $TiCl_4$ and the internal donor(pre-catalyst) later activated by alkyl-aluminium compound. In a typical preparation, adsorbents are added to solid $MgCl_2$; $TiCl_4$ is present in large excess and acts both as a water-scavenger and a reactant, while the donor is added in lower amounts, almost stoichiometric if compared to the number of adsorption sites on $MgCl_2$. The reaction product (pre-catalyst) is then washed with hydrocarbons and activated with an organo-aluminium compound. Heterogeneous Ziegler–Natta catalysts can be prepared by means of mechanical or chemical routes[4,56,57]. In the mechanical route (with solid $MgCl_2$ as starting material), magnesium chloride, pure or concentrated $TiCl_4$ and donors are ball-milled together in the appropriate ratio for several hours; hydrocarbons as reaction mediums are often included in the preparation but are not mandatory. The chemical route[56,57] consists in simultaneously generating active $MgCl_2$ and incorporating donors and titanium tetrachloride. The pre-catalyst can be prepared by chemical routes in three ways:

- dissolution of $MgCl_2$ and donor in suitable solvent (usually ethanol)[58] followed by treatment with $TiCl_4$ (pure or dilute) at a temperature higher than 80 °C and subsequential washing of the precipitate with hydrocarbon;
- treatment of magnesium alkoxides (e.g. $Mg(OEt)_2$, Mg(OR)Cl) with donor and excess of $TiCl_4$ in hydrocarbon medium[59] followed by washing; magnesium chloride is obtained through the reaction between Mg compound and $TiCl_4$ and by-products are removed during the washing step;
- reaction of alkyl-magnesium compound (e.g. MgR_2, MgRCl) with chlorinating agents[60,61] to form $MgCl_2$ and successive hot treatment with donor and $TiCl_4$.

Among the above techniques, those based on pure mechanical treatments were first used in the manufacture of polyolefins owing to their simplicity and low cost, but chemical routes were later preferred because they allowed a better control of polymerization[62,63].

1.2.2 Constituents of the catalyst

1.2.2.1 Crystalline $MgCl_2$

Magnesium dichloride is the most commonly used solid support for the preparation of the heterogeneous Ziegler-Natta catalyst because it provides the catalysts with the highest stereospecificity[4]. As reported by many authors, there are two known crystalline modifications of $MgCl_2$[64,65]: the commercial α form and the less stable ß form. The α-form have a layer structure with a cubic close package stacking of two chlorine layers with interstitial Mg ions in six-fold coordination, while the ß-$MgCl_2$ form shows a hexagonal close packing[66].

Lateral cutsof $MgCl_2$

In $MgCl_2$ bulk all the atoms are surrounded by other atoms of the material and the bonding requirements (saturation of vacancies) are satisfied. On the contrary, the surface of the adsorbent displays lateral cuts with insaturations that can bind an adsorbate. The lateral cuts supposed to be effective for catalysis are named 104 and 110 (indicated by arrows in Figure 4) and expose the five- and four-coordinated (with one and two chlorine vacancies) Mg cations respectively.

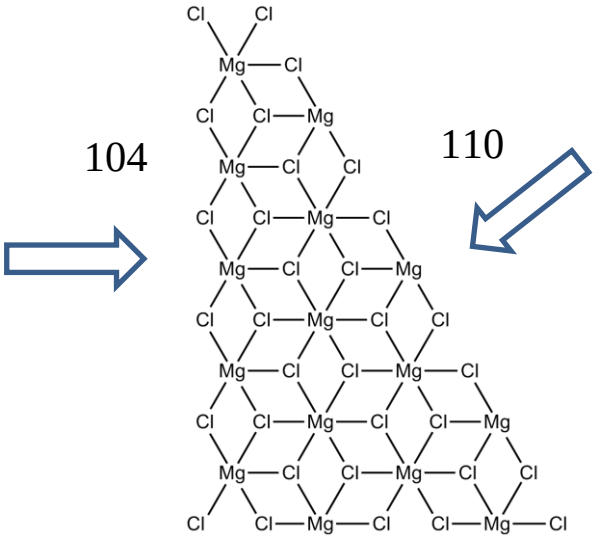

Figure 4: Structure of anhydrous crystalline $MgCl_2$. Lateral cuts 110 and 104 are indicated by arrows.

The idea that adsorption of $TiCl_4$ and donors takes place on insaturations presents on the surface is commonly accepted. Equilibrium crystal shape calculations indicate that the (104) surface, with five-coordinate Mg cations, is the dominant lateral termination in well-formed large crystals, as well as in highly activated $MgCl_2$ samples prepared by ball-milling and that in the latter case a minor fraction of surface Mg sites with a higher extent of coordinative unsaturation (e.g., four-coordinate Mg cations on (110) edges and/or at crystal corners or other defective locations[67,68]) also appear to be present[69].

1.2.2.2 $TiCl_4$ and $TiCl_3$

Titanium tetrachloride is a colourless (or, if impure, pale yellow) fuming liquid very reactive towards Lewis bases in general and water in particular. Titanium tetrachloride is the source of the catalytically active metal. In this compound, titanium have an oxidation state of +4 and is unable to polymerize olefins. In order to become catalytically active, titanium must be reduced to $TiCl_3$ (oxidation state +3); the reaction, performed by means of addition of alkyl-aluminium compounds, activates the catalyst[4].

Titanium trichloride is a paramagnetic solid existing in four different polymorphs named α-, ß-, γ- and δ- $TiCl_3$ (Figure 5). The polymorphs α-, γ- and δ-$TiCl_3$ are violet and have a layered structure. The titanium atoms are distributed in layers every two layers of chlorine, and Ti^{3+}

occupies two-thirds of the available cavities in alternate planes[64,65]. The three forms of $TiCl_3$ differ by the packing mode: α form is hexagonal, γ form is cubic and δ form displays a random sequence of hexagonal and a cubic close packing. The ß-modification is brown and has a fiber structure an hexagonal unit cell[70,71]. There are several methods for the synthesis of different $TiCl_3$ modifications[4], but reduction with Al metal or alkyl aluminum compounds are commonly used.

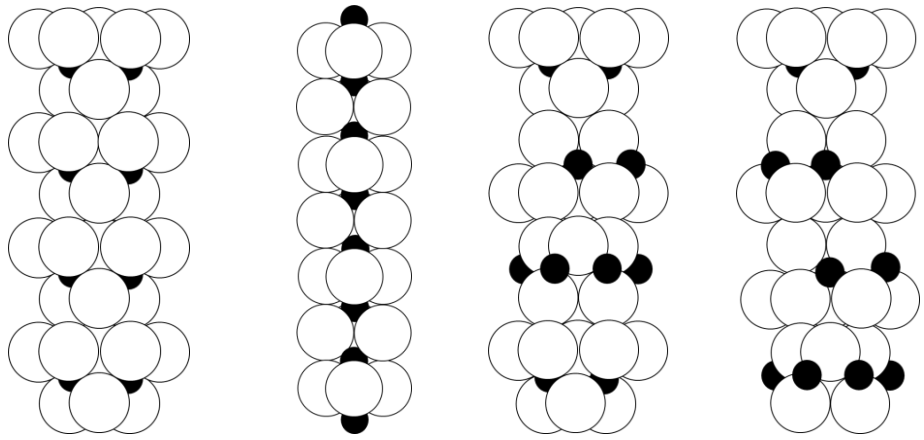

Figure 5: Structures of polymorphs of $TiCl_3$; from left to right α, ß, γ and δ-$TiCl_3$; white circles: chlorine atoms; black dots: titanium atoms.

Although all $TiCl_3$ polymorphs are catalytic active, ß-modification possesses the lowest stereoselectivity on propylene polymerization (40%), while the other polymorphs have a remarkably higher stereoselectivity (90%)[72].

1.2.2.2.1 Binding of $TiCl_4$ to $MgCl_2$

It is commonly accepted that $TiCl_4$ epitaxially adsorb on $MgCl_2$ surface; in particular, adsorption takes place on the lateral cuts of $MgCl_2$ crystals, were insaturations on the magnesium atoms are saturated by chlorides provided by $TiCl_4$.

During the development of the catalyst, several lateral cuts of $MgCl_2$ were considered as possible binding site(s) for $TiCl_4$. In the past, the most probable binding site was supposed to be the 110 lateral cut because more acidic, but no decisive proof confirmed this hypothesis. In Figure 6 possible monomeric (Corradini, "slope" and "edge"[4]) and a dimeric binding structures for the binding of $TiCl_4$ on $MgCl_2$ are visible.

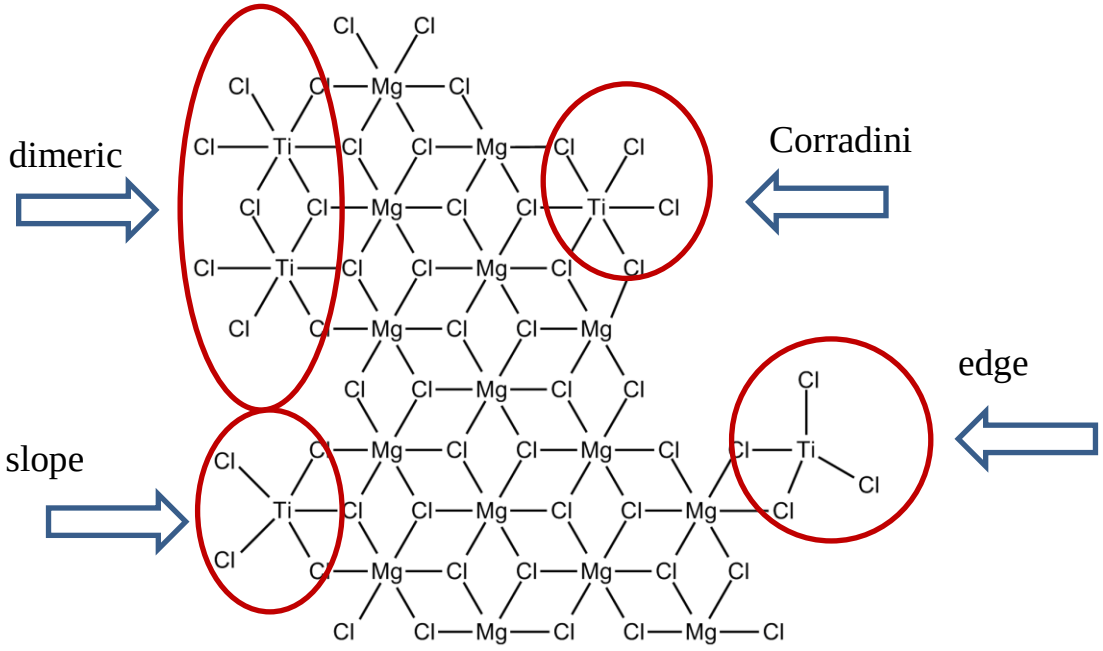

Figure 6: Possible binding modes of $TiCl_4$ on lateral cuts of anhydrous α-$MgCl_2$.

The energy of adsorption from gas phase ($\Delta E_{ads(g \rightarrow surf)}$) of $TiCl_4$ on different lateral cuts of anhydrous $MgCl_2$, considering several different binding modes of $TiCl_4$ (monomeric with different coordination and dimeric) has been studied extensively along time by means of computational approaches. In Table 4 are reported as example some computational results found in literature.

Lateral cut	Adsorbed form	$-\Delta E_{ads(g \rightarrow surf)}$ (kJ mol^{-1})	Ref
110	$TiCl_4$	42/95*	73
		7/120§	7
		54	10
	Ti_2Cl_8	196	73
		46	10
104	$TiCl_4$	34	73
		-5/50§	7
		83	10
	Ti_2Cl_8	135/150*	73
		-2/54§	7

Table 4: Some literature computational results relative to adsorption of $TiCl_4$ from gas phase. *different binding mode; § different DFT approximations.

As visible, the computational results on energy of adsorption range from slightly positive (+2 kJ mol^{-1}) to largely negative (+2 kJ mol^{-1}) values. Calculations yielded very different values of energy of adsorption depending on the binding mode and DFT approximation used. Thus, the computational models have to be validated by means of comparison with experimental results (relative to the adsorption from gas phase) in order to confirm the effectiveness of the models which yield close experimental and computational values and discard the others.

1.2.2.3 Donors

The donors (both internal and external) are oxygen-containing Lewis bases, usually esters, ethers or alkoxysilanes, added to the catalytic system to enhance yields, selectivity and stereospecificity of the final polymer[15]. Donors were not present in Natta's original receipt for the catalyst[1,2] but they were introduced in the catalytic system about a decade later.

Internal and external donors

Donors are classified in two main groups named "internal" and "external donors" (ID and ED). Essentially, internal donors are oxygen-containing molecules (Figure 7) added to $TiCl_4$ before the activation of the precatalyst with alkyl-aluminium compounds, while external donors are added after the activation. In Figure 7 some commonly used industrial internal donors are visible.

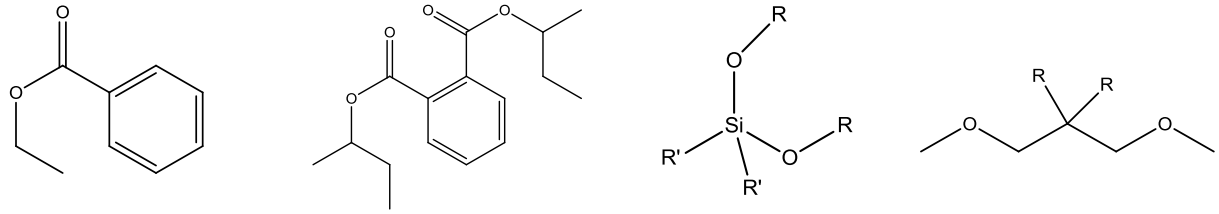

Figure 7: Common industrial internal donors; from left: ethylbenzoate, diisobuthylphthalate, an alcoxysilane, 1-3 dimethyl ether.

The internal donor, added during the impregnation step of magnesium chloride, is the most important. Its nature strongly affects the catalytic performances and the product properties (yield of the polymer, tacticity, and molecular weight distribution). The isotacticity indexes (as percentage of isotactic fraction of product) of several catalysts obtained with different internal donors are reported in Table 4[5]. The addition of the donor always produces an increase in isotactic productivity.

Catalyst	Co-catalyst	Maximum isotactic index (w/w %)
$MgCl_2/TiCl_4$	$AlEt_3$	50
$MgCl_2/TiCl_4$/EB	$AlEt_3$	60
$MgCl_2/TiCl_4$/DIBP	$AlEt_3$	70-80
$MgCl_2/TiCl_4$/DE*	$AlEt_3$	95-99

Table 5: Effect of donors on tacticity of the final product. *1,3 diether.

The ID plays an important role on the active sites formation by shielding a part of the space around the titanium centre[74]. Some IDs such as esters are susceptible to react with aluminium activators by addition of an alkyl residue to carbonyl bond and, thus, are partially consumed when the catalyst is activated.

The external donors are added after the activation of the precatalyst with alkyl-aluminium compounds. External donors are not mandatory, but necessary when ID is able to react with aluminium activators (e.g. esters).

1.2.2.3.1 Binding of donors to $MgCl_2$

Internal donors participate in stereoregulation, directly due to the coordination with the active centers (Ti atoms) or with $MgCl_2$ surface, not far from the Ti species. The coordination turns aspecific Ti sites into stereospecific ones[15,74]. Despite the number of both computational and experimental [8,10,75–78] contributions present in literature about the binding of donors to magnesium chloride, some important questions still need to be answered; in particular, whether the binding of donors takes place on the surface (close to titanium tetrachloride) or directly on the $TiCl_4$ adsorbed on the solid.

Several different structures were considered by researchers for the binding of donors on the surface on both 110 and 104 lateral cuts with different binding modes. In Figure 8 are visible two possible binding modes of EB on $MgCl_2$.

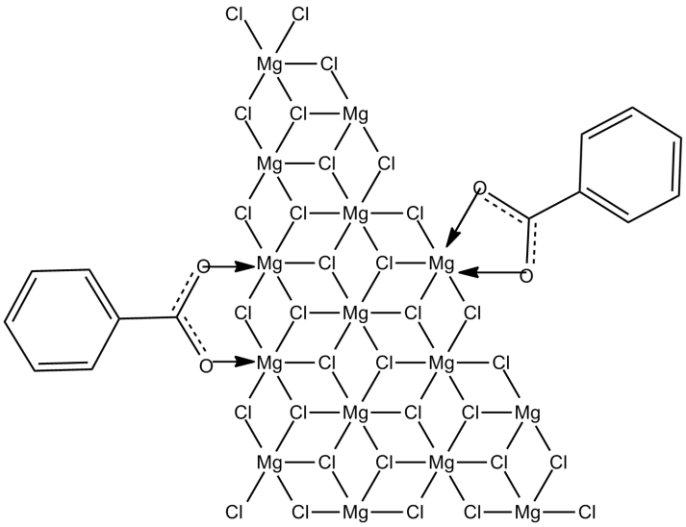

Figure 8: Possible binding modes of EB on lateral cuts of anhydrous crystalline $MgCl_2$

The number of possible binding modes for a given donor essentially depends on the structure of the donor itself. Rigid donors like alkyl-benzoates have a limited number of coordination modalities (in Figure 8 from left to right "chelate" and "bridge" binding of EB to $MgCl_2$), while more functionalized and flexible donors have more modalities.

The question of coordination modes is particularly urgent in the case of industrial donors such as benzoates (e.g. ethylbenzoate) and phthalates (e.g. diisobuthylphthalate, DIBP). For example, considering the coordination of simple monodentate EB on the catalyst surface[7980], it is still unclear if the monoester is coordinated with $MgCl_2$ surface by one or two oxygen atoms of the carboxyl group . Some experimental evidence (^{13}C NMR and DRIFT data) showed that EB forms bidentate complexes rather than monodentate ones[81], while theoretical calculations did not indicate any bidentate structures for monoesters on the $MgCl_2$ surface[75]. Studying adsorption of EB on an activated $MgCl_2$ sample (by DRIFT), it was found that the bands of adsorbed EB could be resolved in two components supposing the existence of two types of EB on the activated $MgCl_2$ surface, maybe correspondent to the binding with five and four-coordinated Mg cations on the (104) and (110) $MgCl_2$ surfaces[76]. In the case of EB these complexes were formed in close proportions, while in the case of phthalate (DIBP) formation of only one type of complexes was most preferable.

In co-adsorption experiments of $TiCl_4$ and donors on $MgCl_2$, the presence of $TiCl_4$ resulted in considerable decrease in the total content of internal donor, which the author interpreted as the competition of the internal donor and $TiCl_4$ for the same surface adsorption sites[80]. Opposite, a different scenario (binding of EB on titanium atom) is suggested by other authors[8] and there is a still on-going discussion on this topic.

Also the adsorption of donors from gas phase ($\Delta E_{ads(g \rightarrow surf)}$) on different lateral cuts of $MgCl_2$ considering several different binding modes (e.g. monodentate, bidentate, chelation) has been studied extensively along time by means of computational calculations. In Table 6 are reported as example some computational results found in literature for several donors.

	Lateral cut	$-\Delta E_{ads(g \rightarrow surf)}$ (kJ mol^{-1})	ref
benzoates	110	122/155 (m)	76
		125(m)	10
		91/125(b)	76
	Co-adsorption	44 (EB on $TiCl_4$)	8
		-2/8 (EB close to $TiCl_4$)*	8
	104	69/112(m)	76
		128(m)	10
		52/65(b)	76
	Co-adsorption	105 (EB on $TiCl_4$)	8
		10/18 (EB close to $TiCl_4$)*	8
phthalates	110	177	10
		134/154*	77
		112/159*	78
		92/144§	82
	104	141/162*	10
		118/152§	82
others	110	161/181*(succinate)	10
		130 (1,3-diether)	10
	104	188 (succinate)	10
		31 (1,3-diether)	10

Table 6: Some literature compurational results relative to adsorption of donors from gas phase. *different binding mode; § different DFT approximations; m: monodentate; b: bidentate.

As in the case of $TiCl_4$, the computational results on energy of adsorption are broad on a large range of values, generally between -100 kJ mol^{-1} and -180 kJ mol^{-1} for binary systems $MgCl_2$-internal donor and validation by comparison with experimental results is necessary to check the effectiveness of computational models.

1.2.2.4 Alkyl-aluminum compounds

Organo-aluminium compounds are extremely water sensitive reagents used in the preparation of heterogeneous Ziegler-Natta catalysts. Organo-aluminium compounds, in particular trimethyl (or ethyl) aluminium and methylaluminoxane (MAO), are widely used to activate the potentially isospecific active sites. In this process, the role of the aluminum compound is to both alkylate and reduce the titanium atom (thus the first titanium-carbon bond is created), in order to obtain the Ti(III)-alkyl specie, which is active towards polymerization.

1.2.3 Polymerization of α-olefins with ZN catalysts

In the last 50 years several polymerization mechanisms have been proposed to explain the polymerization mechanism of olefins by Ziegler-Natta catalysts. The mechanism proposed by Cossee and Arlman[38,39,83] in the middle of the1960s (Figure 9) is generally considered the most reliable.

The most important requirement is that titanium atoms that bind the surface of magnesium chloride possess a vacant coordination site. Polymerization takes place in several steps: first, the incoming olefin binds to titanium in correspondence of a vacancy (step a), shaping a four-center activated complex (step b), then the double bond of the olefin is opened and the olefin is inserted on the close C-Ti bond (step c). An important characteristic of this mechanism is the inversion of the growing chain and the titanium vacancy after every insertion of monomer (structures on the left side); in this way the original stereochemistry of the active site is maintained and polymerization proceeds to isotactic polyolefin. The initial structure of the catalyst is re-formed after the consecutive catalytic cycle (step d).

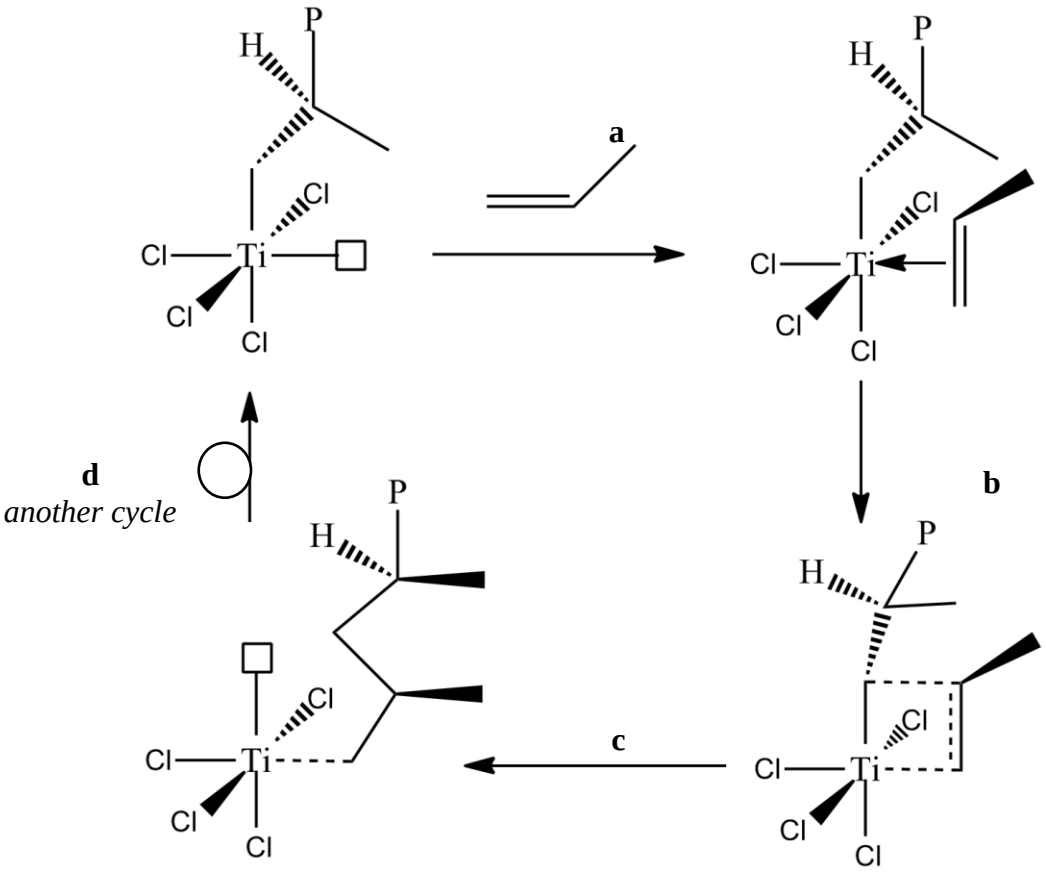

Figure 9: Generally accepted polymerization mechanism of olefins.

In the polymerization of propylene the elongation of the chain takes place with 1,2 insertions of monomer. For a stereospecific elongation of the polymer chain, there must be only one insaturation on the titanium atom and the active center must be chiral. Corradini and his coworkers demonstrated that an asymmetric surrounding of the active site forces the growing chain to adopt a particular orientation in order to minimize the interactions with chlorine atoms present on the surface of the catalyst[84].

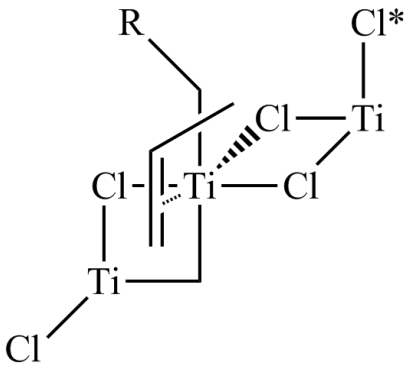

Figure 10: Incoming monomer orientation with respect to the growing polymer.

This implies that in the transition state one of the enantiofaces of the prochiral monomer is preferred over the other as in Figure 10, where the chlorine atom, responsible for the relative orientations of growing chain and incoming monomer, is indicated by an asterisk.

1.3 The process of adsorption

Adsorption is the adhesion of atoms, ions, or molecules from a fluid (gas, liquid or solution) on a solid surface. When adsorption takes place a film of adsorbate is created on the surface of the adsorbent. Adsorption must not be confused with absorption, in which a fluid permeates into solid; adsorption is a process involving the surface of a material, whereas absorption involves the whole volume of solid.

The nature of the binding of the adsorbate strongly depends on the species involved. As a molecule approaches the solid surface, a balance is established between the intermolecular attractive and repulsive forces (both adsorbate-adsorbate and adsorbent-adsorbate interactions come into play). The adsorption process is generally classified as physisorption or chemisorption, depending on which forces play the key-role in the interaction; weaker binding energies are typical of physisorption, whilst stronger characterize covalent bonding. In Table 7 a comparison between physisorption and chemisorption is provided.

	Physisorption	Chemisorption
Heat of adsorption	Low (20-40 kJ mol^{-1})	High (40-400 kJ mol^{-1})
Interactions	Van der Waal's forces	Chemical bonds
Temperature-dependence	Takes place at low T and decreases with increasing T	Takes place at high T
Reversibility	Reversible	Irreversible
Adsorbate-dependence	Related to the ease of condensation of the gas	Not related to the easy of condensation of the gas
Specificity	Not very specific	Highly specific
Structure of film	Multi-molecular layers	Monomolecular layer
Activation energy	Not required	May be required

Table 7: Comparison between physisorption and chemisorption.

Apart from molecular interactions, the overall effect strongly depends on the extent of the surface area and thus the porosity of the adsorbent material. For this reason all industrial adsorbents have large specific surface areas (often in excess of 100 m^2 g^{-1}) and are therefore highly porous or composed of very fine particles. Classification of porous materials is usually based on pores diameter; in Figure 11the classification in micropores, mesopores and macropores is represented.

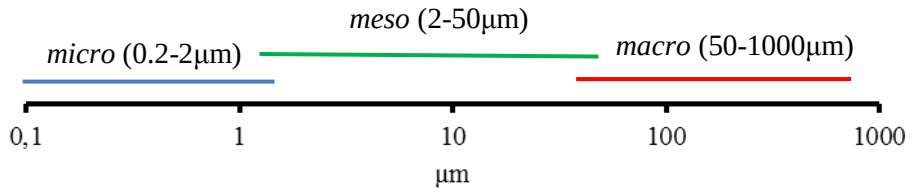

Figure 11: Classification of pores in solid materials.

Micropores and mesopores are important especially in the context of adsorption from gas phase because enhanced adsorbent-adsorbate interactions occur in pores of molecular dimensions. A decrease in the pores width results in both an increase in the adsorption energy and a decrease in

the relative pressure at which the pores filling[85] and the phenomena of capillary condensation occur. Capillary condensation is the process of multilayer adsorption from the vapour phase onto a porous solid proceeding until pore spaces are filled with liquid condensed from the vapour. The unique aspect of capillary condensation is that vapour condensation occurs below the saturated vapour pressure of the pure liquid as a result of an increased number of van der Waals interactions between the vapour molecules inside the confined space of capillary [86,87].

1.3.1 Adsorption types

Adsorption is usually described through isotherms[88–92], which correlate the amount of adsorbate on the adsorbent as a function of its pressure (if gas) or concentration (if liquid) at a certain temperature. The quantity adsorbed is nearly always normalized by the mass of the adsorbent to allow the comparison of different materials, therefore units of measurement include $mg_{ads}\ g_{solid}^{-1}$ and $mmol_{ads}\ g_{solid}^{-1}$ for the ordinate and pressure or concentration for the abscissae. Gases exhibit the greater number of types of adsorption on solids; the possible adsorption isotherms are divided in six different types by IUPAC[93,94]; the related adsorption isotherms are visible in Figure 12.

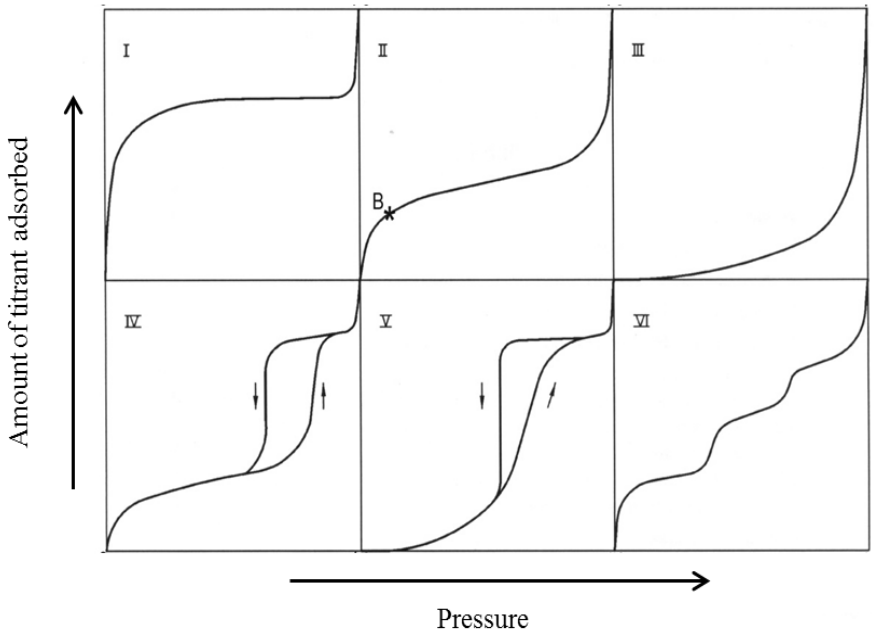

Figure 12: Types of adsorption isotherms.

Type I

Type I adsorption isotherm is characteristic of microporous solids with a relatively small proportion of outer surface. Type I isotherm is concave to the relative pressure axis, rises sharply at low relative pressures and reaches a plateau. The amount of adsorbed titrant approaches a limiting value reaching the saturation pressure. The narrow range of pressure necessary to attain the plateau is an indication of a limited range of pore size and the appearance of a nearly horizontal plateau indicates a small external surface area. The limiting adsorption is dependent on the volume of micropores available.

Type II

Type II isotherm is obtained with non-porous or macroporous adsorbents. Type II isotherm is concave to the pressure axis, then almost linear and finally convex to the pressure axis, indicating the formation of an adsorbed layer whose thickness increases progressively as the pressure increases. The knee of the isotherm at point B (beginning of the middle quasilinear section) is usually considered to represent the complete formation of monolayer and the beginning of multilayer. Moreover, the ordinate of point B gives an estimation of the amount of adsorbate required to cover the unit mass of solid surface with a complete monomolecular layer (monolayer capacity).

Type III

Type III isotherms are not common and are characteristic of non-porous adsorbents with low energy of adsorbent-adsorbate interaction. Type III isotherm is convex to the pressure axis over the complete range of pressure and therefore has no point B; moreover, there is no knee in the curve, meaning that the monolayer formation is missing.

Type IV

Type IV isotherm is similar to type II, but refers to porous adsorbents and shows capillary condensation of gas. At a lower pressure the region of the graph is quite similar to type II and rationalizes the formation of monolayer followed by multilayer. Type IV adsorption exhibits a hysteresis loop, the lower branch of which represents measurements obtained by progressive

addition of gas (the adsorbent), whereas measurements on the upper branch are obtained by progressive withdrawal. The hysteresis loop is usually associated with the filling and emptying of the pores by capillary condensation.

Type V

Types V isotherm is similar to type III, but refers to porous adsorbents; it is initially convex to the pressure axis and levels off at high pressures. As type IV, type V shows capillary condensation of gas and exhibits a hysteresis loop, associated with the mechanism of pore filling and emptying. Such isotherms are relatively rare.

Type VI

Type VI isotherm is characteristic of non-porous adsorbents with homogeneous surface. Type VI isotherm is relatively rare and associated to layer-by-layer adsorption on a highly uniform surface. The sharpness of the steps is dependent on the system and the temperature.

1.3.1.1 Adsorption of solutes

A distinctive feature of adsorption from solution is the competition between the solvent and the solute, which always takes place and has to be taken into account for a complete data treatment. In the case of adsorption from solution, the 'apparent adsorption' of a solute at the liquid-solid interface is usually evaluated by measuring the decrease in its concentration when in contact with the adsorbent. The adsorption isotherm is plotted as amount of adsorbate on solid against the equilibrium concentration.

At low concentrations adsorption from solution isotherms mainly fall into two main groups among those listed by Giles and Smith[95]: concave to the concentration axis and convex and then concave to the concentration axis. The former adsorption isotherms are analogous to Type I of the IUPAC classification and generally associated with monolayer adsorption of the solute and minimal competition with the solvent, while the latter are comparable to Types III or V and explained by a different balance between adsorbate-adsorbate and adsorbate-adsorbent interactions (the former are supposed to be responsible of a “cooperative” adsorption which produces a swing in the second part of the adsorption isotherm).

1.3.2 Adsorption models

The adsorption of molecules on a solid surface is rationalized by means of adsorption models[96,97]. Most models based on both theoretical and empirical bases were developed over the years. A quick description of the main adsorption models is provided below.

1.3.2.1 Langmuir model

Langmuir model is one of the simplest and oldest model used to describe the adsorption of molecules on a solid surface[98,99]. The model is based on several assumptions: (i) a single monolayer is formed on the surface (molecule thickness); (ii) adsorption can only occur at a finite fixed number of identical, equivalent, definite sites; (iii) no lateral interactions exist between adsorbed molecules and the steric hindrance in negligible; (iv) adsorbed molecules cannot move on the surface; (v) solid surface is homogeneous.

Langmuir model is useful to describe type I adsorption isotherms, while types II and III show large deviations. Langmuir adsorption isotherm can be described by several equivalent equations; the commonest are reported below.

$$K_{adsL} = \frac{\theta}{[L](1-\theta)} \qquad \text{Equation 1a}$$

$$L_{ads} = \frac{n_{tot\,L} K_{adsL}[L]}{1 + K_{adsL}[L]} \qquad \text{Equation 1b}$$

In equations 1a,b K_{adsL} is the Langmuir binding constant (M^{-1}), θ is the coverage fraction (adimensional), [L] is the concentration of the adsorbate in solution (mM), L_{ads} is the amount of titrant adsorbed (mmol g^{-1}) and n_{totL} is the maximum adsorption capacity (mmol g^{-1}). In the second, equivalent form, the value of loading (n_{totL}) is present in the numerator and fixes the maximum amount of loadable adsorbent. This form of Langmuir adsorption isotherm is usually used to show the graphs. In Figure 13 the isotherms obtained with different values of K_{adsL} and

n_{totL} are showed. The shape of the curve is dependent on the value of K_{adsL} (Figure 13a), while the plateau represents the total loading (Figure 13b).

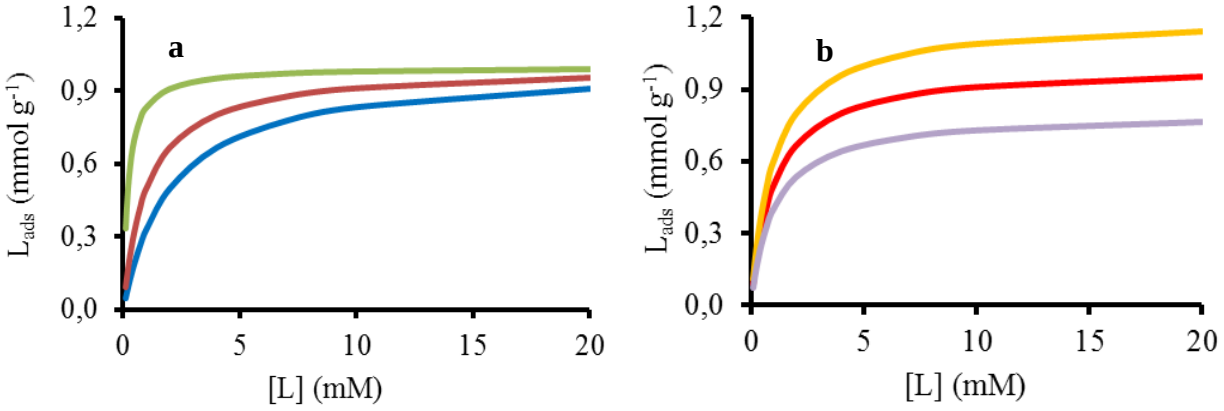

Figure 13: Graphical representation of Langmuir adsorption isotherm. a: n_{totL}=1 mmol g^{-1}, K_{adsL}=500(blue), 1000 (red), 5000 (green), logK_{adsL}=2.7, 3.0, 3.7 respectively. b: K_{adsL}=1000, n_{totL}=1 (red), 1.2 (orange), 0.8 (purple) mmol g^{-1}.

The Langmuir model expressed in form of Equation 1b is easily extendible in order to consider different binding sites (Equation 2a). Each site adds another term of the same form as for that shown in equation 1b:

$$L_{ads} = \sum_{i=1}^{n} \frac{n_{L\_n} K_{adsL\_n}[L]}{1 + K_{adsL\_n}[L]} \qquad \text{Equation 2}$$

where L_{ads} is the amount of moles of titrant adsorbed per gram of solid (mmol g^{-1}), n_{L_n} is the number of moles of site i per gram of solid (mmol g^{-1}), K_{adsL_n} is the Langmuir equilibrium constant of binding (M^{-1}) at site i and [L] is the equilibrium concentration of titrant in solution (mM). Equations 1b and 2 are suitable to fit data obtained by techniques such as UV-Vis spectrophotometry and potentiometry, where the equilibrium concentration of adsorbent is monitored during the experiments.

The rationalization of calorimetric data requires a re-elaborated version of Equation 2 in order to include the molar adsorption enthalpy relative to each binding site. Equations 3a,b describe the calorimetric isotherms relative to single and multi-sites adsorption respectively.

$$\frac{h_{cum}}{w} = \frac{n_L K_{ads\_L}[L]}{1+K_{ads\_L}[L]} * \Delta H_{ads\_L} \qquad \text{Equation 3a}$$

$$\frac{h_{cum}}{w} = \sum_{i=1}^{n} \frac{n_{L\_n} K_{adsL\_n}[L]}{1+K_{adsL\_n}[L]} \Delta H_{adsL\_n} \qquad \text{Equation 3b}$$

In the equations above, h_{cum} is the total heat exchanged (J), w is the weight of the solid sample (g) and ΔH_{adsL} and ΔH_{adsL_n} are the enthalpies of adsorption on the binding site(s). In the calorimetric experiment, however, only the total concentration of titrant added after each injection is known, but the values of free titrant concentration [L] are mandatory for the determination of enthalpy of adsorption by fit. Therefore the values of [L] must be calculated by the values of K_{adsL} and n_L obtained separately by carrying out adsorption experiments with a non-calorimetric techniques (e.g. UV-Vis spectrophotometry).

There are several different adsorption models based on Langmuir's [98,99]. Such models were developed in order to take into account factors such as un-homogeneous surface and lateral interactions. The descriptions of Langmuir-Freundlich and Fowler–Guggenheim models are provided below.

1.3.2.1.1 Langmuir-Freundlich model

Langmuir-Freundlich model takes into account the heterogeneity surface. In this model the product (K_{adsL} [L]) of Langmuir adsorption model (Equations1b and 2) is raised to the Langmuir-Freundlich exponential m_{LF}.

$$L_{ads} = \frac{n_{tot\,LF}(K_{adsLF}[L])^{m_{LF}}}{1+(K_{adsLF}[L])^{m_{LF}}} \qquad \text{Equation 4}$$

where L_{ads} is the amount of adsorbate in the adsorbent at equilibrium (mmol g^{-1}), n_{totLF} is the maximum adsorption capacity, K_{adsLF} is the Langmuir-Freundlich constant (M^{-1}), [L] is the adsorbent equilibrium concentration (mM) and m_{LF} is the LF isotherm model exponential

(adimensional). The Langmuir-Freundlich exponential is a pure number which ranges from 0 to 1 and represents the heterogeneity parameter of the surface; when m_{LF}=1 the model corresponds to Langmuir's and the surface is considered homogeneous (according with the assumption of Langmuir model); on the contrary, when m_{LF}=0 the surface is totally heterogeneous. Figure 14 shows the single-site adsorption isotherms calculated with a constant loading and a binding constant (1 mmol g^{-1} and $\log K_{adsLF}$ =3 respectively) with different values of m_{LF}. By decreasing the value of m_{LF} the loading apparently decreases, while the binding constant apparently increases (the plateau is reached at lower concentrations of free titrant).

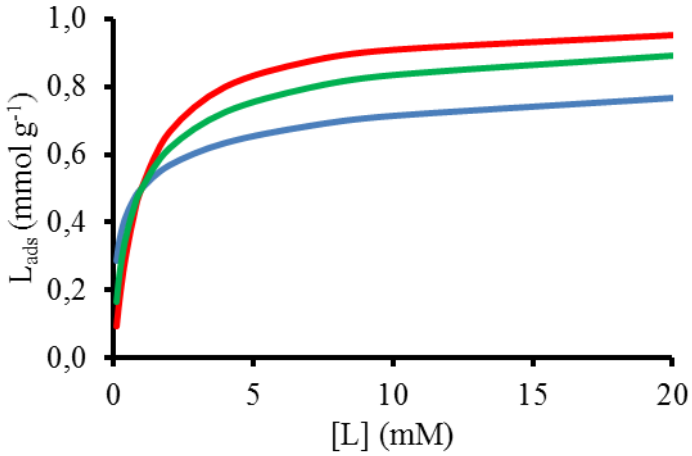

Figure 14: Graphical representation of Langmuir-Freundlich single-site adsorption isotherm. n_{totLF}=1 mmol g^{-1}, $\log K_{adsLF}$=3, m_{LF}=1(red), 0.7 (green), 0.4 (blue).

As in the case of Langmuir model, equation 4 is modified to be applied to calorimetric titrations (Equation 5). Also in this case, during calorimetric experiments the values of [*L*] are unknown and have to be calculated by means of the results obtained by equation 4.

$$\frac{h_{cum}}{w} = \frac{n_{tot\,LF}(K_{adsLF}[L])^{m_{LF}}}{1+(K_{adsLF}[L])^{m_{LF}}}\Delta H_{ads} \qquad \text{Equation 5}$$

1.3.2.1.2 Fowler-Guggenheim model

Fowler–Guggenheim model takes in consideration the lateral interaction between adsorbed molecules and is usually expressed in a form similar to Equation 1a. The basic idea is that the heat

of adsorption varies with loading; if the interaction between the adsorbed molecules is attractive, the heat of adsorption will increase as the loading increases. This means that if the measured heat of adsorption shows an increase with respect to loading, it indicates a favourable lateral interaction among adsorbed molecules. However, if the interaction among the adsorbed molecules is repulsive, the heat of adsorption shows a decrease in loading. When there is no interaction among adsorbed molecules, Fowler–Guggenheim equation (Equation 4) will reduce to Langmuir equation.

$$K_{adsFG} = \frac{\theta}{[L](1-\theta)}^{\frac{2\theta W}{RT}} \qquad \text{Equation 6}$$

where K_{adsFG} is the Fowler-Guggenheim constant (M^{-1}), θ is the coverage fraction (adimensional), [L] is the adsorbent equilibrium concentration (mM), W is the interaction energy among adsorbed molecules (J mol^{-1}), R is the universal gas constant (J mol K^{-1}) and T is the temperature (K).

1.3.2.2 Freundlich model

The Freundlich model [96,98] is an empirical exponential equation which assumes that the amount of adsorbent on the surface is proportional to the Freundlich binding constant K_{adsF} and the n^{-1} power of concentration on the adsorbent [L]. Freundlich adsorption isotherm is expressed in both a linear (Equation 5a) and a logarithmic (Equation 5b) form.

$$\frac{m}{m'} = K_{adsF}[L]^{\frac{1}{n}} \qquad \text{Equation 7a}$$

$$\log\frac{m}{m'} = \log K_{adsF} + \frac{1}{n}\log[L] \qquad \text{Equation 7b}$$

where m is the mass of the adsorbate (g), m' is the mass of the adsorbent (g), K_{adsF} is the Freundlich constant, [L] is the adsorbent equilibrium concentration and n^{-1} is the exponential term. The values of K_{adsF} and n are constants for a given adsorbate and adsorbent at a particular temperature. Being based on an empirical relationship, Freundlich model is useful for comparison purposes with reference values, but the physical interpretation of results is very hard because the

units of measurement (especially *n*) have no physical sense. Thus, obtaining information about the Gibbs free energy of a certain adsorption process from the value of K_{adsF} is impossible. In the cases in which adsorption behaviour can be properly fit by isotherms with a theoretical basis, such isotherms should be used.

1.3.2.3 BET model

The Brunauer-Emmett-Teller (BET) model[91] is an improvement on the Langmuir isotherm which incorporates multilayer adsorption and treats the intermolecular interactions in the adsorbed layer assuming that it is liquid-like. BET theory is based on these hypotheses: (i) gas molecules physically adsorb on a solid in layers infinitely; (ii) there is no interaction between adsorption layers; (iii) the Langmuir theory can be applied to each layer.

The resulting equation gives the surface coverage θ (adimensional) as a function of the relative pressure (P/P_0) and a constant C which measures the strength of the adsorbent. The coverage can be greater than 1.0, which corresponds to multilayer adsorption; this was not possible in the Langmuir model. The "linear" form of BET model (Equation 8a) and its equivalent solved for coverage (Equation 8b) are written below.

$$\frac{1}{\theta(P_0/P-1)}=\frac{1}{C}+\frac{C-1}{C}\frac{P}{P_0} \qquad \text{Equation 8a}$$

$$\theta=\frac{C(P/P_0)}{1+(C-2)P/P_0-(C-1)(P/P_0)^2} \qquad \text{Equation 8b}$$

with

$$C=e^{(E_a-\Delta H_{vap})/RT}$$

where E_a is the adsorption energy, ΔH_{vap} is the enthalpy of vaporization of adsorbent, R is the gas constant and T is the temperature. C is the inverse Boltzmann factor of the 'excess' adsorption energy, exceeding the energy required to liquefy the gas. As the value of C increases (the adsorption is stronger) the pressure where θ =1decreases. At low pressures (P/P_0 > 0.1) the

quadratic term in the denominator of Equation 8b can be ignored and furthermore, if *C*-2~*C*, the BET isotherm resembles the Langmuir isotherm with $C = K/P_0$.. At high pressures ($P/P_0 \rightarrow 1$) all isotherms look the same because molecules in the above layers do not interact with the surface at all. At high pressures the BET isotherm diverges from Langmuir's, meaning that a macroscopically thick layer of adsorbed fluid grows on the surface (wetting). BET adsorption model is able to reproduce adsorption types I, II, and III. When P/P°<<1 and c>>1, it leads to a monolayer formation and Type I adsorption isotherm is obtained; type II isotherm is obtained when the value of C is very high compared to 1 and if C << 1 Type III adsorption isotherm is obtained.

1.3.2.3.1 BET for the determination of surface area

The BET model is useful to determine the surface area of solids. The specific surface area of a powder is determined by physical adsorption of a gas on the surface of the solid and by calculating the amount of adsorbate gas corresponding to a monomolecular layer on the surface. For this purpose, Equation 8a is rewritten using $\theta = L_{ads}/[S]_0$ (Equation 9, where L_{ads} is the amount of adsorbate on surface and $[S]_0$ is the monolayer capacity).

$$\frac{1}{(L_{ads}/[S]_0)(P_0/P-1)} = \frac{1}{C[S]_0} + \frac{C-1}{C[S]_0} P/P_0 \qquad \text{Equation 9}$$

Equation 9 allows the calculation of monolayer capacity and constant *C* from slope and intercept; the equation is plotted as $1/(L_{ads}/[S]_0)(P_0/P-1)$ against P/P_0 in the pressure range of $0.05 > P/P_0 > 0.30$ in order to focus on the area of the isotherm from 0.5 to 1.5 monolayer coverage. The slope and the intercept are evaluated by linear regression analysis and the values of *C* and $[S]_0$ are obtained. The surface area is calculated from $[S]_0$ and the area covered by a single molecule of adsorbate .

2 Experimental section

This section presents reagents, materials and instruments used in this work of thesis. The procedures used for treatment of solvents, preparation of solutions and titration are also reported in the correspondent sections.

2.1 Reagents and materials

2.1.1 Physically activated magnesium chloride

Samples of anhydrous, physically activated $MgCl_2$ were provided by the University of Naples. Activated $MgCl_2$ samples were prepared by mechanical route, milling anhydrous magnesium chloride together with zirconia balls in a planetary miller. The synthetic protocol essentially consisted in:

- loading of planetary ball miller with 5-10g of anhydrous macro-crystalline $MgCl_2$ and 50-80 g of zirconia balls in glove box. This part of the synthetic procedure was improved during the project by adding $SiCl_4$ as a water scavenger or $TiCl_4$ when co-milled $MgCl_2$-$TiCl_4$ samples were necessary;
- Milling of the system through alternate clockwise and counter-clockwise rotation cycles (rotation of 20 min, stop for 5 s, rotation in opposite sense for 20 min) for 4-8 hours at 55-60 °C;
- Recovering of physically activated $MgCl_2$ samples, which were then washed several times with anhydrous heptane, then pentane and drying of solid under vacuum.

Several parameters of preparative procedure (such as milling time, amount of $SiCl_4$, order of milling and drying steps and $MgCl_2$/zirconia balls ratio) were modified during the course of the work using the results of water content on previous samples as feedback in order to reach the conditions that led to the lowest possible water content. Table 8 shows in a more detailed way the conditions used to prepare the physically activated $MgCl_2$ samples considered in this work.

	$MgCl_2$	$SiCl_4$ (mol_{SiCl4}/mol_{H2O})	Milling procedure	$MgCl_2$/balls (g_{MgCl2}/g_{balls})
Preliminary experiments	A	-	M(5h)	0.025
	B	-	M(4h)	0.026
Improvment of methodology	C	9:1*	D(4h)→(5h)	0.035
	D	9:1*	M(8h)→D(4h)	0.034
	E	20:1*	D(5h)→M(8h)	0.034
	F	9:1*	D(4h)→M(8h)	0.065
	G	9:1*	D(5h)→M(4h)	0.055
Optimized procedures	H	20:1*	D(5h)→M(8h)	0.062
	I	20:1*	D(5h)→M(8h)	0.075
	J§	-	M(8h)	0.091

Table 8: Preparative conditions of physically activated $MgCl_2$ samples. M=milling step; D=Drying step with $SiCl_4$. * considering 0.2% w/w H_2O; § co-milled $MgCl_2$-$TiCl_4$ sample.

Since the preliminary experiments (samples A and B) the presence and the effect of water on thermodynamic determinations was evident, thus in the preparation of next samples (C-I) $SiCl_4$ was added to $MgCl_2$ as a water scavenger. For samples C-G the synthetic procedures were slightly modified with the aim of developing the methodology which allowed to obtain the lowest possible water content. In particular, samples C and D were not used to determine the thermodynamic parameters but only for an in-depth analysis of the water content and the results obtained were used as feedback for the synthesis of the next samples. Samples H and I were synthetized with the optimized procedure, while sample J was milled together with 2% w/w of $TiCl_4$ and used to investigate the adsorption of donors in presence of $TICl_4$ (ternary system).

2.1.2 Solvents and solutions

Tetrachloroethane (TCE, >99%), toluene (Tol, >99%) and *n*-heptane (Hept, >99%) were considered as mediums for the adsorption experiments. TCE, toluene and *n*-heptane were purchased form Sigma Aldrich. All solvents were submitted to several drying procedures[100–102] with the aim of finding the best method to obtain the lowest water content possible (paragraph 2.1.2.1). Titanium and silicon tetrachlorides were purchased ($TiCl_4$, Sigma-Aldrich >99%, $SiCl_4$, Fluka, 99%) and used without any further purification. Ethylbenzoate and diethylphthalate were synthetized from the correspondent alcohols and carboxylic acids (procedures reported below). Stock solutions of $TiCl_4$ and donors were prepared in glove box; aliquots of titrants were weighted directly inside a graduated flask, which was then filled with anhydrous solvent.

2.1.2.1 Drying of solvents

The different drying procedures described below, such as treatment with anhydrous salts (calcium and magnesium sulfate), chemical reaction (with hydride or sodium) and trapping (molecular sieves) were taken into consideration in order to remove water from the reaction media. The final water content of the solvent after anhydrification was checked by Karl-Fischer titrations[103,104] on fresh samples at least three times in order to validate the consistence. Not all methodologies were useful for all solvents because of chemical reaction occurring (Table 9), in particular in the case of TCE with sodium and hydrides.

	TCE	Toluene	*n*-heptane
$CaSO_4$	✓	✓	✓
$MgSO_4$	✓	✓	✓
Na/Ph_2CO	R	✓	✓
MS 4Å	✓	✓	✓
Dist. over CaH_2	R	✓	✓
Lowest water content (mM)	*0.72*	*0.27*	*0.06*

Table 9: Drying procedures applied to the solvents. R= reaction.

Calcium and magnesium sulphate ($CaSO_4$ and $MgSO_4$)

Anhydrous $MgSO_4$ (Sigma-Aldrich >99%) was used as received, while $CaSO_4$ was prepared by precipitation from Ca^{2+} and SO_4^{2-} solutions. Calcium sulphate was then washed and dehydrated at 450 K at a reduced pressure for three days. About 10% $w_{salt}/w_{solvent}$ of the sulphates were added to the solvent during the drying procedure; after a few minutes, small crystals of the hydrate salts started to appear in the case of $MgSO_4$. The systems were shacked a few times and stored for 24 hours prior to KF analysis.

Sodium/benzophenone

In a round-bottom flask solvent (100 mL), 0.5-1% w/w sodium and some crystals of benzophenone (as colorimetric indicator) were refluxed under atmosphere of dry nitrogen until a persistent deep blue colour of benzophenone radical appeared (2-4 hours). The solvent was then distilled under nitrogen flux with a protection of $CaCl_2$ against atmospheric moisture. The water content was analysed immediately after cooling.

Molecular sieves (MS)

Molecular sieves (4Å) were washed several times with water, acetone and then again with water (for a total of 8-12 washing steps), pre-dried in an oven at 90° for 2-4 hours and then

transferred inside a vacuum oven at 450 K for three days. Molecular sieves were transferred still hot in a glass ampoule, hermetically closed and used after cooling. Activated molecular sieves (10-20% $w_{MS}/w_{solvent}$) were added to the solvent and left in it for at least three days before determining the water content.

Calcium hydride (CaH_2)

Hydrocarbons were refluxed overnight over CaH_2 under atmosphere of dry N_2. Solvents were then distilled under dry nitrogen flux at ambient pressure and collected in a balloon provided of a protection of anhydrous calcium chloride against atmospheric moisture. Karl-Fischer titrations of water were run immediately after cooling.

Optimized drying procedure for n-heptane

The optimized procedure to dry *n*-heptane (chosen as solvent for titration experiments) consisted in a preliminary anhydrification by distillation over CaH_2 followed by storage on 4 Å molecular sieves. In a 500 mL balloon about 300 mL of *n*-heptane were refluxed under flux of dry nitrogen over CaH_2 (3-5 % w/w) for 24 h. Hydrocarbon was distilled and the vapours were condensed directly in a balloon containing about 20%w/w activated 4 Å molecular sieves. Heptane was stored in glove box for at least 3 days before use.

2.1.2.2 Synthesis of donors

Ethyl benzoate was prepared from the correspondent alcohol and carboxylic acid by acid-catalysed Fischer's synthesis of esters[105,106], while diethylphthalate was obtained from phthalic acid in two steps through phthalic anhydride intermediate prior to the reaction with ethanol.

Ethyl benzoate (EB)

In a 100 mL balloon equipped with a reflux condenser, 1.0 g of benzoic acid was dissolved in 10 mL of anhydrous ethanol with some drops of concentrated sulphuric acid. The system was refluxed overnight with a $CaCl_2$ trap as protection from external moisture and the end of the reaction was monitored by TLC. The reaction mixture was cooled, diluted with 20 mL of diethyl ether, washed with 10 mL of saturated solution of K_2CO_3 and several times with water. The

organic phase was pre-dried over anhydrous $MgSO_4$ and filtrated, then the solvent was stripped under vacuum, leaving an almost colourless oil (0.99g, yield 81%) which was stored in glove box over anhydrous K_2CO_3.

Diethylphthalate (DEP)

A 200 mL beaker with 12.9 g of powdered phthalic acid was placed on an electric heater and covered with an empty 250 mL balloon as cooler; the balloon must not contain water to avoid excessive cooling and allow the water gas formed in the reaction to escape. After being turned on, the heater reached its maximum power in twenty minutes.Aftre melting of phthalic acid (480 K), small snow-like crystals of phthalic anhydride started to appear on the bottom of the empty balloon. Phthalic anhydride crystals were progressively collected by temporarily removing the balloon and scratching the bottom; the procedure was repeated several times. A total of 4.6 g of very pure, sublimated crystalline phthalic anhydride was collected (29% yield). The synthesis of diethylphthalate from phthalic anhydride was run with the same procedure used for the preparation of ethyl benzoate.

2.2 Instruments

2.2.1 UV-Vis spectrophotometric titrations

UV-Vis spectrophotometry was widely used in this work for the determination of concentrations of $TiCl_4$ and IDs in the liquid phase. Electronic spectra were recorded with a Varian Cary 50 spectrophotometer using a quartz cuvette with an optical path of 1 cm and V_{tot} = 3 mL and provided of a hermetic cap. Data were acquired at 298 K with 1 nm resolution over the wavelength range 200-500 nm and 200-700 nm for IDs and $TiCl_4$ respectively.

Figure 15: The UV-Vis spectrophotometer employed (Varian Cary 50). Wavelength range 190-1100 nm, maximum resolution 0.5 nm.

2.2.1.1 UV-Vis spectrophotometric titration of solids

Samples of $MgCl_2$ were titrated by stepwise additions of titrant solution to a stirred dispersion of sample in suitable medium. The adsorption of $TiCl_4$ on $MgCl_2$ was found to be complete within 15 minutes, while equilibration of IDs (DEP in particular) was slower, but grew by more than 95% within one hour, as other authors found[81]. Kinetics of the adsorption of titrants were checked by monitoring changes in titrant concentration after a single addition of a large quantity of donors. Titrations of $MgCl_2$ were typically performed by adding dilute $TiCl_4$ or IDs solutions in strictly anhydrous hydrocarbon ($10<C°_{TiCl4}<100$ mM; $1<C°_{ID}<10$ mM) to a stirred suspension of $MgCl_2$ (30-40 mg mL^{-1} for $TiCl_4$ and 5-20 mg mL^{-1} for IDs, V_0 = 10-20 mL). After each addition and a suitable equilibration time (30 min for $TiCl_4$ and 60 min for IDs), the stirring was stopped, the solid was let settle and an aliquot of transparent liquid phase was collected for UV-Vis spectrophotometric analysis. The experimental data were treated with Microsoft Excel and Solverstat tools[107].

2.2.1.2 UV-Vis spectrophotometric determination of titrants concentrations

During the preliminary experiments of this work of research, UV-Vis spectrophotometric determinations of both $TiCl_4$ and IDs were performed through the direct reading of absorbance of the liquid phase (direct determination or DD) and the concentration determined by means of a calibration line. This methodology was useful for quantitative determinations of organic molecules (IDs), but it was not so accurate for quantitative detection of inorganic titanium, mainly for two

different reasons; (i) $TiCl_4$ is easily hydrolysed (by the residual water in titration system) with consequent formation of suspended TiO_2, which greatly affects the UV-Vis spectrophotometric determination (scattering of UV-Vis spectrophotometric beam); (ii) the concentrations of $TiCl_4$ useful for adsorption on $MgCl_2$ (1-10 mM) were found to be about two orders of magnitude greater than the maximum clearly detectable by UV-Vis spectrophotometry(the maximum of adsorption bands was out of instrumental range).

Thus, a special protocol for the determination of titanium concentration was developed; the method was based on the formation of an inorganic titanium-peroxide complex[108] (hydrogen peroxide method or HPM) and helped to improve the precision and reproducibility of data. A brief description of HPM procedure is provided below and the results obtained by DD and HPM are given in; a comparison between procedures is provided in chapter 3, "results and discussion".

2.2.1.2.1 Determination of titanium concentration: the hydrogen peroxide method

The hydrogen peroxide method (HPM) was based on the formation of a well-coloured Ti-H_2O_2 complex. With simple modifications, this method was used to determinate $TiCl_4$ concentration (after exposure to $MgCl_2$) and $TiCl_4$ content in $MgCl_2$ co-milled samples. This method (see Figure 16 to have visualization of the steps), which works perfectly even outside glove box, essentially consists in:

A. formation of an aqueous solution of Ti^{4+}; the goal was achieved through simultaneous hydrolysis and extraction of a known volume of $TiCl_4$ solution by 10% HCl or dissolution of a known amount of $MgCl_2$-$TiCl_4$ co-milled sample in a known volume of the same acidic solution *Note:* the extraction of Ti^{4+} with concentrated HCl resulted in a pale yellow solution and led to irreproducible results.

B. addition of a known volume of H_2O_2 (strong excess, > 50 eq.) to Ti^{4+} aqueous solution in order to obtain the red Ti-H_2O_2 complex (ε_{418} = 670 M^{-1} cm^{-1}). *Note*: traces of EDTA decrease the evolution of oxygen due to the decomposition of hydrogen peroxide.

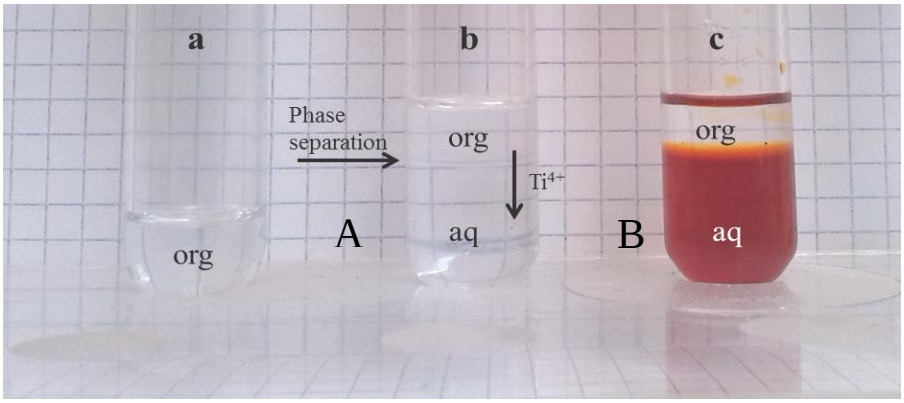

Figure 16: Steps for the formation of Ti-hydrogen peroxide complex; a: $TiCl_4$ solution in heptane; b: addition of 10% HCl; c: addition of H_2O_2.

2.2.2 Calorimetric titrations

During this work of thesis two different calorimeters were used. Calorimetric heads and titration vessels of both instruments were filled, joined together inside the glove-box and connected to the instrument immediately before titration.

The use of two calorimeters was necessary for titrations because of the high reactivity of $TiCl_4$ and, in particular, its inclination to form insoluble/hard working products in the titration capillary; even the smaller amount of water caused precipitation of titanium oxychlorides which block the capillary. The Tronac model 87-558 isoperibolic titration calorimeter equipped with a 25 mL vessel was employed in experiments where the extremely reactive $TiCl_4$ was present, because the Tronac calorimeter's capillary is big enough to allow the (mechanical) cleaning of titration capillary with a small stainless steel tool. The cover of the titration vessel and its connection to the calorimeter were modified in order to ensure the reactions proceeded in an inert atmosphere.

Calorimetric titrations of $MgCl_2$ with IDs were performed by means of TAM III (T.A. Instruments) nanocalorimeter operating in isothermal modality at 298 K and equipped with a 1 mL cell. The use of the very sensitive TAM III was possible only when working with donors, because these compounds are almost inert towards water.

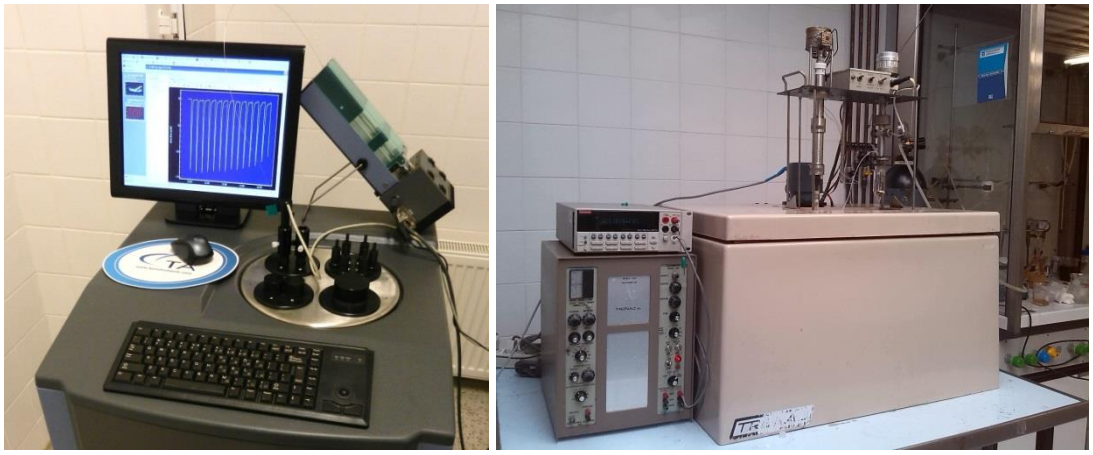

Figure 17: Calorimeters employed in this work. Left: Isothermal titration nanocalorimeter (TAM III), cell capacity 1 mL, sensibility > 10^{-5}J; right: isoperibolic titration calorimeter (Tronac model 87-558), cell capacity 25 mL, sensibility 1J.

2.2.2.1 Calorimetric titration of solids

Calorimetric titrations were performed by stepwise additions of titrant solutions ($50<C°_{TiCl4}<200$mM, $1<C°_{ID}<10$mM) to a stirred suspension of solid in anhydrous hydrocarbon ($10<MgCl_2<40$ mg mL^{-1} for $TiCl_4$, $5<MgCl_2<20$ mg mL^{-1} for ID); one hour passed between one addition and the next. In experiments with samples E-I $SiCl_4$ a water scavenger was introduced in the titration cell (50 eq. supposing 0.2% w/w of water). Dilution heats were measured by running analogous experiments in absence of solid phase or, if possible, obtained by extrapolation from last titration points, in which no adsorption takes place and the heat exchange is due to dilution.

2.2.2.2 Calorimetric titration of solutions

Calorimetric titrations in homogeneous phase (e.g. $TiCl_4$ with DEP) were performed by Tronac calorimeter through a single, slow addition of titrant into the calorimetric cell. In a typical experiment, 20 mL of $TiCl_4$ 10 mM were titrated with IDs solutions (50-130 mM). Dilution heats of titrants were measured by running analogous experiments where titrant solutions were added to the solvents. The calculation of the enthalpy and Gibbs free energy changes was performed by the computer tools HyperDeltaH[109] and Solverstat[107].

2.2.3 Karl-Fischer determination of water

Karl Fischer (KF) titrations[103,104] were used to quantify the water content of solvents and $MgCl_2$ samples. Determinations of water were performed at 298 K with a Metrohm 684 KF Coulometer using a methanol-based KF reagent (Fluka, HYDRANAL-Coulomat AD).

Figure 18: Metrohm 684 Karl-Fischer Coulometer for determination of water. Working solution: HYDRANAL - Coulomat AD – methanol based, sensibility 0.1 ppm w/w.

The titration of solvents was performed by adding known amounts of solvent to pre-dried of KF solution (automatically performed by the instrument) according with the manual; a special methodology was developed to allow the titration of solid $MgCl_2$ samples, because this KF apparatus is designed for titration of liquids.

2.2.3.1 Karl-Fischer titration of magnesium chloride

The water content of $MgCl_2$ samples was determined by titration of $MgCl_2$ solution in pre-dried KF reagent. Little modifications in the titration procedures allowed the determination of both total and bulk amount of water (surface water excluded).

2.2.3.1.1 Determination of total water

The titration procedure consisted in:

A. in glove box, loading of weighted amount (about 100 mg) of $MgCl_2$ in a 5 mL plastic syringe, protecting the hole of the needle against humidity with a rubber cap;

B. dissolution of $MgCl_2$ sample in pre-dried KF solution (2-3 mL of liquid; solubility limit of $MgCl_2$ in methanol 50 mg mL^{-1} [110]) collected directly from the titration apparatus (trough septum) by quickly removing the rubber cap. *Attention!* Dissolution of anhydrous $MgCl_2$ in KF solution is *strongly exothermic*! Temperature can rise enough to allow the solvent to boil inside the syringe;
C. after cooling to room temperature, injection of $MgCl_2$ solution into KF apparatus and determination of total water.

2.2.3.1.2 Determination of bulk water

The titration procedure is very similar to the one used for the determination of the total amount of water. However, the two procedures differ because a new point (A') was inserted between points A and B, in which $MgCl_2$ sample was pre-treated with $TiCl_4$ solution as a water scavenger. The pre-treatment of the samples with $TiCl_4$ does not dissolve $MgCl_2$ but remove the water on magnesium chloride "accessible" to $TiCl_4$ (surface), allowing bulk water content to be determined.

A→ *A*

A'→ *B*: withdrawing $TiCl_4$ solution in dry *n*-heptane (1 mL of 100 mM $TiCl_4$, 1-4 equivalents. considering a total water content of 0.2% w/w) through a needle after quickly removing the rubber cap, which is then put back into place. Shaking the heterogeneous system for a few minutes.

B→ *C*

C→ *D*

Attention! In presence of $TiCl_4$ the heat evolved during the dissolution of $MgCl_2$ is greater than the heat described in the previous paragraph! Reaction *runs-out* easily and the procedure must be carried out with great care and attention!

2.2.4 Glove box

Glove box must be used in order to ensure strictly anhydrous experimental conditions. The water content of glove box was maintained below 0.1 ppm (detection limit of sensor); molecular sieves and copper-based catalysts ensuring dry and anoxic internal atmosphere (nitrogen) were periodically regenerated through a treatment with heating and hydrogen-nitrogen mixture (90% N_2, 10% H_2). The manipulation of reactants (solvents, solutions and solid samples) and the preparation of titration experiments (preparation of titration apparatus) were performed inside glove box. Before being introduced inside GB, also glassware, tools, etc. were thermally treated to eliminate water during one hour-long (at least) treatment in a vacuum oven; heating temperature was chosen depending on the materials used (glass/metallic parts: 408 K; plastic/rubber/delicate parts: 323 K). Items were transferred still hot inside the glove box.

Figure 19: Glove box employed (MBBROWN model MB 150 GI).

2.2.5 B.E.T.

The textural characteristics of all samples were measured according to the B.E.T. equation (see paragraph 1.3.2.3)[91] by nitrogen adsorption isotherms at -196 ºC. Pore size distributions were calculated by applying the Barrett–Joyner–Halenda (BJH) method[94,111] to the isotherms desorption branch. These measurements were carried out in a Tristar 3000 gas adsorption analyser (Micromeritics). Prior to the adsorption measurements, degasification of the samples was carried out at 150ºC for 1h.

Figure 20: Gas adsorption analyzer.

3 Results and Discussion

This chapter describes the results obtained from the study of thermodynamic interactions between the components of the heterogeneous Ziegler-Natta catalysts. The results are divided in three sections, each one divided in sub-sections according to the scheme below.

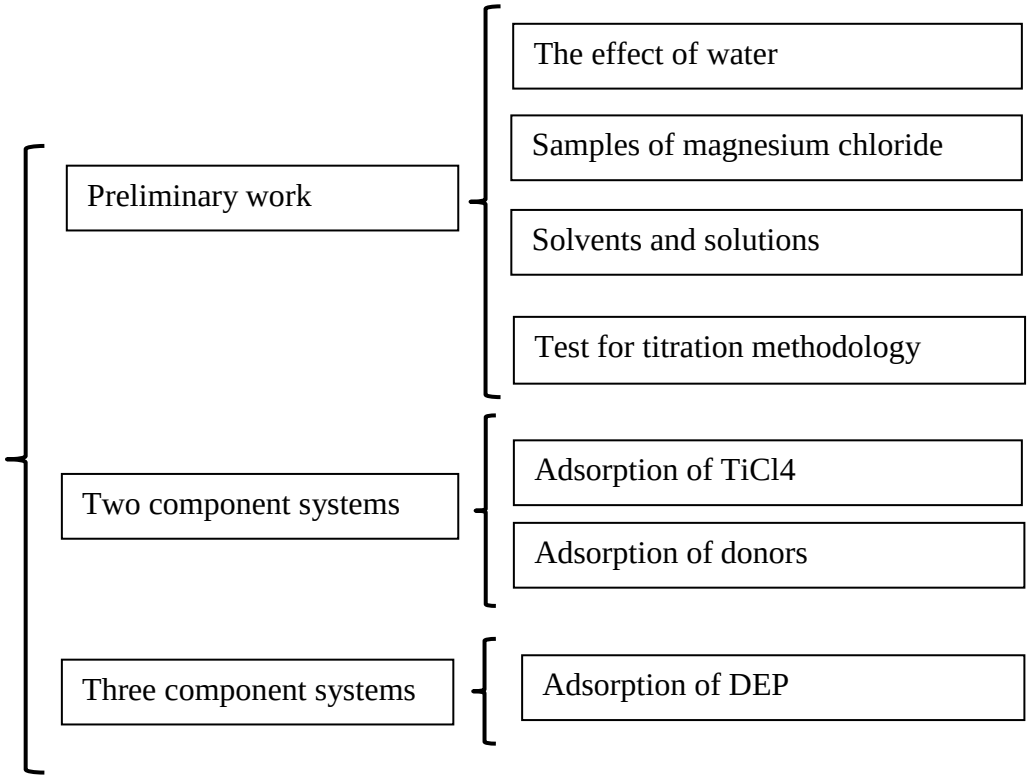

3.1 Preliminary work

Most of the preliminary work was focused on the study of the effect of water on experimental data and on the way to remove this molecule during calorimetric and UV-Vis spectrophotometric experiments. Part of the work consisted also in validating the titration methodology by means of titration of silica with pyridine (Py) in anhydrous cyclohexane[112].

3.1.1 The effect of water

When exposed to air, $TiCl_4$ or its concentrated solutions strongly fumes, while anhydrous $MgCl_2$ readily adsorbs moisture until a complete dissolution occurs (it is deliquescent) [113,114]. The hydrolysis of both chlorides is known to be highly favoured and exothermic[115,116], and the high reactivity is reflected on instrumental signals (particularly on the calorimetric ones) when water is present inside the titration apparatus. The effect of water was evident since the firsts experiments.

3.1.1.1 Hydrolysis of $MgCl_2$

Magnesium chloride readily adsorbs water until the formation of liquid hydrates $MgCl_2*nH_2O$ occurs. In the almost dry systems under examination the amount of water is very low (hydration is limited to the surface of anhydrous $MgCl_2$) and it is bound to the insaturations present on the surface[117].

$MgCl_2 + H_2O \rightarrow MgCl_2\text{-}OH_2$ *Filling of insaturations*

Both 104 and 110 lateral cuts of $MgCl_2$ (with one and two vacant sites on Mg atoms respectively) bind water; the overall reaction is very exothermic[115]. The heat of interaction between water and physically activated anhydrous $MgCl_2$ was quantified through titrations of $MgCl_2$ suspensions in *n*-heptane with a saturated solution of water in *n*-heptane ($[H_2O]$=1.6 mM at 298 K, analyzed by Karl-Fischer titration, see Table 13). The calorimetric titrations were run using the high sensitive TAM III nanocalorimeter; the graph in Figure 21 plots the molar enthalpy of reaction per mole of water (ΔH_{ads}) as a function of volume of titrant. The values at infinite dilution (evidenced by circles in Figure 21) were obtained by extrapolation at V_{add}=0.

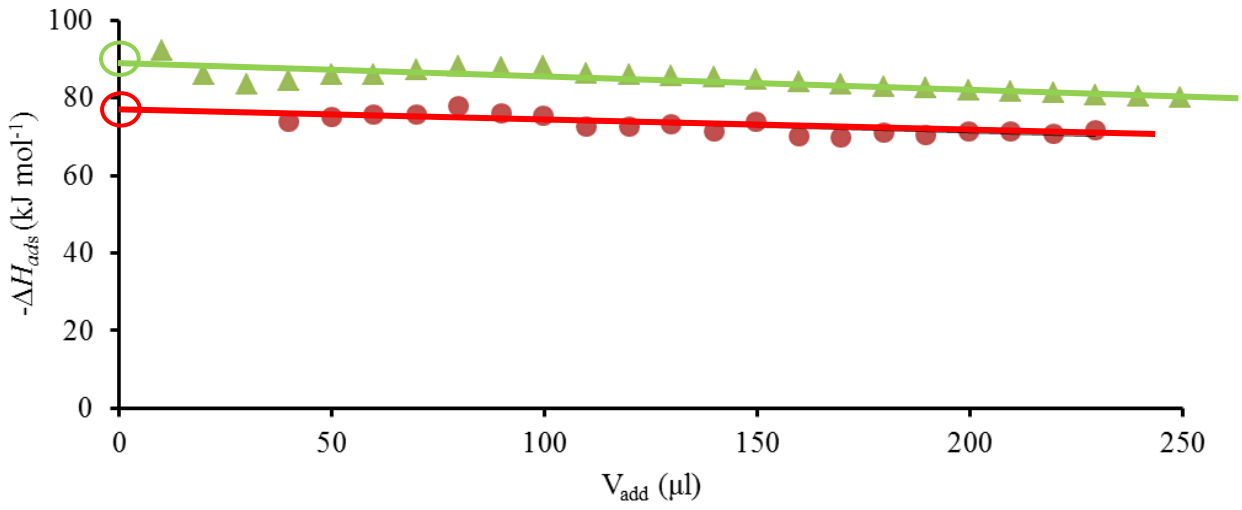

Figure 21: Calorimetric titration of $MgCl_2$ (B) with *n*-heptane saturated with water. Green triangles: $MgCl_2$=22.4mg, V_0=0.7mL, C_{H2O}=1.6 mM, 12.5 µL additions; red dots: $MgCl_2$=7.9 mg, V_0=0.7mL, C_{H2O}=1.6 mM.

Calorimetric experiments showed an overall heat of interaction water-anhydrous $MgCl_2$ of -84±5 kJ mol^{-1} per mole of water, close to the results relative to binding of water to $MgCl_2$ lateral cuts obtained by DFT calculations considering the different phase of reactants[117]. This highly favored reaction underlines the importance of working in very dry conditions to obtain clear thermodynamic information.

3.1.1.2 Hydrolysis of $TiCl_4$

Hydrolysis of $TiCl_4$ is a highly favoured exothermic multi-step reaction, accompanied by evolution of hydrochloric acid. If there is enough water, the hydrolysis proceeds until the formation of solid TiO_2:

$TiCl_4 + 2H_2O \rightarrow TiO_2 + 4HCl$ *Complete hydrolysis of $TiCl_4$*

Hydrolysis occurs through several steps[118] by reactions of chlorides displacement (accompanied by evolution of hydrochloric acid) and elimination of water (when not less than two hydroxyl groups are bond to Ti atom). If water is sub-stoichiometric, predicting the exact final composition of hydrolysis products is impossible, because a mixture of Ti-oxychlorides (e.g. TiOCl(OH), $TiCl_3OH$) is formed essentially randomly according with the following reaction:

$TiCl_4 + nH_2O \rightarrow TiCl_{(4-n)}(OH)_n + nHCl$ *Formation of Ti-oxychlorides*

Hydrolysis heat of $TiCl_4$ was experimentally detected by stepwise calorimetric titration of *n*-heptane saturated with water (H_2O = 1.6 mM) with $TiCl_4$ solutions. For this purpose, the Tronac calorimeter was used in order to avoid damages due to $TiCl_4$ reactivity. Figure 22 shows the experimental data points of cumulative heat evolved plotted against the molar ratio $TiCl_4/H_2O$.

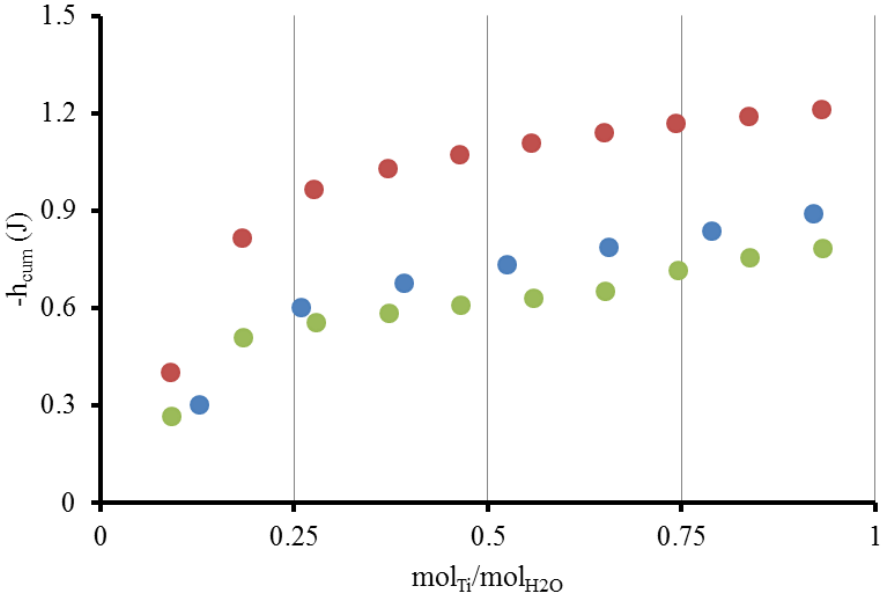

Figure 22: Calorimetric titrations of water with $TiCl_4$ in *n*-heptane. V_0=20mL, $C°_{H2O}$=1.6 mM (saturated solution), C_{TiCl4}= 25.1mM (blue, green), 36.4 mM (red).

All titrations show a very exothermic reaction in the first part of titration, when water is present in excess and $TiCl_4$ is supposed to completely hydrolyse. The change of slope in correspondence of a molar ratio $TiCl_4/H_2O$ of about 0.25 is supposed to correspond to a "tetrahydroxo titanium" like specie, where $TiCl_4$ is completely hydrolysed. Based on the slopes of straight lines obtained from the first titration points (prior to molar ratio 0.25), the initial step of $TiCl_4$ hydrolysis in *n*-heptane corresponds to -128±11 kJ mol_{Ti}^{-1}. Also in this case, calorimetric data evidence that removal of water is mandatory, in particular for calorimetric titrations.

3.1.1.3 $SiCl_4$ as water scavenger for titrations

Silicon tetrachloride, despite being less reactive toward water than $TiCl_4$, is a useful water scavenger, removing residual water from the system when added inside the titration cell three hours before titrations. Reaction products (silicon oxychlorides, SiO_2) and unreacted $SiCl_4$ were supposed not to adhere to $MgCl_2$ surface, because atoms of magnesium and silicon usually adopt a different geometry; in fact, magnesium atoms in $MgCl_2$ adopt an octahedral geometry[64,65], while the same geometry for silicon compounds is very rare[119].

The reactivity of $SiCl_4$ towards $MgCl_2$, $TiCl_4$ and LBs was anyway investigated to check if the silicon compound interacts with other components of the catalytic system apart from water. The interaction of IDs with $SiCl_4$ was studied by means of UV-Vis spectrophotometry, monitoring the changes in LBs spectra upon additions of titrant. In Figure 23 an example of titration of EB with $SiCl_4$ is provided.

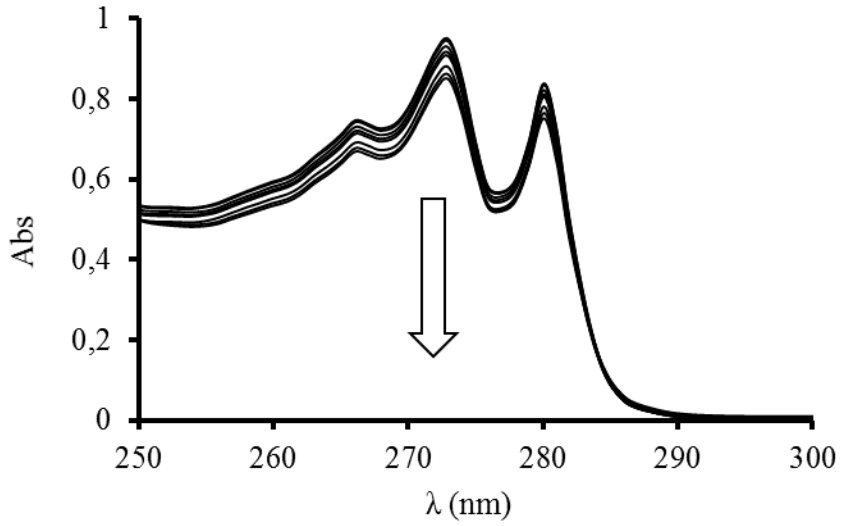

Figure 23: Titration of EB with $SiCl_4$. $C°_{EB}$=1.27 mM, total $SiCl_{4\,add}$>100 eq.

No significant changes in shift and/or intensity of the UV-Vis spectrophotometric band of donors were observed during titrations (the change in intensity visible in Figure 23 was due to a dilution of the initial EB solution), evidencing that silicon tetrachloride was unreactive towards IDs in the experimental conditions. UV-Vis spectrophotometric titrations of $MgCl_2$ and $TiCl_4$ with

$SiCl_4$ were unfeasible because, in addition to problems due to $TiCl_4$ reactivity (if present), the wavelengths at which silicon tetrachloride adsorbs are out of instrumental range (<190 nm).

Calorimetric titrations were therefore performed on $TiCl_4$ and $MgCl_2$ systems (Tronac): no heat was evolved thus indicating that no interaction occurred. As example, Figure 24 shows the instrumental calorimetric output of the titration of $SiCl_4$ with $TiCl_4$ (the signals correspondent to pre- and post-titration calibrations are also visible). The addition of titrant started at about 3000s (in correspondence of the small peak) and ended after about 20 minutes.

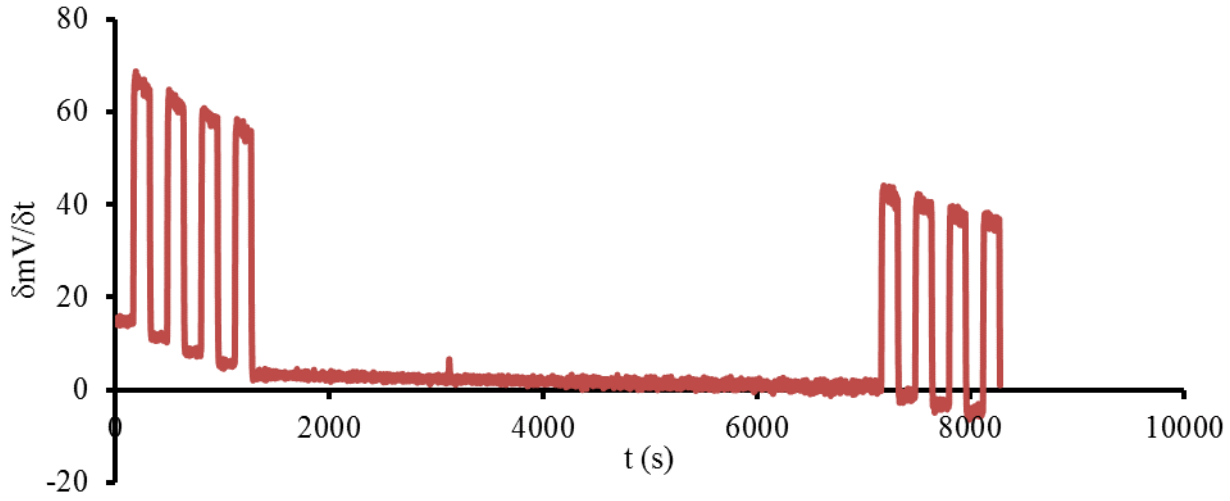

Figure 24: Calorimetric titration of $SiCl_4$ with $TiCl_4$. V_0=20mL, $C°_{SiCl4}$=16mM, 4 mL C_{TiCl4}=100mM.

Considering the experimental results, silicon tetrachloride resulted a potentially useful water scavenger because no reaction with any other component of the catalytic system was observed. Its efficiency as water scavenger is described in section 3.2.1 "Adsorption of TiCl4 on MgCl2".

3.1.2 Samples of magnesium chloride

Samples of $MgCl_2$ were provided by the University of Naples in amounts which ranged from 0.5 to 2 grams for each batch. The results provided by this work are part of a still unexplored field, therefore not all the batches were used to determine thermodynamic parameters, because some of them were employed for explorative experiments and characterization purposes. Table 10 shows how samples of physically activated $MgCl_2$ were used.

$MgCl_2$	BET analysis	Water content	$TiCl_4$	DEP	EB	Ti determination
A	x	-	x	-	-	-
B	x	-	x	x	-	-
C	-	x	-	-	-	-
D	-	x	-	-	-	-
E	x	x	x	x	-	-
F	x	x	x	-	-	-
G	x	-	-	x	-	-
H	-	-	-	x	x	-
I	-	-	-	-	x	-
J§	-	-	-	x	-	x

Table 10: Uses of $MgCl_2$ samples. § Co-milled $MgCl_2$-$TiCl_4$ sample.

Samples A and B were used for preliminary investigations (section 3.2.1.1 "Preliminary experiments (”). Samples C-F were used to investigate the water content of samples; in particular, with samples C and D the influence of the order of milling and drying in the preparative steps on the final water content was checked and therefore repeated with samples E and F, which were prepared with a more optimized procedure and also used for titration experiments. Samples G-J were finally prepared with an almost optimized synthetic procedure and used exclusively for titrations.

3.1.2.1 Morphology of $MgCl_2$ (Samples A,B,E-G)

Textural characteristics of several $MgCl_2$ samples were obtained by BET analysis trough adsorption of nitrogen at 77 K. In Table 11 the values of surface area, pore volume and pore size of the five different $MgCl_2$ samples analysed for this work are provided.

Sample	Surface Area ($m^2\ g^{-1}$)	Pore Volume ($cm^3\ g^{-1}$)	Pore size (Å)
A	57.8	0.471	326
B	44.0	-	-
E	64.6	0.292	181
F	65.6	0.322	196
G	52.8	0.434	329

Table 11: Results of BET analysis on physically activated $MgCl_2$ samples

Surface area, average pore volume and average pose size varied depending on the preparative conditions. Surface area was the most reproducible parameter with a standard deviation lower than 10% (57.0 $m^2\ g^{-1}$). Volume of pores is distributed in a larger relative range of values (average pore volume 0.380 $cm^3\ g^{-1}$, standard deviation 20%), while values of pore size strongly diverged. No clear relationship was established between the synthetic procedure and the results of morphological analysis.

3.1.2.2 Water content on $MgCl_2$ (samples C-F)

Karl-Fischer determinations of water content on $MgCl_2$ were performed on samples C-F. Every sample was titrated with both methodologies presented in the experimental section in order to detect both total and bulk water. The results of Karl-Fischer determinations are listed in Table 12.

Sample	Total water (% w/w)	Treatment: ($TiCl_4$, time)	Treated sample (bulk water % w/w)	Difference (surf. water % w/w)
C	0.95	1 eq, 10 min	0.62	0.33
		2 eq, 60 min	0.61	0.34
		4 eq, 150 min	0.57	0.38
D	2.35	1 eq, 10 min	2.00	0.35
		2 eq, 60 min	1.96	0.39
E	0.96	2 eq, 60 min	0.87	0.09
F	0.96	2 eq, 60 min	0.68	0.28

Table 12: Water content detected in $MgCl_2$ samples.

The treatment of $MgCl_2$ with $TiCl_4$ was found to be effective for the removal of water from the surface ("accessible" water). The process was almost complete in mild conditions (1 eq. $TiCl_4$, 10 min). Through the comparison of water contents in each samples before and after the treatment a residual amount of about 0.3-0.4 % w/w of water was detected, even after a more drastic treatment (more $TiCl_4$ and longer treatment time, samples C-D). Given the high reactivity of $TiCl_4$ with water, the result could be explained by the presence of water "un-accessible" to $TiCl_4$ in the experimental conditions. In this way, the water present in the original $MgCl_2$ sample (with no treatment) can be classified as "bulk" (un-accessible, 4^{th} column, treated sample) and "surface" (accessible, 5^{th} column, difference) water. The values obtained for batch D were close to those provided by the University of Naples about the same sample, where 0.3 % w/w water was detected by means of heterogeneous titration (determination of surface water) with trialkyl-aluminum compound. The "accessible" water was considered able to influence both calorimetric and UV-Vis spectrophotometric determinations of $TiCl_4$ and donors adsorption, and thus had to be removed. Although the diffusion of water form bulk to surface was possible, the process was supposed negligible in the experimental time scale (maximum 24 h in the case of calorimetric titrations with donors).

3.1.3 Solvents and solutions

Heptane, toluene and TCE were selected as possible solvents; hydrocarbons (both aliphatic and aromatic) were considered because often used during catalyst preparation[120], while TCE was previously used to investigate homogeneous $TiCl_4$-donors interactions[121,122]. Polar protic solvents such as ethanol, despite being sometimes used to prepare ZN pre-catalysts[56,58,59,123], were not considered because strongly hygroscopic and reactive towards both $MgCl_2$ and $TiCl_4$.

Heptane was found to be the best solvent because of the minimum reachable water content (Table 13) and its UV-Vis spectrophotometric properties: UV-Vis spectrophotometric adsorption band of *n*-heptane (cut-off around 200 nm) does not overlap the adsorption bands of $TiCl_4$ and donors, while toluene and TCE adsorption bands of adsorbents are partially overlapped with the that of solvent (cut-off around 280 nm). Figure 25 shows the UV-Vis spectra of internal donors and $TiCl_4$ in *n*-heptane; in the case of $TiCl_4$, spectra was quickly recorded on a very fresh solution in order to minimize the loss of $TiCl_4$ due to hydrolysis.

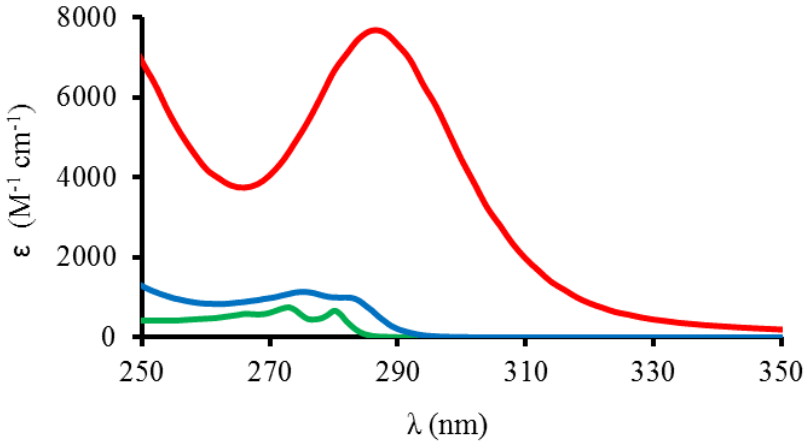

Figure 25: UV-Vis spectra of $TiCl_4$ (red), DEP (blue) and EB (green) in anhydrous *n*-heptane.

3.1.3.1 Water content in solvents

The water content in dry solvents was checked through Karl-Fischer titration. Table 13 shows the amount of water in the solvents after different drying procedures (reported in the experimental section). Water contents of the solvent as received and at equilibrium with water are

also inserted for comparison purposes; the determinations were repeated at least three times to check their consistency.

	n-heptane (mM)	Toluene (mM)	TCE (mM)
As received	0.75	3.11	3.81
H_2O sat.	1.60	23.37	90.5
$CaSO_4$	0.07	0.27	0.72
$MgSO_4$	0.63	7.12	23.8
CaH_2	0.12	n.d.	R
Na/Ph_2CO	0.13	n.d.	R
MS 4Å (three days)	0.09	6.41	3.6
MS 4Å (two weeks)	0.06	4.27	2.4

Table 13: Final water content of solvents anhydrified with different procedures. R= Reaction; n.d.=not detected.

Independently from the drying method used, the trend of water content found was TCE > toluene > *n*-heptane. Among all procedures, the treatment with MS was the most effective for water removal, but long a large amount MS was necessary to achieve complete drying. The combination of reflux over CaH_2 followed by distillation and condensation over activated MS was chosen as final drying procedure for aliphatic hydrocarbons. The procedure allowed a quick pre-drying of solvent (by CaH_2), followed by a slower but efficient anhydrification by MS[102], and allowed also the reaching of a minimum water content of 0.06 mM within two weeks.

3.1.3.2 $TiCl_4$ in different solvents

Solutions of titanium tetrachloride exhibit different behaviours depending on the solvent in which they are dissolved. The hydrolytic process leads to the formation of a very fine white

precipitate and takes place in a period ranging from hours to months. A brief description of behaviour of $TiCl_4$ solutions in different solvents is provided below.

n-Heptane: titanium tetrachloride is perfectly miscible with anhydrous n-heptane in all proportions. Concentrations ranging from 1 mM to 1000 mM were tested. Solutions with a concentration higher than 10 mM can be stored in glove box for months without any appreciable change of concentration. In fact, despite traces of water were inevitably present in the solvent (<0.1 mM), $TiCl_4$ concentration remained essentially constant because the amount of hydrolysed $TiCl_4$ was negligible. On the contrary, in more dilute solutions the concentrations of $TiCl_4$ and water were comparable and the effect of hydrolysis was marked. Figure 26 shows the UV-Vis spectra of dilute 0.22mM $TiCl_4$ solution collected immediately after the preparation (3 min, red) and within 8 and 23 minutes (blue and green respectively).

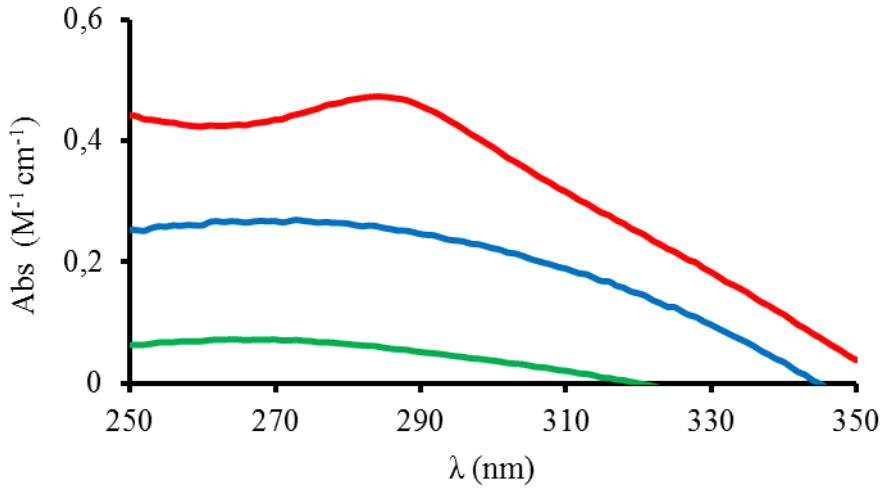

Figure 26: Time-evolution of 0.22 mM $TiCl_4$ solution in *n*-heptane (C_{H2O} < 0.1 mM).

The downturn of the adsorption band clearly indicated that dilute $TiCl_4$ solutions quickly reacted with residual water. The change of shape of the band during hydrolysis was rationalized considering, beside insoluble reaction products, the formation of partially hydrolyzed titanium species which may be partially soluble (e.g. $TiCl_3$-O-$TiCl_3$, given that water is the limiting reagent) and affect the spectra.

Toluene: titanium tetrachloride is easily soluble in anhydrous toluene. A range of concentrations up to 45 mM was tested. $TiCl_4$ solutions in toluene exhibit an intense yellow-orange colour (depending on concentration) due to the formation of sandwich charge-transfer complexes[124–126]. Titrations with $TiCl_4$ in toluene were unfeasible because of the almost complete cut-off in the UV region due to the adsorption band of the sandwich-complex. Freshly prepared solutions looked clear, with no turbidity, but hydrolysis products tend to precipitate in a period which ranges from few days to weeks, depending on concentration.

Tetrachloroethane (TCE): $TiCl_4$ is soluble in TCE; a range of concentrations up to 45 mM was observed. Freshly prepared solutions appeared colourless and clear but within 10-30 hours a tiny white hydrolysis product was settling on the bottom of the flask. Meanwhile, the solution changed its colour to dark brown.

3.1.3.3 Determination of $TiCl_4$ in solution

Quantitative determination of titanium concentration was mandatory for thermodynamic determinations. The hydrogen peroxide method (HPM), based on the formation of water soluble red titanium-peroxo complex, was developed as an alternative to direct determination (DD) for the quantification of metal. In fact, although titanium tetrachloride adsorbs in the accessible UV region of electromagnetic spectra (λ_{max}=290 nm) determinations by direct reading (DD) were abandoned after preliminary experiments because of problems during the manipulation of $TiCl_4$ solutions for UV-Vis spectrophotometric reading. Figure 27 shows the molar extinction coefficients of $TiCl_4$ and Ti-peroxo complex.

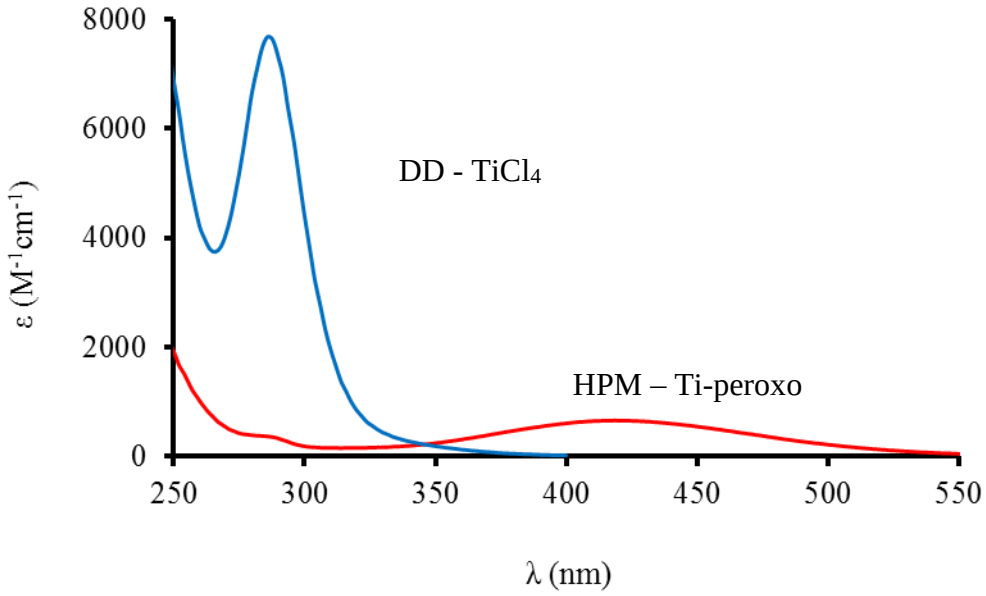

Figure 27: Molar adsorption coefficients of $TiCl_4$ in *n*-heptane (blue line) and Ti-peroxo complex in HCl 10% (red line).

Although the molar adsorption coefficient at λ_{max} of $TiCl_4$ in hydrocarbon (obtained by DD) was several times greater than the Ti-peroxo complex (by HPM) and the methodology simpler, direct determination of titanium was affected by several inconveniences:

(i) due to high extinction coefficient (ε) in hydrocarbons, the absorbance at λ_{max} was out of the instrumental range in experimental conditions. In preliminary experiments the reading of absorbance was performed in correspondence of a shoulder (330-340 nm), inevitably increasing the noise/signal ratio; the dilution of solutions was not possible because solvents inevitably introduced amounts of water with consequent hydrolysis of $TiCl_4$.

(ii) calibration line of $TiCl_4$ in hydrocarbon greatly deviates from linearity at concentrations lower than 4 mM (circles, Figure 28), when concentration of residual water became comparable with that of $TiCl_4$;

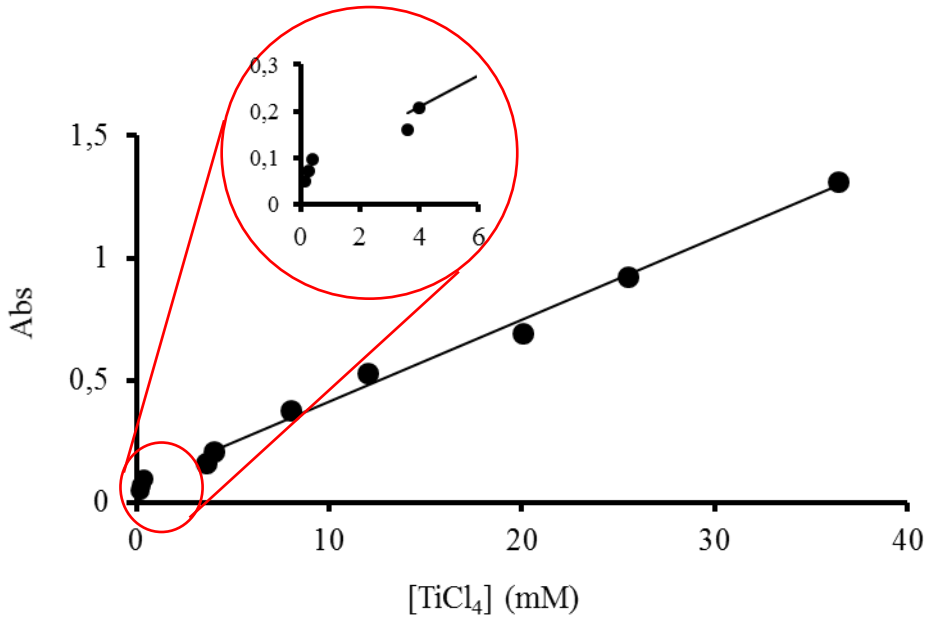

Figure 28: Calibration lines of $TiCl_4$ in *n*-heptane at 340 nm.

(iii) after a few readings a thin film of titanium dioxide stick on the inner walls of the cuvette, considerably increasing the noise/signal ratio going on with titration because of light scattering.

A comparison between the two methods is provided in Table 14. Although hydrogen peroxide method was more time consuming (procedure in paragraph 2.2.1.2.1), it was very useful for our purposes. The lower molar adsorption coefficient allowed readings to be performed in correspondence of the maximum of the band (see point (i)), and the aqueous environment allowed problems due to hydrolysis and light scattering to be avoided (see points (ii) and (iii)).

Method	$\varepsilon_{reading}$ (M^{-1} cm^{-1})	$\lambda_{reading}$ (nm)	calibration line (R^2)
DD	147	350 (shoulder)	0.9922
HPM	760	418 (max)	0.9998

Table 14: Comparison between DD and HPM.

3.1.4 Test for titration methodology (pyridine adsorption on silica)

The titration method was tested through the determination of thermodynamic parameters of adsorption of pyridine (Py) on silica in anhydrous cyclohexane (Cyc) according with Drago's methodology[112]. Such titration was chosen as a benchmark because it was performed with the same instruments (UV-Vis spectrophotometer and isoperibolic calorimeter), in very similar titration conditions (anhydrous hydrocarbon) as the ones used for Ziegler-Natta systems.

3.1.4.1 Gibbs free energy of adsorption

Several values of binding constant (K_{ads}) were obtained as a result of the data fitting of different adsorption models. The concentration of free pyridine ([Py]) after each addition, necessary to fit the data, was determined by means of a calibration line obtained by injections (nine in total) of pyridine solution to cyclohexane and by recording the UV-Vis spectra after each addition. Figure 29 shows the UV-Vis spectra used for the determination of the calibration line visible in the frame.

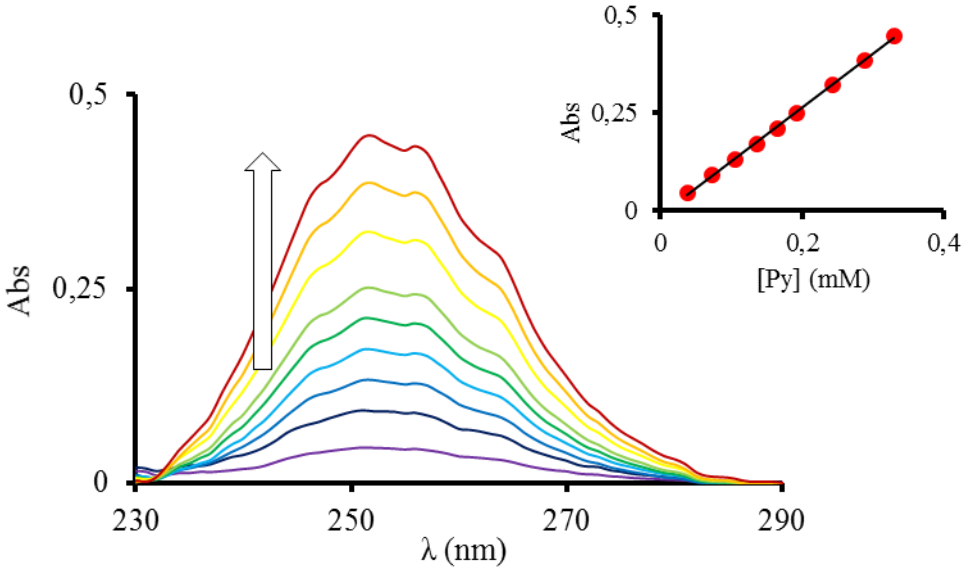

Figure 29: UV-Vis spectra of pyridine in the range 0.02-0.40 mM in anhydrous cyclohexane; frame: calibration line at $\lambda_{max.}$=252 nm.

Figure 30 shows the experimental titration points obtained for the titration of silica with pyridine in cyclohexane, together with the calculated adsorption isotherms. The aliquots of liquid phase collected after each addition were diluted with cyclohexane in order to achieve a concentration useful for determinations. The amount of pyridine on silica (Py_{ads}) was calculated from the difference between the total amount of pyridine in the solution and the total amount of pyridine added to it.

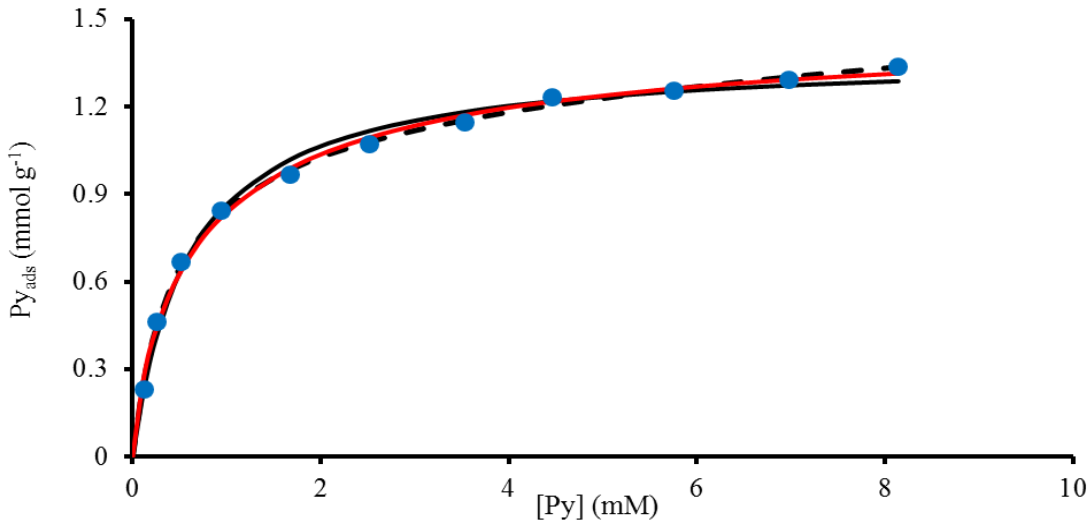

Figure 30: UV-Vis spectrophotometric adsorption isotherm of pyridine on silica in cyclohexane at 298 K. V_0= 20 mL, SiO_2 = 113.8 mg, C° Py =144 mM, 0.2mLx11 additions; black lines: Langmuir model (full line: one binding site; dot line: two binding sites); red line: Langmuir-Freundlich model.

Langmuir (with one and two binding sites) and Langmuir-Freundlich (LF) adsorption models were considered for the fitting of experimental data. Results of data fit are summarized in Table 15, together with those acquired from the literature. Loading values in the "literature" column were normalized for the surface area of samples to allow a better comparison (surface areas of silica: Drago: 590 m^2 g^{-1}, this work: 490 m^2 g^{-1}). In two-site Langmuir model subscripts L_A and L_B indicate different binding sites.

Model	Parameter	Literature[112]	This work
Langmuir1	n_{totL} (mmol g^{-1})	1.32	1.38 ± 0.03
	logK_{adsL}	3.43	3.24 ± 0.06
	ΔG_{adsL} (kJ mol^{-1})	-19.6	-18.4 ± 0.1
	adj R^2	-	0.990
Langmuir2	n_{L_A} (mmol g^{-1})	0.71	1.15 ± 0.11
	logK_{adsL_A}	4.23	3.38 ± 0.15
	ΔG_{adsL_A} (kJ mol^{-1})	-24.1	-19.3 ± 0.9
	n_{L_B} (mmol g^{-1})	0.71	0.79 ± 0.09
	logK_{adsL_B}	2.50	1.74 ± n.d.
	ΔG_{adsL_B} (kJ mol^{-1})	-14.3	-9.9 ± n.d.
	n_{tot} (mmol g^{-1})	1.42	1.94
	adj R^2	-	0.999
LF	n_{totLF} (mmol g^{-1})	-	1.50 ± 0.02
	logK_{adsLF}	-	3.12 ± 0.05
	ΔG_{adsLF} (kJ mol^{-1})	-	-17.8 ± 0.3
	m_{LF}	-	0.81
	adj R^2	-	0.995

Table 15: UV-Vis spectrophotometric results of fit for adsorption of pyridine on silica in anhydrous cyclohexane. n.d.: not determined

The values of logK_{adsL} and n_{tptL} obtained in this work by means of one-site Langmuir model are close to those reported in literature, with both parameters differing from Drago's values by less than 5%. The results obtained using LF model show greater deviations (both about 10%) of logK_{adsLF} and n_{totLF} compared to one-site Langmuir model, and a partially inhomogeneous surface according with $m_{LF}<1$. Despite slight differences, both one-site models led to almost the same value of Gibbs free energy of adsorption found in literature (-19.6 kJ mol^{-1}) using one-site Langmuir model.

Differences arose when two-site Langmuir model was used for comparison. Both in the literature and in the present work one of the two binding constants was found to be higher than the constant obtained fitting the data for the one-site model, while the other one resulted lower.

However, the literature indicates the presence of equal amounts of different binding sites with binding constants higher and lower than the constant obtained with one site model by about one order of magnitude ($\log K_{adsL\_A}$=4.23, $\log K_{adsL\_B}$=2.50), while in this work different amounts of different binding sites with binding constants lower than those reported in literature ($\log K_{adsL\_A}$ =3.38, $\log K_{adsL\_B}$=1.74) were found. Errors on $\log K_{adsL\_B}$ and n_{L_B} could not be calculated because of the limited number of experimental data points.

Considering the similarity of results obtained with the one-site model and the complexity of the heterogeneous systems in general, the methodology resulted useful to perform UV-Vis adsorption experiments and obtain the Gibbs free energy(s) of adsorption.

3.1.4.2 Enthalpy of adsorption

The enthalpy of adsorption of pyridine on silica was obtained through calorimetric titrations by means of TAM III nanocalorimeter at 298 K by stepwise addition of pyridine solution to stirred suspended SiO_2. Figure 31 shows the calorimetric outputs of two titrations; the experiments were performed in the same experimental conditions (amount of silica, volume of cyclohexane and pyridine concentration) except for the stirring rate (red, 150 and blue, 200 rpm), with the aim of obtaining information also on the effect of stirring on calorimetric signal.

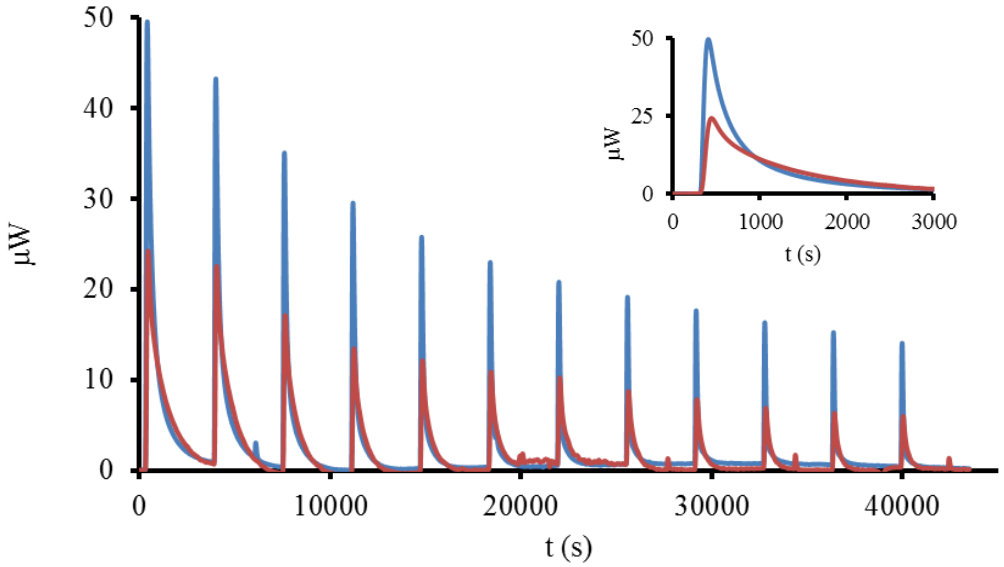

Figure 31: Calorimetric titration of SiO_2 with pyridine in anhydrous cyclohexane (instrumental output); SiO_2 = 4.3mg (blue), 4.1mg (red), V_{tot}= 0.8mL, C_{Py} = 50 mM; 0.016 mLx11 additions in both titrations; blue line: 200 rpm; red line: 150 rpm. Frame: enlargement of first peak

Adsorption of pyridine on silica in cyclohexane is exothermic and faster in correspondence of higher stirring rates, as visible in the frame of Figure 31: the calorimetric peak correspondent to 200 rpm (first peak) decreases sharply (the higher the stirring rate, the faster the adsorption). The graph in Figure 32 plots the cumulative heat obtained for both titrations against the volume of titrant added.

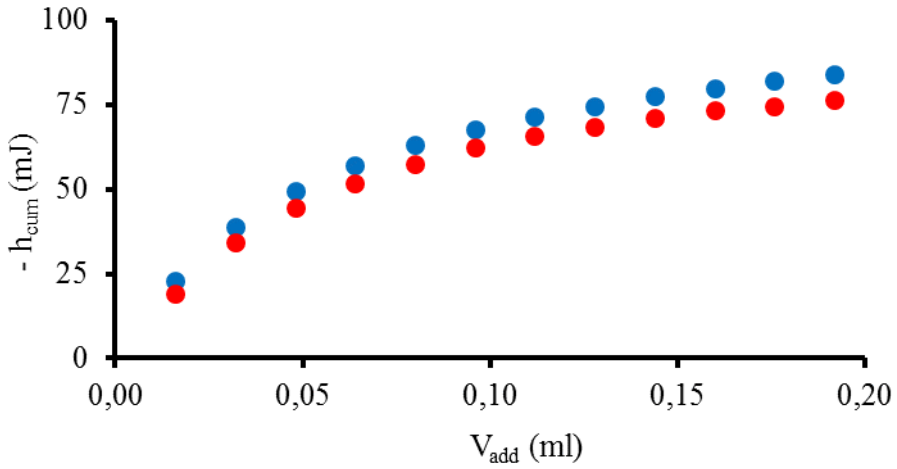

Figure 32: Cumulative titration heat of SiO_2 with pyridine on SiO_2. Same experimental conditions of previous figure; blue: 200 rpm; red 150 rpm.

Data at 200 rpm were used for calculations of enthalpy because calorimetric signals were more defined and easier to integrate. The calorimetric adsorption isotherms of pyridine at 200 rpm are visible in Figure 33; the concentrations of pyridine correspondent to each addition (mandatory for the fit) were calculated using the values of loading and binding constant obtained through UV-Vis spectrophotometric determinations using the same adsorption model. As visible in Figure 33, all models resulted in almost the same adsorption isotherms; the results of fitting of enthalpy are inserted in Table 16.

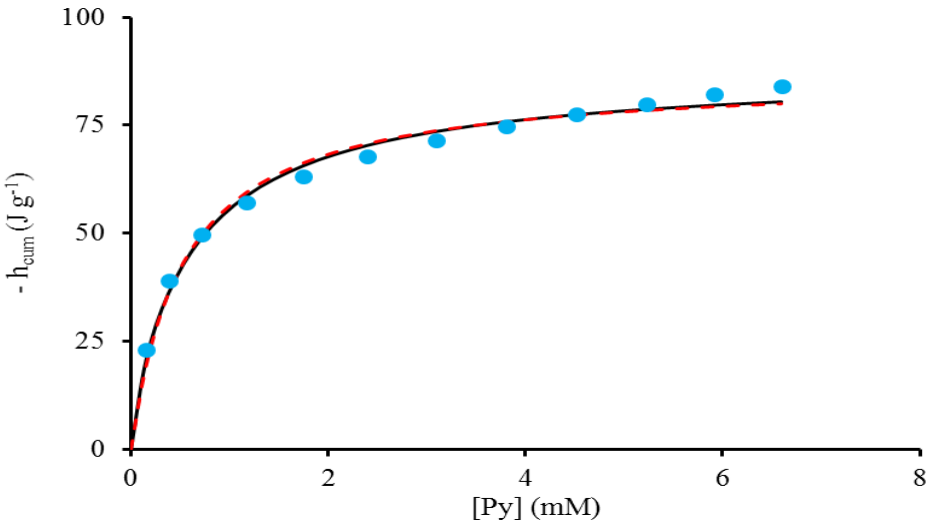

Figure 33: Calorimetric adsorption isotherm (full black line: one-site Langmuir model; dot red line: Langmuir-Freundlich model) of pyridine on silica at 200 rpm. Same experimental conditions as Figure 31.

Model	Parameter	Literature[112]	This work
Langmuir1	ΔH_{adsL} (kJ mol^{-1})	n.r.	-27.1±1.3
	adj R^2	n.r.	0.990
Langmuir2	ΔH_{adsL_A} (kJ mol^{-1})	-52.7	-34.1±1.3
	ΔH_{adsL_B} (kJ mol^{-1})	-22.2	-12.3±2.2
	adj R^2	n.r.	0.996
LF	ΔH_{adsLF} (kJ mol^{-1})	n.r.	-28.9±1.2
	adj R^2	n.r.	0.995

Table 16: Results of fitting for calorimetric titration of pyridine on silica in anhydrous cyclohexane. n.r.: not reported.

The experimental value of ΔH_{adsL} obtained by one-site Langmuir model was not comparable with Drago's data because the author found that "one binding site model was incompatible with both calorimetric and spectrophotometric data" and results were not reported. The results of fitting considering two binding sites led to different values of enthalpy, but the absence of detailed

information about the surface of silica did not allow the rationalization of the difference. It must be underlined that the results of fitting of calorimetric experiments are closely related to UV-Vis results, thus errors on parameters obtained through UV-Vis determinations (especially in the amount of binding sites) may greatly affect the values of enthalpy obtained through fitting.

Nevertheless, considering the aim of the titration (to test the working procedure), the methodology is suitable for calorimetric titrations of heterogeneous systems in anhydrous conditions.

3.2 Two component systems ($MgCl_2$-$TiCl_4$ and $MgCl_2$-IDs)

The binary systems $MgCl_2$-adsorbent ($TiCl_4$ or IDs) are described in this section. For each adsorbent, UV-Vis spectrophotometric experiments are first commented and followed by calorimetric ones. This sequence was chosen because UV-Vis spectrophotometric results are mandatory to calculate the amount of titrant adsorbed during calorimetric titrations and thus to determine the adsorption enthalpy. After the experimental results, the comparison with DFT results obtained by University of Naples is provided.

3.2.1 Adsorption of $TiCl_4$ on $MgCl_2$

Adsorption of $TiCl_4$ on activated $MgCl_2$ was studied with the same methodology described for the titration of silica with pyridine. This section starts with a sub-section named “preliminary experiments”, where the results of early investigations on $TiCl_4$ adsorption are described, along with the related problems and the solutions adopted. In successive sections, the results of optimized procedures are provided.

3.2.1.1 Preliminary experiments (samples A,B)

Single addition experiments

The first preliminary UV-Vis spectrophotometric and calorimetric experiments were carried out through a single large addition of $TiCl_4$ to stirred suspensions of $MgCl_2$ with the aim to check the intensity of the signals. UV-Vis spectrophotometric changes were monitored by direct

determination (DD) of titanium, performed by reading the absorbance in correspondence of the shoulder of band (340 nm).

UV-Vis spectrophotometric and calorimetric preliminary data were indicative of low loading of $TiCl_4$ on $MgCl_2$ and slightly exothermic process. This evidenced the need to increase the reagents amounts in the following experiment in order to avoid noisy signals, especially in calorimetric titrations.

Stepwise addition experiments

The information obtained from single addition experiments was therefore used to plan stepwise titrations; the amounts of $MgCl_2$ were increased in order to better monitor changes between total and adsorbed $TiCl_4$ (UV-Vis) and to enhance calorimetric signals.

The quantification of titanium through UV-Vis spectrophotometry was still performed by direct reading of the absorbance of solution. The experimental points of stepwise titrations (samples A and B) and the related adsorption isotherms obtained by Langmuir and Langmuir-Freundlich models are illustrated in Figure 34, and the values of loading and binding constant obtained are written in Table 17.

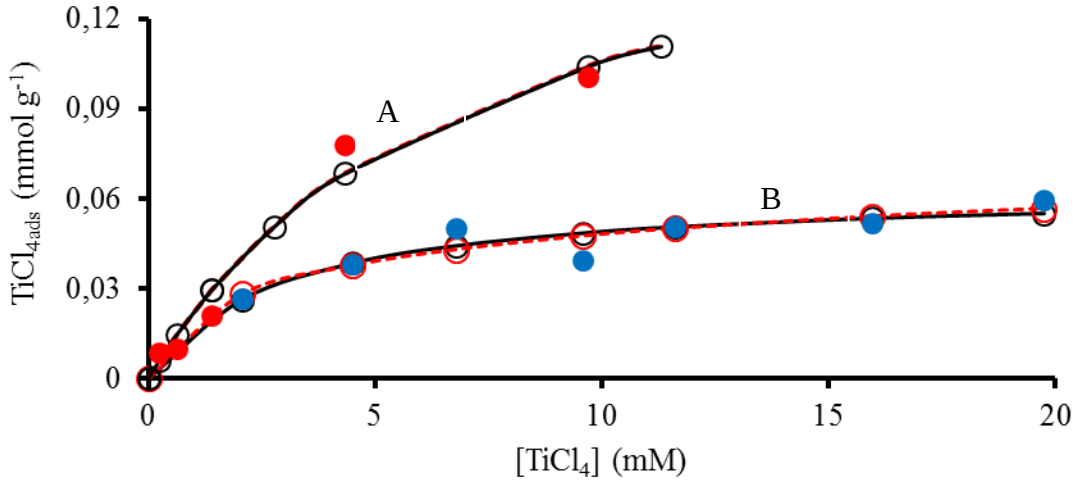

Figure 34: Experimental points and adsorption isotherms for titrations of $MgCl_2$ with $TiCl_4$. A: red, $MgCl_2$=180mg, V_0=15 mL, C_{TiCl4}=100 mM, 5x0.05-0.1 mL additions; B: blue: $MgCl_2$=320 mg, V_0=10 mL, C_{TiCl4}=100 mM, 7x0.3 mL additions. Dots: experimental points; full black lines: one-site Langmuir model fit; red dot line: Langmuir-Freundlich fit.

Model	Parameter	A	B	Average*
Langmuir1	n_{totL} (mmol g^{-1})	0.18 ± 0.03	0.06 ± 0.0	0.12±0.78
	logK_{adsL}	2.15 ± 0.33	2.54 ± 0.3	2.35±0.28
	ΔG_{adsL}	-12.3 ± 1.9	-14.5 ± 2.(	-13.4±1.6
	adj R^2	0.969	0.778	-
LF	n_{totLF} (mmol g^{-1})	0.18 ± 0.03	0.19 ± 0.0	0.14±0.62
	logK_{adsLF}	2.15 ± 0.33	2.14 ± 0.0(	2.15±0.19
	ΔG_{adsLF}	-12.3 ± 1.9	-12.2 ± 0.3	-12.3±1.1
	m_{LF}	0.999	0.951	-
	adj R^2	0.971	0.792	-

Table 17: Fitting of UV-Vis adsorption of $TiCl_4$ on A and B samples (preliminary experiments).

Both $MgCl_2$ samples weakly interacted with $TiCl_4$, with average logK_{ads} of 2.35±0.28 (ΔG_{adsL} =-13.4±1.6 kJ mol^{-1}) and 2.15±0.19 (ΔG_{adsLF} =-12.3±1.1 kJ mol^{-1}) for one-site Langmuir and Langmuir Freundlich models respectively. Other models were considered for the description of the adsorption process, but they led essentially to the same results of the one-site Langmuir model; fit by two-sites Langmuir model resulted in different amounts of sites with almost the same binding constants (e.g. logK_{ads_A}=2.14 and logK_{ads_B}=2.15 for sample A), while Fowler-Guggenheim model yielded un-reasonable results about lateral interaction. The loading of $TiCl_4$ on samples A and B was very different; sample A was able to load about three times the amount of titanium loaded by sample B, despite the difference in surface area was not so large (57.8 and 44 m^2 g^{-1} for samples A and B respectively). The difference in maximum loading clearly indicated that, besides the surface area, it is dependent also on other parameters (morphology) and thus on the preparation of samples (Table 8).

Calorimetric titrations were performed on B sample at 298 K through a stepwise addition of $TiCl_4$ solution to a stirred suspension of $MgCl_2$. The data acquisition software of isoperibolic Tronac calorimeter was expressly developed to perform stepwise titrations of heterogeneous systems; the "stepwise" mode allowed the control of the delay time between consecutive additions in order to study the relatively slow processes of adsorption of a solute. Calorimetric experiments show in all cases a first, high calorimetric peak followed by lower signals (Figure 35); depending on experimental conditions, the heat evolved with the first addition of $TiCl_4$ can be up to one order of magnitude greater than the heat detected during further additions (Figure 35, frame; second addition around 200s).

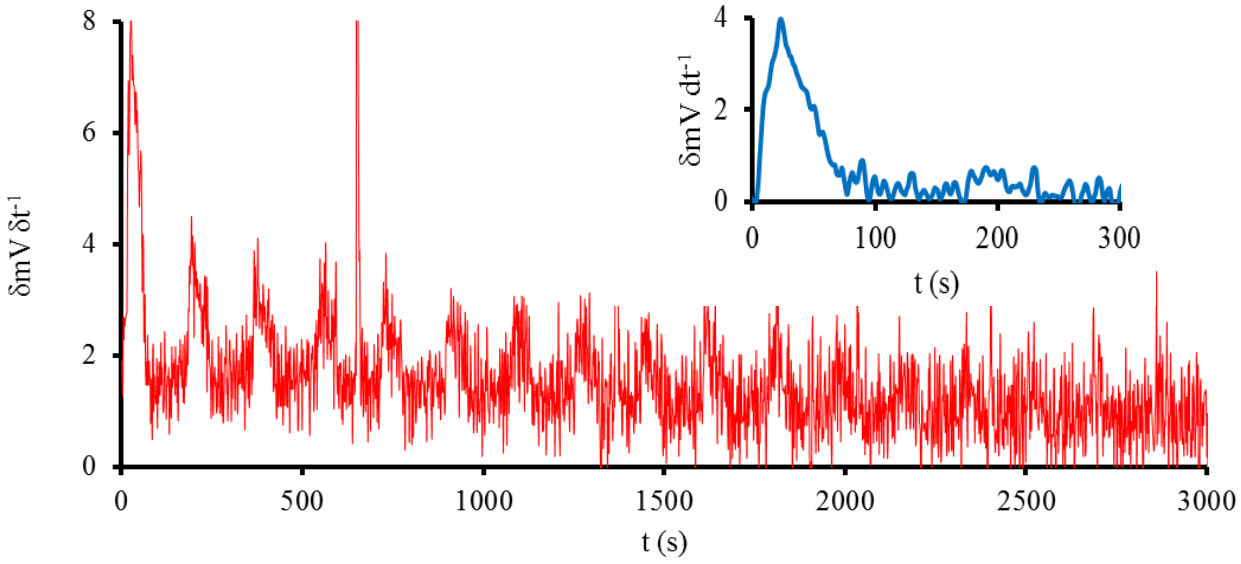

Figure 35: Calorimetric titration of sample B with $TiCl_4$ (no $SiCl_4$ as water scavenger): $MgCl_2$=160 mg, V_0=20 mL, C_{TiCl4}=100 mM, 0.2mL x18 additions.

The intensity of the first peak was attributed to the hydrolysis of water present in the $MgCl_2$ sample or in the calorimetric titration system (e.g. walls of cell, solvent). Until molecules of water (accessible to $TiCl_4$) were present inside the titration apparatus, $TiCl_4$ acted as a water scavenger in a very exothermic reaction. Experiments also showed that after the first addition $TiCl_4$ was enough to chemically remove "accessible" water inside the calorimetric apparatus, allowing the calculation of a maximum water content lower than 1% w/w (supposing complete hydrolysis of $TiCl_4$), higher but consistent with contents successively detected (samples C-F, Table 12).

The loading capacity and the binding constant obtained through UV-Vis spectrophotometric determinations were used to calculate the amount of $TiCl_4$ adsorbed after each addition. An enthalpy of adsorption slightly lower than -20 kJ mol^{-1} was estimated from the ratio between heat evolved and amount of $TiCl_4$ adsorbed considering additions 2-4 in Figure 35. High experimental uncertainties were associated to the data because of a high signal-to-noise ratio, but, on the whole, a slightly exothermic process was confirmed for $TiCl_4$-$MgCl_2$ interaction.

From preliminary experiments the need to improve titration methodologies in both UV-Vis spectrophotometric and calorimetric determinations emerged; apart from the removal of water from the systems, a better determination of $TiCl_4$ concentration during UV-Vis spectrophotometric was necessary in order to obtain less scattered data-points (for improvement of adj. R^2, Table 17). The titration methodology started to be improved with sample E (after an in-depth study on the water content in samples C-D); silicon tetrachloride was added as a water scavenger to a $MgCl_2$/hydrocarbon suspension prior to all experiments, while the hydrogen peroxide method (HPM) was used to determine the concentration of free titanium. Moreover, the amount of $MgCl_2$ used in the experiments was further increased. Typically, 100-500 mg of magnesium chloride were used for UV-Vis spectrophotometric titrations, while calorimetric experiments required 500-800 mg. Due to the relatively small amounts of $MgCl_2$ provided for each batch (800-2000 mg), the number of titrations performed for every sample was limited.

3.2.1.2 Gibbs free energy of adsorption of $TiCl_4$ (samples E, F)

UV-Vis spectrophotometric titrations performed in *n*-heptane with optimized methodology led to well–defined UV-Vis spectra and more accurate adsorption isotherms compared to the preliminary experiments, according with the higher values of adj R^2 obtained (>0.99, Table 18). In Figure 36 the experimental points and the adsorption isotherms calculated through the one-site Langmuir model of samples E and F are depicted (full lines, sample F was titrated twice) together with the adsorption isotherm obtained by simultaneous fit of whole data-points of sample F (dotted line, F_exp1+F_exp2).

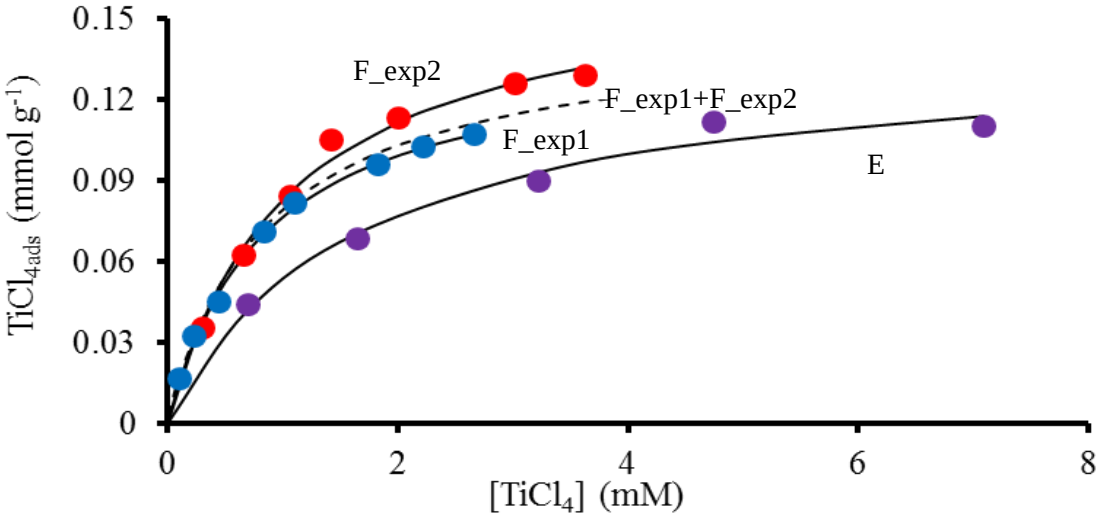

Figure 36: Langmuir adsorption isotherms of $TiCl_4$ on $SiCl_4$ pre-treated $MgCl_2$ samples. E: purple, $MgCl_2$=215mg, V_0=15 mL, C_{TiCl4}=100 mM, 0.2-0.3mL x5 additions F_exp1: blue, $MgCl_2$=529mg, V_0=15 mL, C_{TiCl4}=200 mM, 10x0.05 mL additions; F_exp2: red, $MgCl_2$=417mg, V_0=20 mL, C_{TiCl4}=200 mM, 0.02-0.04 mL x7 additions. Dots: experimental points; full black lines: one-site Langmuir model fit; black dot line: F_exp1 and F_exp2 fit together (one-site Langmuir fit).

In Table 18 the results of best fit are shown. For sample F, in addition to results relative to individual titrations, the parameters obtained by simultaneous fit of both experiments (F_exp1+F_exp2) and the average of the whole experiments are listed for comparison purposes.

Model	Parameter	E	F_exp1	F_exp2	F_exp1+F_exp2	Average*
Lang.	n_{totL}(mmol g^{-1})	0.140±0.008	0.141±0.003	0.171±0.006	0.16±0.01	0.15±0.02
	logK_{adsL}	2.79±0.18	3.07±0.05	2.94±0.10	2.98±0.07	2.94±0.13
	ΔG_{adsL}(kJ mol^{-1})	-15.9±1.0	-17.5±0.3	-16.9±0.6	-17.0±0.4	-16.8±0.7
	adj R^2	0.997	0.999	0.998	-	-
LF	n_{totLF}(mmol g^{-1})	0.144±0.008	0.141± 0.002	0.171±0.006	0.16±0.02	0.14±0.03
	logK_{adsLF}	2.76±0.05	3.07±0.05	2.94±0.10	2.98 ± 0.10	2.92±0.14
	ΔG_{adsLF}(kJ mol^{-1})	-15.6±0.3	-17.5±0.3	-16.9±0.6	-17.0±0.6	-16.7±0.8
	m_{LF}	0.958	1	1	-	-
	adj R^2	0.998	0.999	0.998	-	-

Table 18: UV-Vis spectrophotometric results of fit for adsorption of $TiCl_4$ on $MgCl_2$ at 298 K (optimized titration methodology). *calculation of errors based on simultaneous fit of experimental points with logK_{ads}=average.

The loading is more homogeneous compared to the preliminary experiments, ranging from 0.14 to 0.17 mmol g^{-1} (Table 18), while binding constants are higher than those found previously (Table 17), independently from the sample and model considered. The values used for discussion are pertinent to the simpler Langmuir adsorption model. The values of binding constants relative to the adsorption of $TiCl_4$ on different $MgCl_2$ samples indicate a weak interaction with an average Gibbs free energy of adsorption of -16.8±0.7 kJ mol^{-1}.

When other models (e.g. two-sites Langmuir, Fowler–Guggenheim models) were used to describe adsorption, scenarios were similar to those previously described and no significant improvement of fit was registered, in particular with sample F.

3.2.1.3 Enthalpy of adsorption of $TiCl_4$ (sample F)

The UV-Vis spectrophotometric results of E and F samples were similar, therefore the calorimetric study was carried out focusing on sample F, which was prepared in large quantity for calorimetric purposes. Silicon tetrachloride (>50 eq.) was added as a water scavenger in the calorimetric vessel prior to titration with $TiCl_4$. As mentioned, due to the low heat of adsorption, larger amounts of sample were used to enhance the calorimetric signal and decrease the signal-to-noise ratio. In Figure 37 the instrumental output relative to the titration of sample F with titanium tetrachloride in presence of $SiCl_4$ is depicted as an example.

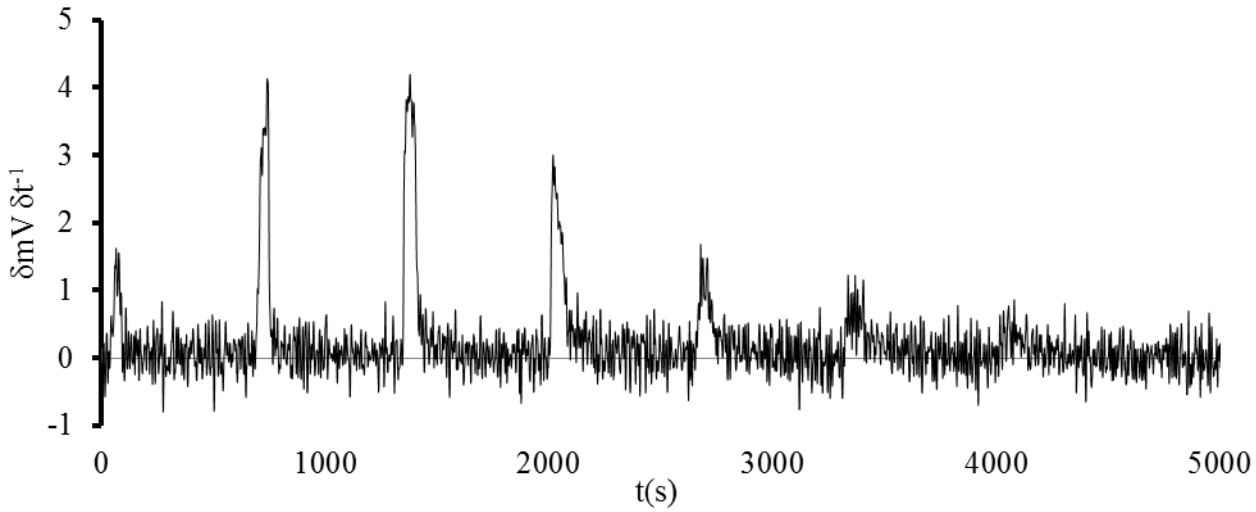

Figure 37: Instrumental calorimetric output of titration of sample F: $MgCl_2$=683mg, $SiCl_4$>50eq. (water scavenger), V_0=20 mL, C_{TiCl4}=54 mM, 0.2mLx7 additions shown.

The efficiency of $SiCl_4$ in the removal of "accessible" water is evident considering the first peak of the thermogram. In absence of $SiCl_4$ the first peak was several times higher than the successive ones (Figure 35) because, besides the heat of adsorption, extra heat was provided by reactions of hydrolysis. The intensity of the first peak in Figure 37 is thus a good indication that water "accessible" to $TiCl_4$ was completely removed by $SiCl_4$ pre-treatment. The intensity of the first peak was lower than the intensity of the second because the capillary connecting the syringe to the titration cell is always not completely filled in order to avoid pre-mixing of reactants before the beginning of the experiment. In fact, pre-mixing may take place during pre-calibrations in case of excessive temperature changes (thermal expansion of solvent). The consecutive peaks

corresponding to the different additions of titrant show that the released heat decreases with the progress of the experiment and indicates that $TiCl_4$ adsorption decreases to zero at the end. Figure 38 shows two calorimetric titrations on sample F, as the cumulative heat exchanged (h_{cum}) as a function of the total amount of $TiCl_4$ added ($TiCl_{4\ add}$) normalized to the weight of $MgCl_2$. The value of cumulative heat reached a plateau before the value of 0.14-0.17 mmol g^{-1} (Table 18), clearly indicates a lower loading than expected. Despite great care used in sample manipulation and preservation, the trend was observed with all aged samples and the decreased loading was explained by supposing an uptake of the traces of water during the manipulation.

The loading of sample in each calorimetric titration was determined through the projection of crossing points of red and blue straight lines (evidenced by circles) on the *x*-axis. The almost horizontal straight lines were extrapolated from the points of the plateau (correspondents to additions without an evolution of heat when the total loading was reached), while the oblique straight lines were obtained from the first titration points (when calorimetric signals are well-defined and $TiCl_4$ is mostly adsorbed). The so obtained loadings were slightly conditioned by the points used for their determination, but always resulted in the range 0.070-0.076 mmol g^{-1}.

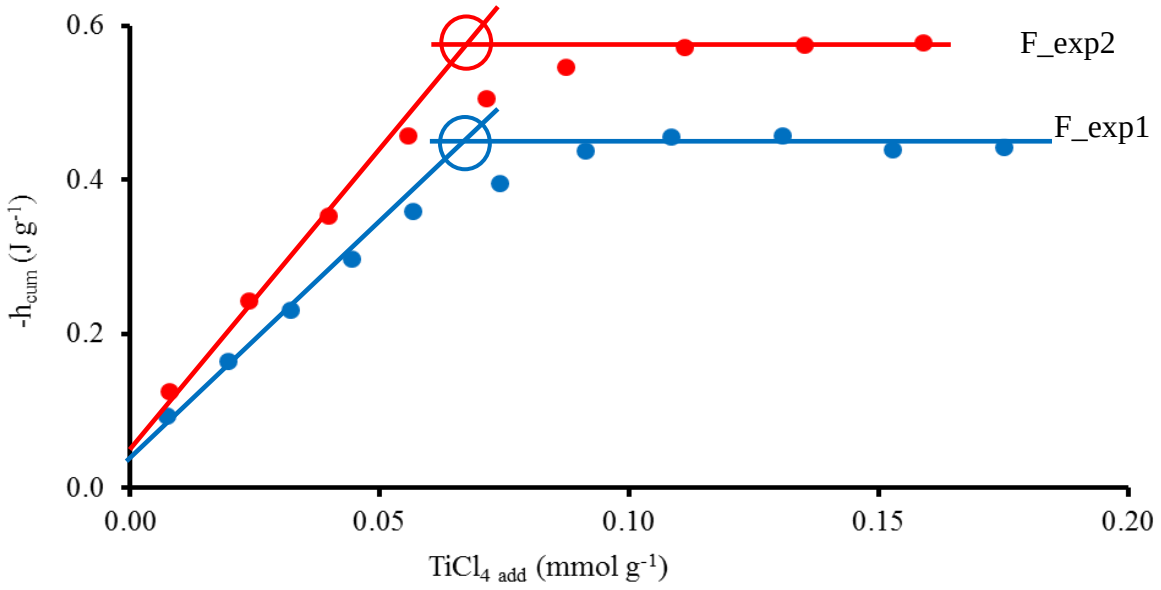

Figure 38: Stepwise calorimetric titrations of sample F (two titrations); F_exp1: blue: $MgCl_2$=740mg, V_0=20 mL, C_{TiCl4}=36 mM, 11x0.2mL additions; F_exp2: red: $MgCl_2$=683mg, V_0=20 mL, C_{TiCl4}=54 mM, 9x0.2 mL additions.

The value of logK_{adsL}=2.98 (Table 18, column F_exp1+F_exp2) and the loadings extrapolated by calorimetric experiments (0.072 and 0.074 mmol g^{-1} for F_exp2 and F_exp1 respectively) were used for the calculation of the concentration of "free" $TiCl_4$ after each addition and remained constant in the fitting of enthalpy of adsorption. Only the data-points correspondent to well-defined calorimetric peaks (4-6 points) were used for fitting.

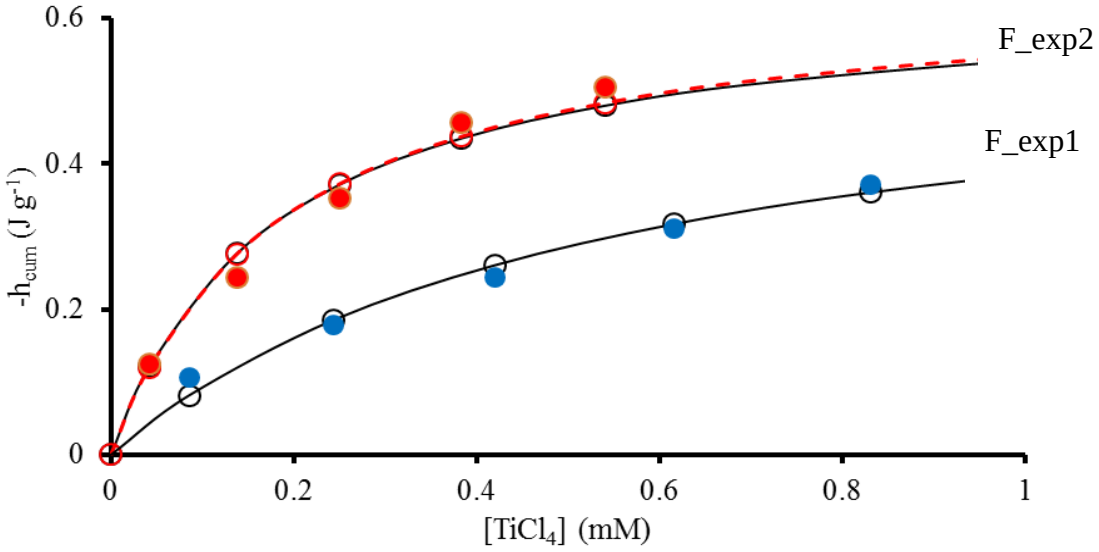

Figure 39: Calorimetric adsorption isotherms of $TiCl_4$ on $MgCl_2$ in n-heptane (sample F, two titrations). Same experimental conditions reported in the previous Figure. Dots: experimental points; full black lines: one-site Langmuir model fit; red dot line: Langmuir-Freundlich fit.

The adsorption isotherms illustrated in Figure 39 were calculated by means of five titration points. The parameters fitted by Langmuir model are reported in Table 19. As in the case of UV-Vis, the values obtained by simultaneous fitting of both experiments and the average are provided (column F_exp1+F_exp2) together with the values relative to single experiments.

	Parameter	F_exp1	F_exp2	F_exp1+F_exp2	Average*
Langmuir	n_{totL} (mmol g^{-1})	0.074	0.072	-	0.073
	ΔH_{adsL} (kJ mol^{-1})	-11.4±0.9	-13.4±0.9	-12.3±1.3	-12.4±1.8
	adj R^2	0.997	0.998	-	-

Table 19: Results of fit by of calorimetric adsorption isotherms of $TiCl_4$ on $MgCl_2$. *calculation of errors based on simultaneous fit of experimental points with logK_{ads}=average.

Since fitting of UV-Vis spectrophotometric data was not improved using other models (e.g. Table 18, m_{LF}=1 for sample F; Langmuir-Freundlich model resembles Langmuir's, thus results do not need to be indicated), Langmuir adsorption model was the only one used to describe the calorimetric data, providing a good description of the process (adj R^2>0.997). The average enthalpy of adsorption of $TiCl_4$ on $MgCl_2$ was ΔH_{adsL} = -12.4±1.8 kJ mol^{-1}.

The study of the effect of the number of points used for the fit on ΔH_{adsL} (Table 20) together with the calculation of enthalpy of adsorption at infinite dilution also points to values close to those indicated in Table 18. The results obtained using a different amount of data-points (among those that led to a clear calorimetric signal) for F_exp1 and F_exp2 are summarized in Table 20, while Figure 40 plots the partial molar enthalpy of adsorption (parΔH_{ads}, correspondent to the ratio between partial heat evolved after each addition and partial amount of titrant adsorbed) against the amount of titrant added.

			N° of fitting data-points				
			6	*5*	*4*	*3*	*2*
	n_{tot} (mmol g^{-1})	logK_{adsL}	ΔH_{adsL} (kJ mol^{-1})				
F_exp1	0.074	2.98	*-10.7*	*-11.4*	*-11.8*	*-13.1*	*-14.4*
F_exp2	0.072	2.98	*-12.9*	*-13.4*	*-14.1*	*-14.5*	*-15.6*

Table 20: Fitting of ΔH_{adsL} considering different number of data-points.

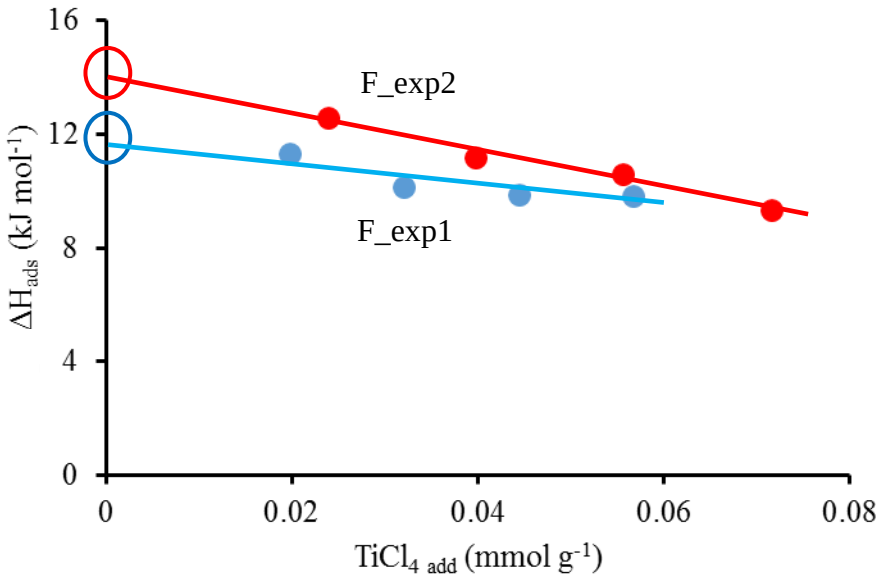

Figure 40: Partial enthalpy of adsorption of $TiCl_4$ on $MgCl_2$. Blue: F_exp1; red: F_exp2; enthalpy at infinite dilution evidenced by circles.

The enthalpy of adsorption at infinite dilution was obtained by the intercept of the straight lines obtained by linear regression of data. The points correspondent to additions 2-5 were used to calculate the value of intercept; the first points were not included in the fit because they fell outside the straight line formed by the others. The so determined enthalpy of adsorption was -11.7 and -14 kJ mol^{-1} for F_exp1 and F_exp2 respectively, very close to the values reported in Table 19. In conclusion, the adsorption of $TiCl_4$ on $MgCl_2$ from hydrocarbon solution was confirmed to be a weak, exothermic process (slightly negative ΔH_{adsL} and $\log K_{adsL}$~3). None of the calorimetric titrations revealed enthalpies of adsorption more negative than -20 kJ mol^{-1}. The values of ΔG_{adsL}=-16.8±0.7 (Table 18) and ΔH_{adsL} = -12.4 ± 1.8 kJ mol^{-1} (Table 19) will be used in the next part of discussion.

3.2.1.4 Entropy of adsorption of $TiCl_4$

The entropic term of the process at 298 K calculated from the values of Gibbs free energy and enthalpy of adsorption (ΔG_{adsL}=-16.8±0.7, ΔH_{adsL} = -12.4 ± 1.8 kJ mol^{-1}) is $T\Delta S_{ads}$=+4.4 kJ mol^{-1} in *n*-heptane. The slightly positive ΔS_{ads} favoring the adsorption process is rather unexpected, since a reagent ($TiCl_4$) loses translational/rotational degrees of freedom after binding on surface.

The effect of the solvent was taken into consideration to rationalize the almost zero entropy. The basic idea is that (i) desorption of solvent molecules weakly adsorbed on $MgCl_2$ surface upon competition with $TiCl_4$ may partially compensate the loss of entropy of $TiCl_4$ and (ii) adsorption of titanium tetrachloride liberates free volume in the bulk of the solvent, allowing a solvent reorganization and thereby increasing the total entropy. The overall entropy is the sum of all the individual contributions (adsorption of $TiCl_4$, desorption and reorganization of solvent), which, however, are very difficult to estimate individually.

Experiments were thus repeated in cyclohexane, based on the idea that a shift from a conformationally flexible linear alkane (*n*- heptane) to a more constrained solvent (cyclohexane) should give hints on the entropy changes in the adsorption process; in fact, cyclohexane has a lower conformational entropy and therefore its desorption from the surface should yield a smaller solvent reorganization upon $TiCl_4$ capture and thus a more negative value of $T\Delta S_{ads}$ for the overall process.

Spectrophotometric and calorimetric experiments in cyclohexane supported such hypothesis. Gibbs free energies of adsorption were essentially the same in both solvents (ΔG_{ads} =-16.8±0.7 and -16.2±0.5 kJ mol^{-1} in *n*-heptane and in cyclohexane respectively, Table 21), but the adsorption enthalpy was slightly more negative than in *n*-heptane (ΔH_{adsL}=-14.7±1.9 and -12.4±1.8 kJ mol^{-1} in cyclohexane and heptane respectively). Thus, the whole process in cyclohexane ($T\Delta S_{adsL\ Hept}$=+4.4 kJ mol^{-1} and $T\Delta S_{adsL\ Cyc}$ = +1.5 kJ mol^{-1}) was less entropy favored than that in *n*-heptane.

	ΔG_{adsL} (Average) (kJ mol^{-1})	ΔH_{adsL} (Average) (kJ mol^{-1})	$T\Delta S_{adsL}$ (kJ mol^{-1})
n-heptane	-16.8±0.7	-12.4±1.8	+4.4
cyclohexane	-16.2±0.5	-14.7±1.9	+1.5

Table 21: Entropy of adsorption in *n*-heptane and cyclohexane of $TiCl_4$ on $MgCl_2$.

The small, yet measurable, effect of the solvent supported the proposed hypothesis of "solvent effect", bur not fully explained the "nearly-zero" entropy of adsorption. Very recently[127], solid state ^{1}H-NMR studies on anhydrous $MgCl_2$ performed by other research groups belonging to Dutch Polymer Institute (DPI) revealed the presence of acidic protons on the surface of $MgCl_2$

even after strong treatments for water removal. In that study, samples of physically activated $MgCl_2$ prepared by the University of Naples were treated against water in several ways. Thermal (heating at 523 K under flux of dry gas) and chemical (addition of $SiCl_4$ at ~330 K) treatments and a combination of both were used for this purpose. ^{1}H-NMR analysis, independently from the treatment of sample, revealed an amount of surface water which ranged from 1 to 5% mol_{H2O}/mol_{MgCl2} present in form of both hydroxide groups and "water". The experiments demonstrated ubiquity of water and that its removal from $MgCl_2$ is very difficult and thus, complete removal was not achieved by $SiCl_4$ treatment during the titrations in the already mentioned experimental conditions.

The way in which surface-water interacts with $TiCl_4$ is unknown, and even computational calculations are lacking. However, the presence of residual water after $SiCl_4$ pre-treatment partially rationalizes the almost neutral entropy of adsorption found. In fact, it is plausible that the more reactive $TiCl_4$ was able to react (at least partially) with water molecules escaped to pre-treatment. The hydrolytic reaction is associated to leaving hydrochloric acid which compensates the loss of entropy of titanium tetrachloride. Calorimetric evidence of this hydrolytic reaction was not found during experiments, but considering the noisy calorimetric signals this process may pass unnoticed in case of slow reaction rates. On the other hand, residual water may also not react with $TiCl_4$, but allow modification/reorganization of solid surface with consequent change of the thermodynamic parameters of adsorption respect to perfectly dry surface.

3.2.1.5 Adsorption of $TiCl_4$ from gas phase

Beside the determination of thermodynamic parameters, goal of this work of thesis was to use the experimental results as a benchmark for computational results. It must be underlined that DFT calculations considered the adsorption from gas vacuum, while experiments were performed in solution; therefore some terms had to be added to the experimental values in order to consider the different phase of reactants. The thermodynamic cycle shown in Figure 41 was used to obtain the parameters of adsorption from gas phase.

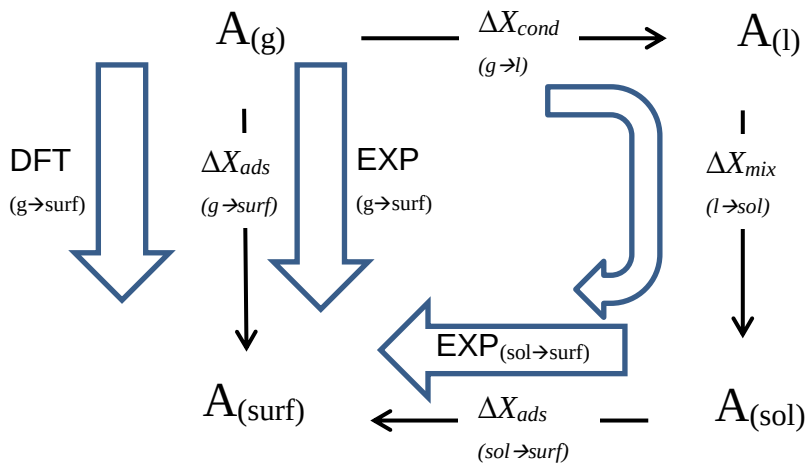

Figure 41: Thermodynamic cycle for the comparison between calculated and experimental values. ΔX = thermodynamic parameter (ΔG, ΔH or ΔS), A=adsorbent ($TiCl_4$, DEP or EB).

The cycle included the terms which take into account the condensation and mixing processes according with

$$\Delta X_{ads(g\rightarrow surf)} = \Delta X_{ads(sol\rightarrow surf)} + \Delta X_{cond(g\rightarrow l)} + \Delta X_{mix(l\rightarrow sol)} \qquad \text{Equation 10}$$

where X is a generic thermodynamic function. The enthalpy of mixing of $TiCl_4$ ($\Delta H_{mix(l\rightarrow sol)}$) was experimentally determined through calorimetry by means of additions of pure $TiCl_4$ to anhydrous *n*-heptane, while the Gibbs free energy of the same process ($\Delta G_{mix(l\rightarrow sol)}$) was estimated from the entropic change of mixing of pure liquids and experimental enthalpy of mixing according. The thermodynamic values relative to condensation process ($\Delta X_{cond(g\rightarrow l)}$) were obtained from the literature.

Enthalpy of mixing

The enthalpy of mixing of $TiCl_4$ and anhydrous *n*-heptane was determined by addition of pure liquid $TiCl_4$ to the anhydrous solvent. The graph in Figure 42 plots the partial molar entropy of mixing (parΔH_{mix}, correspondent to each addition) against the added volume. The mixing of $TiCl_4$ with anhydrous *n*-heptane was found to be endothermic. The associated enthalpy change at infinite dilution (C=0, evidenced by circle) calculated by linear regression was $\Delta H_{mix(l\rightarrow sol)}$=+1.8±0.1 kJ mol^{-1}.

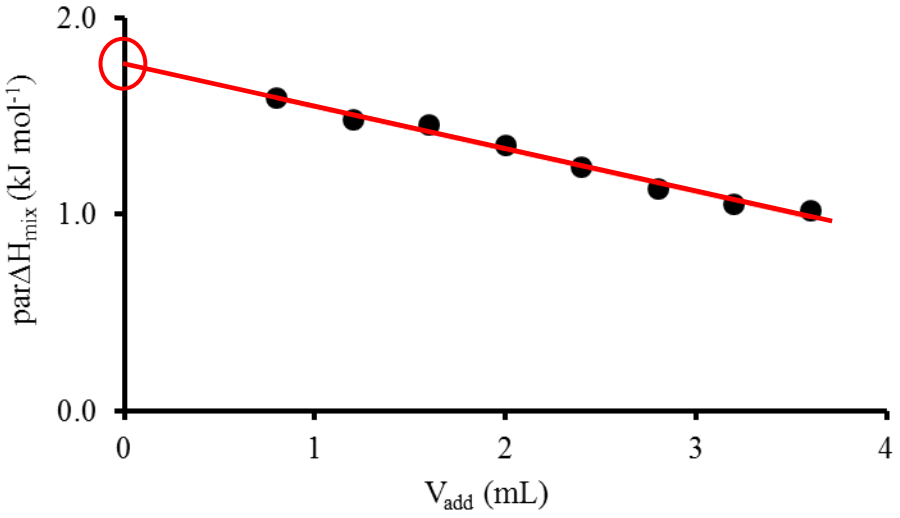

Figure 42: Partial molar enthalpy of mixing of $TiCl_4$ in *n*-heptane. V_0=20 mL, 0.4mLx8 additions.

Gibbs free energy of mixing

Gibbs free energies of mixing of $TiCl_4$ and *n*-heptane were calculated using the experimental enthalpy of mixing ($\Delta H_{mix(l \rightarrow sol)}$ = +1.8±0.1 kJ mol^{-1}) and the calculated ideal entropy of mixing $\Delta S_{mix,id}$ according with Equation 11, while the specific entropy can be calculated with Equation 12:

$$\Delta G_{mix} = \Delta H_{mix} - T\Delta S_{mix,id} \qquad \text{Equation 11}$$

$$\Delta S_{mix,id} = -nR(x_1 \ln x_1 + x_2 \ln x_2) = -nR[x_1 \ln x_1 + (1-x_1)\ln(1-x_1)] \qquad \text{Equation 12}$$

where *n* the total number of moles, R is the gas constant, and x_1 and x_2 are the molar fractions of $TiCl_4$ and *n*-heptane respectively. The graph in Figure 43 plots the calculated entropic term $T\Delta S_{mix,id}$ of mixing of $TiCl_4$ and *n*-heptane correspondent to a wide range of $TiCl_4$ concentration.

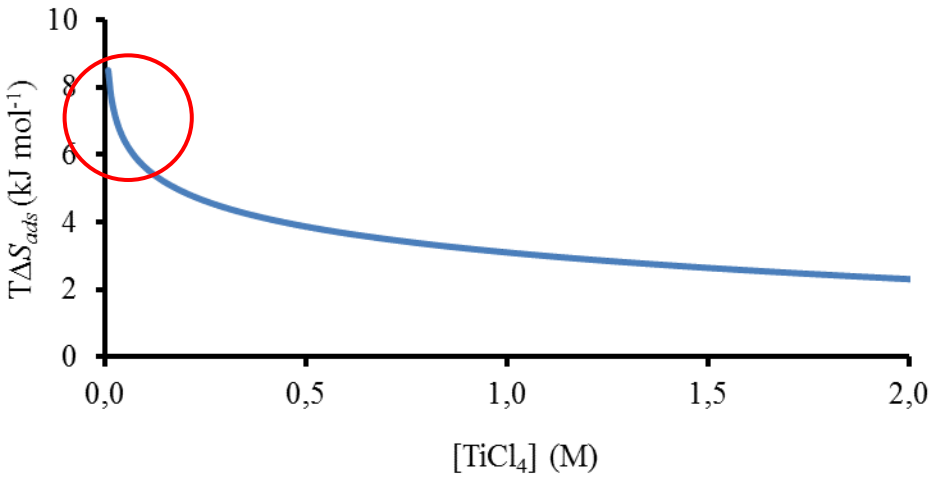

Figure 43: Entropic change of mixing of $TiCl_4$ and *n*-heptane relative to different final $TiCl_4$ concentrations.

The part of the graph evidenced by the red circle corresponds to the concentrations of $TiCl_4$ used in the experiments and the relative entropic change (about 6-8 kJ mol^{-1}), close to the value relative to infinite dilution +8.2 kJ mol^{-1}. Calculated Gibbs free energy of mixing is thus ΔG_{mix}=-6.4±0.1 kJ mol^{-1}.

Thermodynamic values adsorption from gas phase

The thermodynamic values of adsorption of $TiCl_4$ from gas phase to surface ($\Delta X_{ads\ (g \rightarrow surf)}$) was calculated according to the scheme that can be seen in Figure 41. In Table 22 the values associated to the steps of the thermodynamic cycle are provided; the values reported in the last row of table are referred to adsorption from gas phase, and thus are those to compare with computational results; Table 23 provides the DFT values obtained at the University of Naples during the course of this DPI cooperation project for the binding of $TiCl_4$ on $MgCl_2$.

	ΔG (kJ mol^{-1})	ΔH (kJ mol^{-1})	TΔS (kJ mol^{-1})
ΔX_{ads} (sol→surf)	-16.8	-12.4	+4.4
ΔX_{cond}(g→l)	-15.9[128,129]	-37[130]	-
ΔX_{mix} (l→sol)	-6.4	+1.8	-
ΔX_{ads} (g→surf)	-39.1	-47.6	-8.5

Table 22: Gibbs free energies and enthalpies relative to the thermodynamic cycle for correction of phase applied to adsorption of $TiCl_4$.

DFT	ΔG_{ads} (g→surf) (kJ mol^{-1})	ΔH_{ads} (g→surf) (kJ mol^{-1})	TΔS_{ads} (g→surf) (kJ mol^{-1})
clu_4	-40.2	-104.6	-64.4
clu_5	2.1	-52.7	-54.8
hole_4	-33.1	-100	-66.9
step_4	-38.9	-100.6	-61.7
step_5	-41	-102.5	-61.5

Table 23: Results of DFT calculations for the adsorption of $TiCl_4$ on $MgCl_2$.

The different computational values correspond to the binding of $TiCl_4$ on different clusters (clu, hole, step) and on different types of Mg atoms (_4: tetra-coordinated Mg atom belonging to 110 lateral cut; _5: penta-coordinated, Mg atom belonging to 104 lateral cut). The clu_4 and clu_5 structures expose an edge with tetra and penta-coordinated Mg atoms, respectively, mimicking 110 and 104 lateral cuts of a perfect $MgCl_2$ crystal; in hole_4 structure a few $MgCl_2$ units along the edge are missing, while in step_4 and step_5 structures half of the edge of $MgCl_2$ cluster was removed. The structures of clusters are illustrated below (Figure 44).

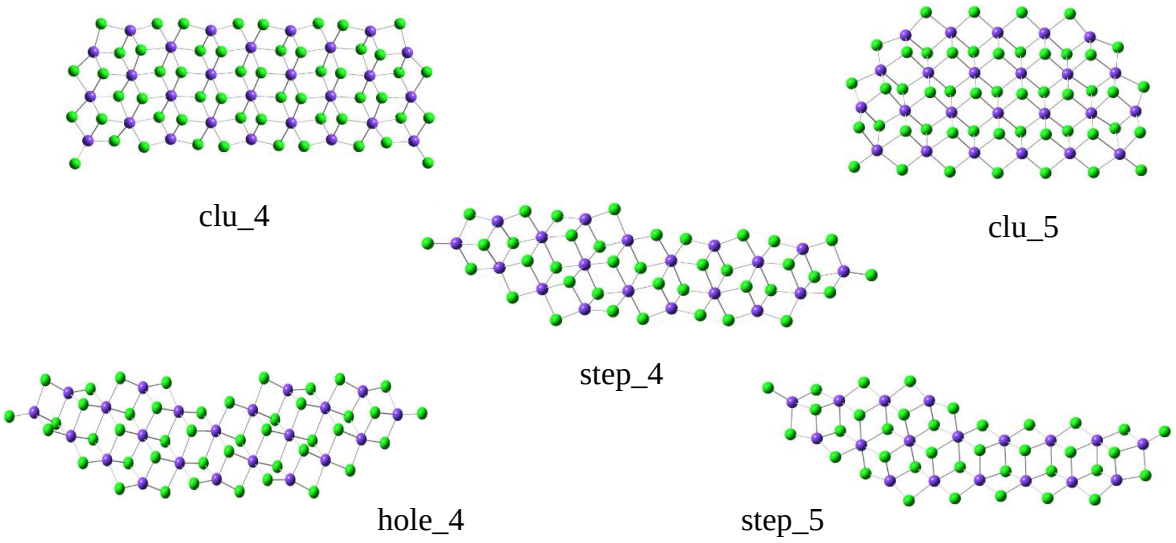

Figure 44: Clusters of $MgCl_2$ used for DFT calculations.

The set of values of $\Delta X_{ads\ (g\rightarrow surf)}$ reported in Table 22 does not match any set of values in Table 23, but show a genera overestimation of enthalpy respect Gibbs free energy of adsorption. Depending on the experimental $\Delta X_{ads\ (g\rightarrow surf)}$ value considered ($\Delta G_{ads(g\rightarrow surf)}$ or ($\Delta H_{ads(g\rightarrow surf)}$), all results of DFT models can be validated or discarded. The contrast is even more evident with entropy. Independently from the computational model, the entropic computational term associated to the adsorption from gas phase was in the range -55/-65 kJ mol^{-1}, much more negative than the experimental range for the same process (-8.5 kJ mol^{-1}).

The large difference in entropy found between experimental and computational results suggest the presence of factors that drastically influenced the process of adsorption of $TiCl_4$ on physically activated $MgCl_2$, such as presence of water recently evidenced[127]. In fact, the presence of water on the surface of $MgCl_2$ means that the experimental values obtained during this work were relative to a system which is different from the one simulated by DFT, which considered the binding of $TiCl_4$ on a "naked" surface of magnesium chloride. Thus, the use of experimental results as a benchmark for computational calculations was not possible because the two sets of data correspond to different processes (adsorption on "hydrated" and "dry" surface for experimental and DFT results respectively). The experimental values, however, are referred to a real system and may be thus useful to describe the pre-catalysts behavior.

3.2.2 Adsorption of donors

The study of adsorption of diethylphthalate and ethylbenzoate on physically activated $MgCl_2$ was performed with the same methodology used for $TiCl_4$. The more sensitive isothermal calorimeter TAM III was used for the determination of reaction heats because no hydrolytic problems occurred inside the syringe and the titration capillary during the experiments.

3.2.2.1 Kinetics of adsorption (sample B)

Since the first experiments, adsorption of donors was immediately found to be slower than absorption of $TiCl_4$, and to proceed for several hours after the mixing of reagents. In Figure 45 the graph of a titration of $MgCl_2$ with DEP interrupted for 24 hours is illustrated as an example. The red and blue points represent the experimental values collected on the first and second day respectively, while the green points represent the position in which the blue points (second titration day) were expected to be. The shifts are indicated by the arrows.

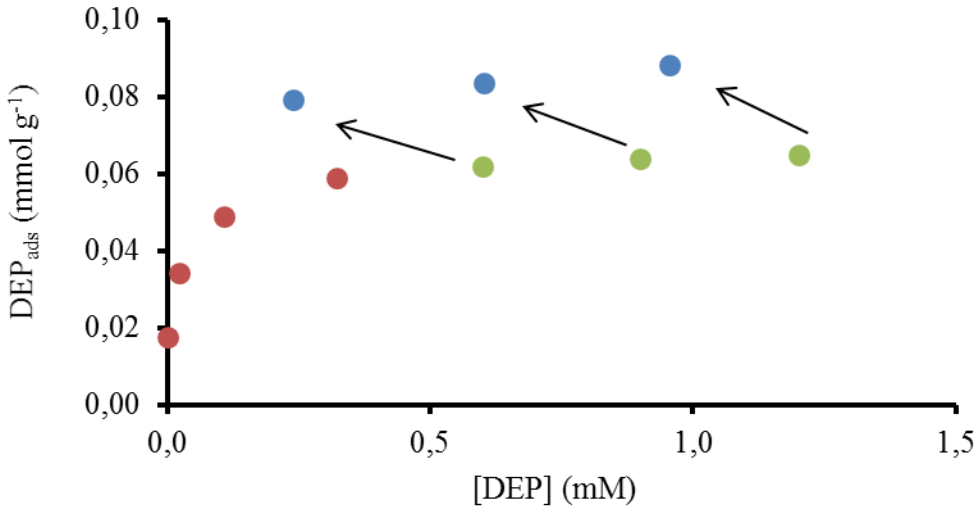

Figure 45: Two days UV-Vis titration of $MgCl_2$ (sample B) with DEP.

The second day loading of samples was higher than expected (a shift of about 30% towards the top), while concentration of DEP was lower (shift to the left). The shift evidenced a kinetic of adsorption, which had thus to be considered when choosing the interval between consecutive additions of titrant during the experiments.

The kinetic behavior of DEP was investigated by a single, large addition of titrant to $MgCl_2$ suspension. The adsorption process was monitored by UV-Vis spectrophotometric determination of donor concentration on aliquots of liquid phase collected at different times. Figure 46 visualizes the UV-Vis spectra of the original solution (black dotted line) and those obtained after 3, 14, 21, 31, 57 and 115 minutes from mixing (from blue to red lines), while the frame shows the related loading of magnesium chloride against time.

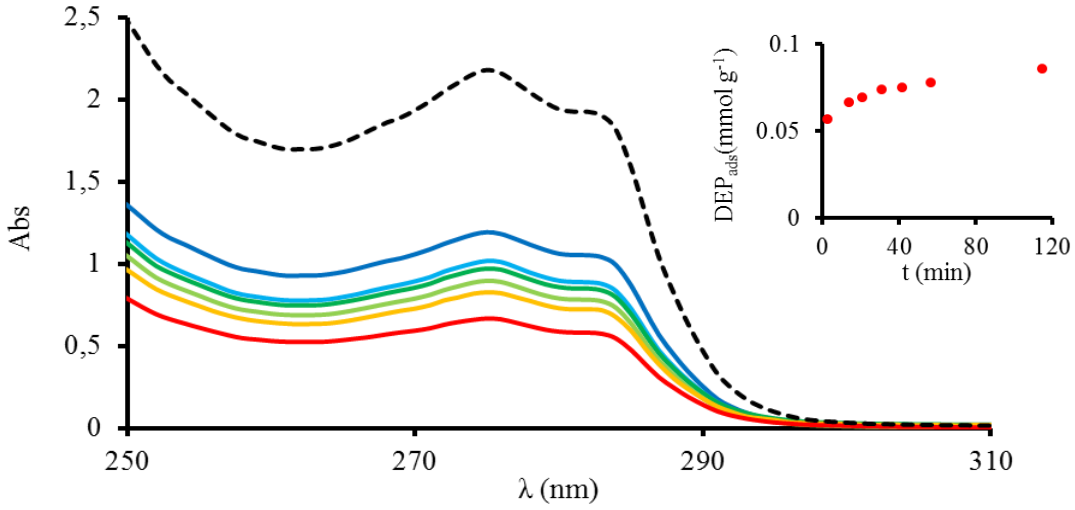

Figure 46: Evolution of UV-Vis spectra of DEP solution after addition of $MgCl_2$. $MgCl_2$ (sample B)=162 mg, V_0=10 mL, $C°_{DEP}$= 1.97 mM. In the frame loading of sample as function of time.

Initially, adsorption of DEP was fast, reaching about 70% of the final loading within three minutes; the process then slowed down and continued for several hours, but reached 95% of the final loading within one hour. The effect of the amount of time between additions on the binding constant was consequently investigated by means of three titrations with DEP. For each titration, different intervals between additions were chosen (15, 30 and 60 min). The experimental points with the related adsorption isotherms (obtained by one-site Langmuir model), are visible in Figure 47, while in Table 24, the numerical results of fit are tabulated.

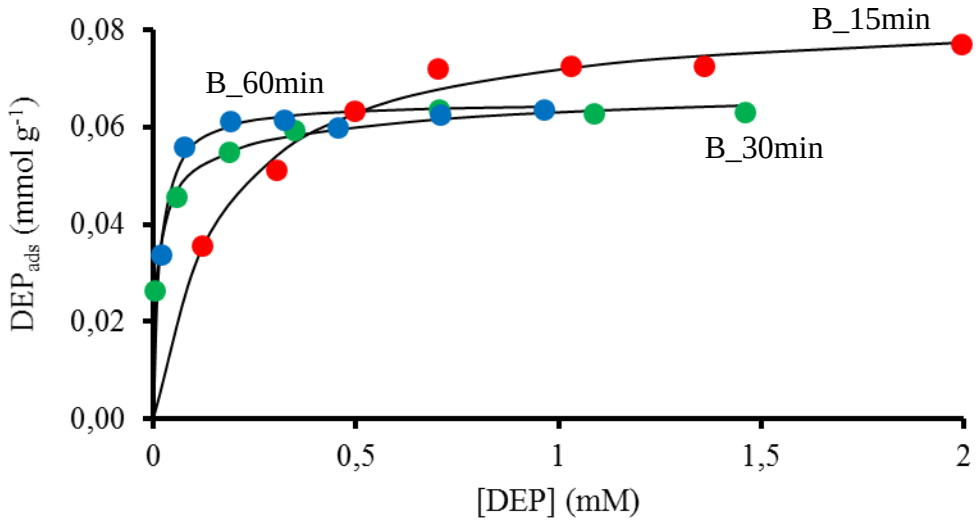

Figure 47: Adsorption of DEP on $MgCl_2$ (B) at different time between additions. Red: 15 min, $MgCl_2$=48mg, V_0=15 mL, C_{DEP}=100 mM, 7x0.035-0.05 mL additions; green: 30 min, $MgCl_2$=75mg, V_0=10 mL, C_{DEP}=100 mM, 7x0.2-0.4 mL additions; blue: 60 min, $MgCl_2$=34mg, V_0=10 mL, C_{DEP}=100 mM, 7x0.02-0.04 mL additions.

Model	Parameter	B_15min	B_30min	B_60min
Langmuir1	n_{totL} (mmol g^{-1})	0.084±0.09	0.060±0.003	0.065±0.00
	$\log K_{adsL}$	3.77±0.22	5.21±0.13	4.92±0.12
	ΔG_{adsL} (kJ mol^{-1})	-21.5±1.3	-29.7±0.7	-27.4±0.7

Table 24: UV-Vis spectrophotometric results of fit for adsorption of DEP on $MgCl_2$ (B) with different time between additions (15, 30 and 60 minutes).

In Table 24 the drastic effect of the different amounts of time between consecutive additions on $\log K_{adsL}$ is evident; in fact, the binding constants of experiments B_15min and B_30min differ by more than one order of magnitude. However, considering the limits of errors, almost identical adsorption isotherms were obtained for experiments B_30min and B_60min. A similar experiment performed with EB led to similar results, with the only difference that adsorption was slightly faster, reaching 95% of the total loading within 30 minutes.

In the experimental protocol, a 60 min interval between additions was chosen for both donors because the interval was long enough to minimize its influence on the results of fit and it allowed the collection within a day of sufficient amount of data points (6-9) sufficient to fit the experiments, which are impossible to carry out with longer times (e.g. 3-4 points collected with 2 h between additions).

3.2.2.2 Gibbs free energy of adsorption of donors (samples E, G-I)

Loading, binding constant and Gibbs free energy of adsorption of donors on physically activated $MgCl_2$ were determined with the same methodology used for the determinations with $TiCl_4$. Titrations with donors were also performed in presence of $SiCl_4$ and required lower amounts of $MgCl_2$ and more dilute solutions of titrants (1-10 mM). Titrations were performed on fresh samples of magnesium chloride with an interval of one hour between additions in all experiments.

UV-Vis spectrophotometric adsorption isotherms (and the related experimental points) obtained in *n*-heptane by titration of several $MgCl_2$ samples with both ethylbenzoate and diethylphthalate are chosen as an example. Exemplificative titrations are reported in Figure 48 (DEP) and Figure 49 (EB); the adsorption isotherms were obtained by data-fitting with one-site Langmuir (black full lines) and Langmuir-Freundlich models (red dot lines). For every donor, two different samples were used for the investigations.

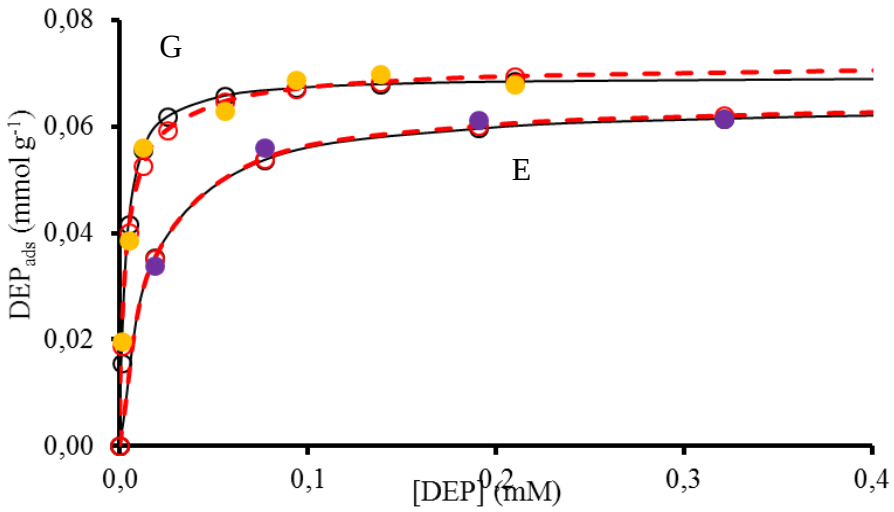

Figure 48: UV-Vis spectrophotometric adsorption isotherm of DEP on $MgCl_2$. Sample E: purple, $MgCl_2$=49 mg, V_0=15 mL, C_{DEP}=100 mM, 4x0.2 mL additions; sample G: orange, $MgCl_2$=73 mg, V_0=15 mL, C_{DEP}=10 mM, 7x0.015 mL additions. Dots: experimental points; full black lines: one-site Langmuir model fit; red dot line: Langmuir-Freundlich fit.

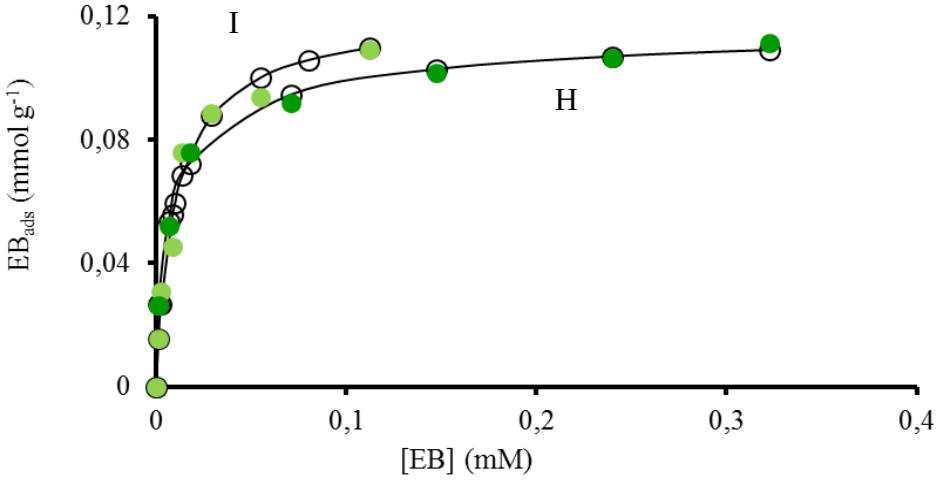

Figure 49: UV-Vis spectrophotometric adsorption isotherm of EB on $MgCl_2$. Sample H: dark green, $MgCl_2$=73 mg, V_0=15 mL, C_{EB}=15 mM, 6x0.15 mL additions; sample I: light green: $MgCl_2$=98 mg, V_0=15 mL, C_{EB}=10 mM, 8x0.15 mL additions. Dots: experimental points; full black lines: one-site Langmuir model fit; red dot line: Langmuir-Freundlich fit.

The values of loading and binding constant obtained are inserted in Table 25 (adsorption of DEP) and Table 26 (adsorption of EB). Again, the adsorption of donors was well described by Langmuir adsorption model, with a value of adj. R^2 higher than 0.99 in most of the experiments. As found for adsorption of $TiCl_4$, other models did not improve significantly the goodness of fit;

as example, the values obtained by Langmuir-Freundlich (see Table 25 and Table 26) were slightly different from those calculated by Langmuir model; however, considering the corresponding limits of error, the values of parameters well match.

Model	Parameter	E	G	Average*
Langmuir	n_{totL} (mmol g^{-1})	0.065 ± 0.001	0.070 ± 0.002	0.068±0.004
	logK_{adsL}	4.81 ± 0.11	5.51 ± 0.12	5.2±0.5
	ΔG_{adsL} (kJ mol^{-1})	-27.4 ± 0.6	-31.4 ± 0.7	-29.7±2.9
	adj R^2	0.971	0.997	-
LF	n_{totLF} (mmol g^{-1})	0.065 ± 0.001	0.073 ± 0.003	0.069±0.06
	logK_{adsLF}	4.79 ± 0.11	5.45 ± 0.09	5.13±0.46
	ΔG_{adsLF} (kJ mol^{-1})	-27.4 ± 0.5	-31.1 ± 0.5	-29.2±2.6
	m_{LF}	0.998	0.768	0.884
	adj R^2	0.983	0.998	-

Table 25: UV-Vis spectrophotometric results of fit for adsorption of DEP on $MgCl_2$ (samples E and G). *calculation of errors based on simultaneous fit of experimental points with logK_{ads}=average.

Model	Parameter	H	I	Average*
Langmuir	n_{totL} (mmol g^{-1})	0.107±0.003	0.118±0.0	0.113±0.00
	logK_{adsL}	5.18±0.17	5.02±0.22	5.1±0.1
	ΔG_{adsL} (kJ mol^{-1})	-29.6±1.0	-28.6±1.1	-29.1±0.6
	adj R^2	0.996	0.994	-
LF	n_{totLF} (mmol g^{-1})	0.120±0.005	0.123±0.0	0.122±0.00
	logK_{adsLF}	5.03±0.18	4.97±0.19	5.00±0.08
	ΔG_{adsLF} (kJ mol^{-1})	-28.7±0.1	-28.4±0.9	-28.5±0.4
	m_{LF}	0.751	0.903	0.777
	adj R^2	0.999	0.997	-

Table 26: UV-Vis spectrophotometric results of fit for adsorption of EB on $MgCl_2$ (samples H and I). *calculation of errors based on simultaneous fit of experimental points with logK_{ads}=average.

The results of fitting indicated that different donors had different loadings (see plateau of experimental points), in both cases lower than the loading detected for $TiCl_4$ (0.14-0.17 mmol g^{-1}). Fresh samples of magnesium chloride were able to load 0.11-0.12 mmol g^{-1} of EB, about 40% higher than the average loading of DEP found (0.068 mmol g^{-1}). The result was rationalized considering the different steric hinder of donors (the bigger DEP molecules required more space to bind on the $MgCl_2$ surface). The values of loading for donors determined on fresh samples match with those found in literature (from 0.06 to 0.15 mmol g^{-1})[131,132] relative to the adsorption of aromatic esters (ethyl benzoate and diisobutylphthalate) in similar experimental conditions.

Both internal donors interacted with the surface of $MgCl_2$ much more strongly than $TiCl_4$. EB and DEP were found to possess a very similar affinity for physically activated $MgCl_2$, in contrast with the expected greater value for the bidentate DEP. Binding constants of donors were not less than two orders of magnitude higher than that $TiCl_4$ independently of the sample

employed. The fit of UV-Vis spectrophotometric data allowed the determination of average $\log K_{adsL}$=5.2±0.5 (correspondent to ΔG_{ads} = -29.7±2.9 kJ mol^{-1}) for DEP and $\log K_{adsL}$=5.1±0.1 for EB (ΔG_{ads}=-29.1±0.6 kJ mol^{-1}).

3.2.2.3 Enthalpy of adsorption of donors (samples G-I)

Calorimetric titrations of $MgCl_2$ with IDs were run by TAM III nanocalorimeter. Stirring rate (150 rpm) were regulated in order to reach a compromise between goodness of calorimetric data and baseline noise (the higher the rate, the higher the noise). Preliminary experiments of single additions of a great excess of donors (to ensure the maximum saturation of the system) were run to estimate the order of magnitude of the total heat evolved per gram of $MgCl_2$. Experiments of stepwise addition of IDs to $MgCl_2$ suspensions were then carried out.

As in UV-Vis spectrophotometric determinations, the amounts of $MgCl_2$ used for titrations were lower (10-35 mg) than those used in the $MgCl_2$-$TiCl_4$ system; $SiCl_4$ was added as a water scavenger and additions of donors were performed with an interval of one hour between each other. Two different samples of $MgCl_2$ were used. The same samples employed for UV-Vis determinations were used for titrations with EB, but only sample G was used for titrations with DEP because sample E was finished; therefore, another batch (sample H) had to be used. The integrals of the ITC peaks (heats) of two representative titrations of DEP and EB are illustrated in Figure 50 as cumulative heat (h_{cum}) against the amount of donor, both normalized for the weight of $MgCl_2$ (as in $MgCl_2$-$TiCl_4$ system, see Figure 38). A representative calorimetric output of titration of $MgCl_2$ (sample G) with DEP is visible in the frame.

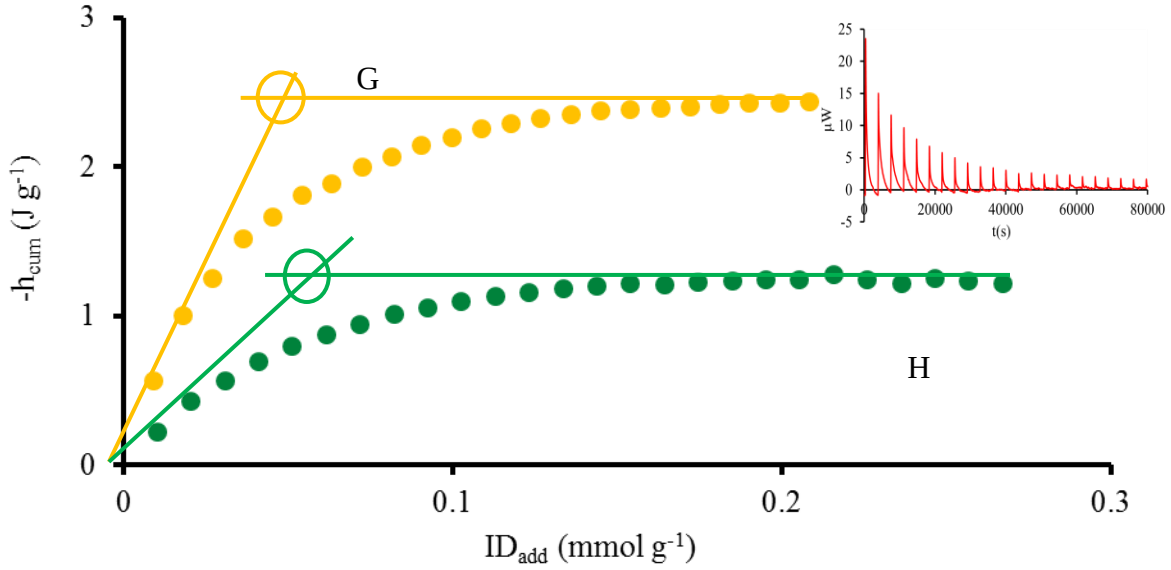

Figure 50: Exemplificative stepwise calorimetric titrations of $MgCl_2$ with donors; DEP, orange, sample G: $MgCl_2$=25mg, V_0=0.7 mL, C_{DEP}=22mM, 0.01mLx 25 additions, calorimetric output in the frame; EB, light green, sample H: $MgCl_2$=13mg, V_0=0.7 mL, C_{EB}=10 mM, 0.01mLx25 additions.

The calorimetric titration clearly indicated an exothermic process. The loading of $MgCl_2$ for each experiment (evidenced by circles) was determined with the method of straight lines (see Figure 38 and related paragraph), and also in this case the loading of $MgCl_2$ was lower for aged samples. Data elaboration was performed as explained for $MgCl_2$-$TiCl_4$ system. "Calorimetric loading" was used with average binding constants of $\log K_{ads}$ =5.2 and $\log K_{ads}$=5.1 for DEP and EB respectively (Table 25 and Table 26) to calculate the concentration of free donors during calorimetric titrations [ID], necessary for the fitting. In Figure 51 and Figure 52 exemplificative isotherms obtained for DEP and EB respectively (two for each donor) with two different samples of $MgCl_2$ are illustrated. The results of the analysis of calorimetric data by Langmuir model on the basis of the adsorption constants previously determined by UV-Vis spectrophotometric titrations allowed the calculation of the values of enthalpy of adsorption listed in Table 27 for DEP and Table 28 for EB.

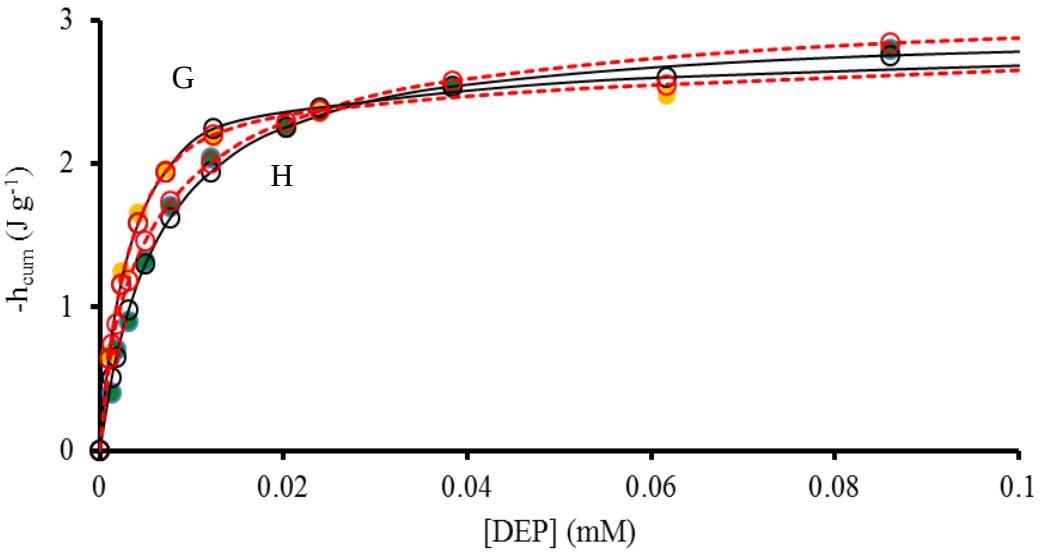

Figure 51: Calorimetric adsorption isotherms of DEP on $MgCl_2$ in *n*-heptane. Sample G: orange: $MgCl_2$=25mg, V_0=0.7 mL, C_{DEP}=22mM, 25x0.01 mL additions; H: dark green: $MgCl_2$=29mg, V_0=0.7 mL, C_{DEP}=28 mM, 12x0.02 mL addition. Dots: experimental points; full lines: one-site Langmuir model fit; dot red lines: Langmuir-Freundlich fit.

Model	Parameter	G	H	Average*
Langmuir	n_{tot} (mmol g^{-1})	0.064	0.04	0.052
	ΔH_{adsL} (kJ mol^{-1})	-59.2±2.2	-63.2±1.8	-61.2±2.1
	adj R^2	0.978	0.984	-

Table 27: Results of fit from calorimetric adsorption isotherm of DEP on $MgCl_2$. *calculation of errors based on simultaneous fit of experimental points with logK_{ads}=average.

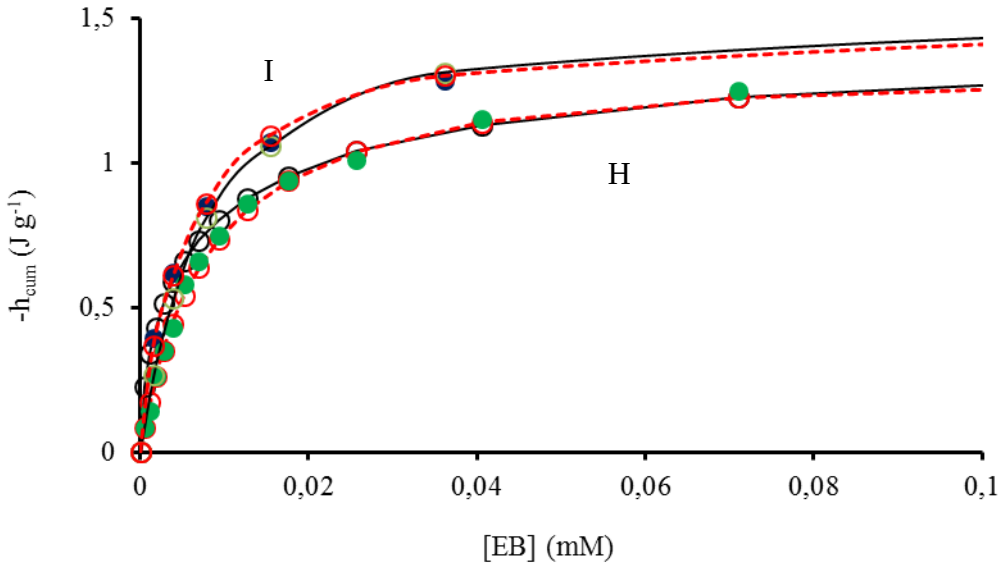

Figure 52: Calorimetric adsorption isotherms of EB on $MgCl_2$ in *n*-heptane. H: dark green: $MgCl_2$=13mg, V_0=0.7 mL, C_{EB}=10 mM, 25x0.01mL additions; I: dark blue, $MgCl_2$=32mg, V_0=0.7 mL, C_{EB}=30 mM, 25x0.01mL additions. Dots: experimental points; full lines: one-site Langmuir model fit; dot lines: Langmuir-Freundlich fit.

Model	Parameter	H	I	Average*
Langmuir	n_{totL} (mmol g^{-1})	0.068	0.053	0.061
	ΔH_{adsL} (kJ mol^{-1})	-26.1±1.7	-28.9±2.1	-27.5±2.3
	adj R^2	0.982	0.987	-

Table 28: Results of fit from calorimetric adsorption isotherm of EB on $MgCl_2$. *calculation of errors based on simultaneous fit of experimental points with logK_{ads}=average.

As previously found for $TiCl_4$, the values of loading for all samples were generally lower than those previously detected by UV-Vis spectrophotometric determinations on the same batch of $MgCl_2$; in particular, the difference is evident in the case of samples H and I titrated with EB, which loading decreased from ~0.11 mmol g^{-1} to ~0.06 mmol g^{-1} after several manipulations.

On the whole, the binding of both IDs was more exothermic than $TiCl_4$. Data clearly evidenced a higher enthalpy of adsorption ΔH_{adsL} of DEP compared to EB, with average enthalpies of adsorption of ΔH_{adsL} =-61.2±2.1 kJ mol^{-1} and ΔH_{adsL} =-27.5±2.3 kJ mol^{-1} for DEP

and EB respectively, with a trend which met the expectations considering the bidentate nature of DEP as compared to the monodentate EB.

3.2.2.4 Entropy of adsorption of donors

The entropic terms of adsorption at 298 K of IDs calculated by fitting the data with Langmuir model ($T\Delta S_{adsL}$) are inserted in Table 29, together with the respective values of Gibbs free energies and enthalpies of adsorption.

	ΔG_{adsL} (Average) (kJ mol^{-1})	ΔH_{adsL} (Average) (kJ mol^{-1})	$T\Delta S_{adsL}$ (kJ mol^{-1})
DEP	-29.7±2.9	-61.2±2.1	-31.5
EB	-29.2±2.6	-27.5±2.3	+1.7

Table 29: Thermodynamic parameters of adsorption of donors from *n*-heptane on $MgCl_2$.

In the experimental conditions (impregnation from dilute solutions, 298 K), DEP show a largely negative adsorption entropy ($T\Delta S_{adsL}$ = -31.5 kJ mol^{-1}), as expected for an adsorption process; on the other hand, adsorption of EB was essentially entropy-neutral ($T\Delta S_{adsL}$ = +1.7 kJ mol^{-1}) as found for $TiCl_4/MgCl_2$ system.

Again, rationalizing the entropy change in these systems is very hard; $T\Delta S_{adsL}$, calculated from measurements, is the entropy change *in the system* and thus, several contributions are present. Factors such as desorption of solvent molecules partially but not fully explain the almost zero entropy of adsorption of EB (effect of solvent was proved to affect the calculation of entropy of just a few kJ mol^{-1}). The recent evidence of residual water on $MgCl_2$ surface[127] suggest that beside acid-base interactions between incoming donor molecule and surface (saturation of coordination-vacant magnesium sites), other interactions such as hydrogen bonding may establish between solid surface and adsorbent. A similar argumentation was provided by Drago previously[112] to interpret negative ΔS_{ads} for pyridine adsorption on acid sites of silica particles dispersed in cyclohexane.

3.2.2.5 Adsorption of donors for gas phase

The thermodynamic parameters of adsorption from gas phase $\Delta X_{ads\ (g \rightarrow surf)}$ were calculated according with the scheme in Figure 41 as for $TiCl_4$.

Enthalpy and Gibbs free energy of mixing of donors

The enthalpies of mixing of DEP and EB were experimentally determined by means of isothermal calorimeter TAM III by stepwise additions of pure donor into pure anhydrous *n*-heptane at 298 K. In Figure 53 the instrumental outputs experiments are illustrated, while the graph in Figure 54 plots the partial molar enthalpy of mixing against the amounts of IDs added.

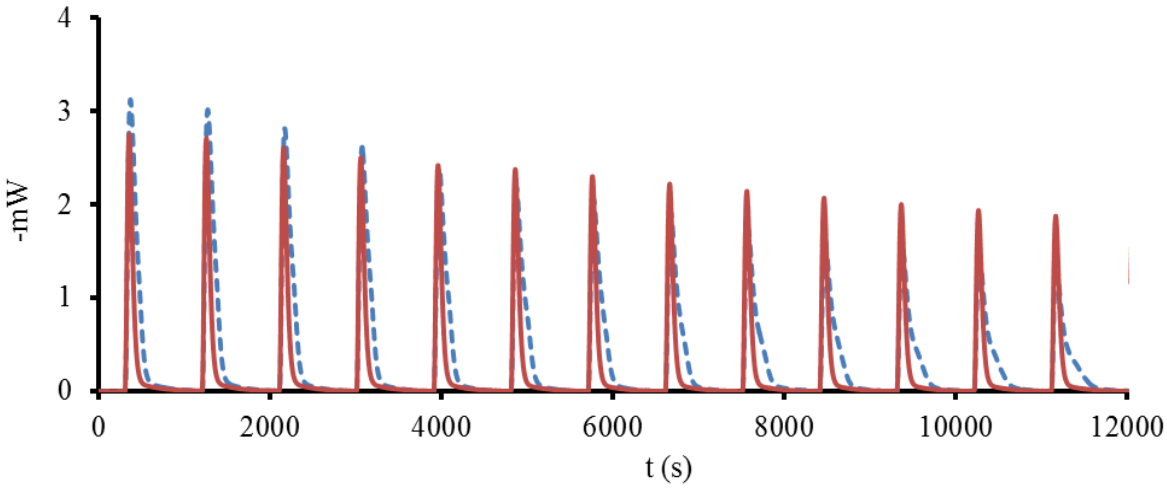

Figure 53: Calorimetric output of dissolution heat of DEP (dotted, blue) and EB (red). V_0 = 0.7mL, undiluted IDs, additions of 7(DEP)-10(EB) µL.

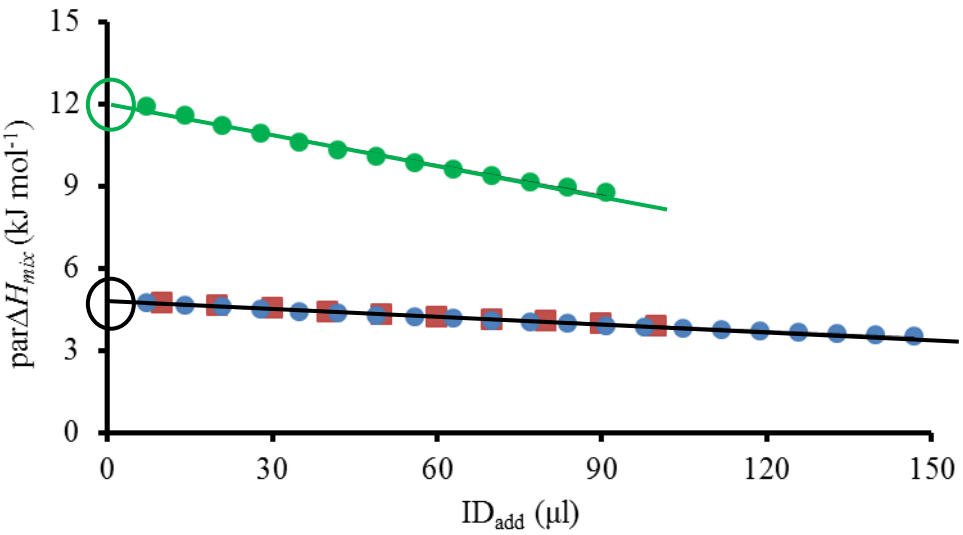

Figure 54: Partial molar enthalpies of mixing of DEP (green) and EB (red and blue, two experiments) in anhydrous *n*-heptane. V_0=0.7 mL, additions of 7-10µl.

The enthalpies of mixing of both DEP and EB with *n*-heptane were positive, and the process with DEP was more endothermic than the process with EB. Enthalpies of mixing at infinite dilution, calculated as with $TiCl_4$ and evidenced by circles in Figure 54, were $\Delta H_{mix(l\rightarrow sol)}$=+12.1±0.1 kJ mol^{-1} for DEP and $\Delta H_{mix(l\rightarrow sol)}$= +4.7±0.1 kJ mol^{-1} for EB.

Gibbs free energy of mixing $\Delta G_{mix(l\rightarrow sol)}$) of -2.3 kJ mol^{-1} for EB was determined by the experimental $\Delta H_{mix(l\rightarrow sol)}$ and calculated value of $T\Delta S_{mix(l\rightarrow sol)}$ (+7 kJ mol^{-1}); in the case of DEP a similar calculation resulted in positive value of $\Delta G_{mix(l\rightarrow sol)}$=+6.1 kJ mol^{-1} ($\Delta H_{mix(l\rightarrow sol)} > T\Delta S_{mix(l\rightarrow sol)}$), correspondent to the formation of two liquid phases. Since phase separation did not take place in the experimental conditions, $\Delta G_{mix(l\rightarrow sol)}$= 0 kJ mol^{-1} was used in the thermodynamic cycle.

Thermodynamic values adsorption from gas phase

The tables below show the thermodynamic values associated to the different steps of the thermodynamic cycle visible in Figure 41 relative to the adsorption of DEP (Table 30) and EB (Table 31) on magnesium chloride.

		ΔG (kJ mol^{-1})	ΔH (kJ mol^{-1})	TΔS (kJ mol^{-1})
DEP	$\Delta X_{ads\ (sol \rightarrow surf)}$	-29.7	-61.2	-31.5
	$\Delta X_{cond\ (g \rightarrow l)}$	-36[133]	*-82**[134]	-
	$\Delta X_{mix\ (l \rightarrow sol)}$	0	+12.1	-
	$\Delta X_{ads\ (g \rightarrow surf)}$	-65.7	-131.1	-65.4

Table 30: Gibbs free energies and enthalpies relative to the thermodynamic cycle for correction of phase applied to adsorption of DEP. *$\Delta X_{cond\ (g \rightarrow l)}$ of dimethylphthalate.

		ΔG (kJ mol^{-1})	ΔH (kJ mol^{-1})	TΔS (kJ mol^{-1})
EB	$\Delta X_{ads\ (sol \rightarrow surf)}$	-29.2	-27.5	+1.7
	$\Delta X_{cond\ (g \rightarrow l)}$	-16[135]	-59[135]	-
	$\Delta X_{mix\ (l \rightarrow sol)}$	-2.3	+4.7	-
	$\Delta X_{ads\ (g \rightarrow surf)}$	-47.5	-81.8	-34.3

Table 31: Gibbs free energies and enthalpies relative to the thermodynamic cycle for correction of phase applied to adsorption of EB.

Adsorption of donors from gas phase *(g→surf)* is characterized by more negative values of Gibbs free energy, enthalpy and entropy compared to adsorption from solution *(sol→surf)*. The entropic term became negative for both donors ($T\Delta S_{ads(g \rightarrow surf)}$= -65.4 kJ mol^{-1} for DEP and $T\Delta S_{ads(g \rightarrow surf)}$ = -34.3 kJ mol^{-1} for EB), as expected for an adsorption process.

Table 32 and Table 33 show the thermodynamic parameters of adsorption from gas phase calculated by DFT for the adsorption of internal donors considering several coordination modes (chelate and bridge structures and different conformers). Calculations were performed at the University of Naples using the clusters of $MgCl_2$ listed in Figure 44.

		$\Delta G_{ads(g \rightarrow surf)}$ (kJ mol^{-1})	$\Delta H_{ads\ (g \rightarrow surf)}$ **(kJ mol^{-1})**	$T\Delta S_{ads\ (g \rightarrow surf)}$ **(kJ mol^{-1})**
DMP	Clu_4 a$^{£}$	-87.1	-145.7	-58.6
	Clu_4 b$^{£}$	-117.6	-175.8	-58.2
	Clu_4 a*	-69.5	-115.9	-46.4
	Clu_4 b§	-86.6	-152.4	-65.8
	Clu_5 a*	-55.7	-104.6	-48.9
	Clu_5 b§	-95.8	-157.4	-61.6
	Clu_5 b§	-100.9	-163.3	-62.4

Table 32: DFT results for adsorption of dimethylphthalate (DMP) on $MgCl_2$; £ = chelation, §=bridge, * = monodentate, a-e = different conformers.

		$\Delta G_{ads\ (g \rightarrow surf)}$ **(kJ mol^{-1})**	$\Delta H_{ads\ (g \rightarrow surf)}$ **(kJ mol^{-1})**	$T\Delta S_{ads\ (g \rightarrow surf)}$ **(kJ mol^{-1})**
EB	Clu_5 a	-52.7	-98.3	-45.6
	Clu_5 b	-53.6	-99.2	-45.6
	Clu_5 c	-57.3	-102.6	-45.3
	Clu_4 d	-72.8	-123.1	-50.3
	Clu_4 e	-73.3	-116.4	-43.1

Table 33: DFT results for adsorption of EB on $MgCl_2$; a-e = different conformers.

The set of experimental results referred to adsorption from gas phase are close to those of some computational models (e.g. Clu_4a* in Table 32 and Clu_5a,b in Table 33); in the case of donors, also the experimental values of entropy of adsorption from gas phase (-65.4 kJ mol^{-1} and -34.3 kJ mol^{-1} for DEP and EB respectively) were close to the results provided by simulations (in the ranges of -45/-65 kJ mol^{-1} and -43/-50 kJ mol^{-1} for DEP and EB respectively) and suggest the binding of phthalates and benzoates to 110 and 104 lateral cuts respectively.

However it must be kept in mind that comparison and conclusions have be performed with great care in the light of the experimental evidence of partially hydrated $MgCl_2$ surface[127], which makes the "dry" binary $MgCl_2$-ID(s) system closer to a ternary "hydrated" H_2O-$MgCl_2$-ID(s). Further studies on the real nature of $MgCl_2$ solid surface and investigation of thermodynamic relationships between the whole components of the system have to be performed to elucidate more in detail the adsorption of donors.

3.3 Three component systems ($MgCl_2$-$TiCl_4$-DEP)

In the last months of this work of research the three components system $MgCl_2$-$TiCl_4$-DEP started to be investigated through titrations of sample prepared by co-milling of $TiCl_4$ and $MgCl_2$ (sample J) with the donor. Efforts were focused on DEP because of its higher calorimetric signals and better UV-Vis detection.

Beside heterogeneous titration, homogeneous titration of $TiCl_4$ with DEP in *n*-heptane was performed to investigate the equilibrium in liquid phase, which may play an important role in the case of $TiCl_4$ release in solution.

3.3.1 Titanium content in co-milled $TiCl_4$-$MgCl_2$ sample

Total titanium content in co-milled $MgCl_2$-$TiCl_4$ sample provided by University of Naples was determined by means of hydrogen peroxide method (dissolution of sample in 10% HCl, addition of H_2O_2) and repeated three times to check consistence. The results of total amount of titanium in the sample determined with such procedure are inserted in Table 34.

sample	w_{sample} (mg)	w_{Ti} (mg)	Average Ti content (% w_{Ti}/w_{sample})
J	15.33	0.289	1.91(0.05)
	5.39	0.106	
	13.28	0.251	

Table 34: Titanium content in co-milled $MgCl_2$ (sample J).

The total average titanium content of sample J was found to be 1.91% w_{Ti}/w_{sample}, correspondent to 0.41 $mmol_{Ti}/g_{sample}$, in good agreement with the values of 2% w_{Ti}/w_{sample} found by ICP at the University of Naples where sample J was prepared. The amount of titanium in the co-milled sample was around three times greater than that loadable by adsorption on fresh samples; the greater amount of titanium in sample J was explained by the very different conditions of impregnation of $TiCl_4$ (ball-milling of $MgCl_2$ and concentrated or pure $TiCl_4$), harsher than those used in our experimental protocol (adsorption from dilute solutions).

3.3.2 Adsorption of DEP on co-milled $MgCl_2$-$TiCl_4$ sample

3.3.2.1 Gibbs free energy of adsorption

UV-Vis titrations for the determination of Gibbs free energy of adsorption were performed in conditions similar to those used for the binary $MgCl_2$-DEP system. Figure 55 shows the UV-Vis adsorption isotherm obtained by titration of sample J with dilute DEP solution. The UV-Vis spectra correspondent to each addition were more scattered than those obtained for binary $MgCl_2$-donor systems, similar to what observed during preliminary titrations of $MgCl_2$ with $TiCl_4$ (direct determination of Ti), when deposition of very fine solid particles was observed on the walls of the cuvette. The analysis of titanium content in solution at the end of adsorption experiment was performed by hydrogen peroxide method in order to check if desorption of titanium occurred.

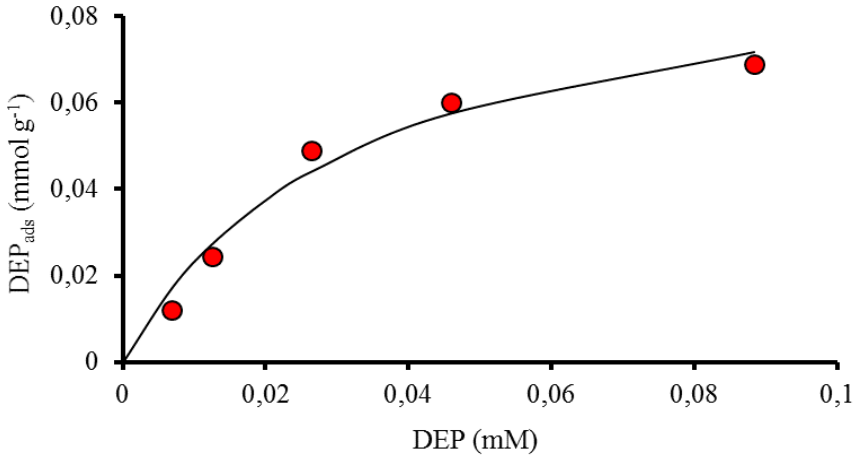

Figure 55: UV-Vis spectrophotometric adsorption isotherm of DEP on co-milled sample. $MgCl_2$ (J)=166mg, V_0=20 mL, C_{DEP} =21 mM, 8x0.1 mL additions.

The results of fitting of experimental points by means of Langmuir model are written in Table 35. As in the previous cases, fitting was not improved using other adsorption models (with Langmuir-Freundlich m_{LF}=1) and results are thus not reported. Data relative to binary $MgCl_2$-DEP binary system are also given for comparison purposes.

Model	Parameter	J	Binary system*
Langmuir	n_{totL} (mmol g^{-1})	0.098 ± 0.008	0.068±0.004
	logK_{adsL}	4.5 ± 0.2	5.2±0.5
	ΔG_{adsL} (kJ mol^{-1})	-25.6 ± 1.1	-29.7±2.9
	adj R^2	0.993	-

Table 35: UV-Vis spectrophotometric results of fit for the adsorption of DEP on co-milled $TiCl_4$-$MgCl_2$ (sample J); *average.

Results of fitting indicated that the presence of $TiCl_4$ on $MgCl_2$ affected the adsorption of DEP. In presence of $TiCl_4$ the binding constant of DEP was slightly lower than that previously found on pure $MgCl_2$ (ΔlogK_{ads}=0.7); considering the limits of errors, the two values did not differ much, but the variation is non negligible. The experiment also evidenced that the presence of

$TiCl_4$ did not led to lower values of loading of DEP, as the loading of fresh sample J was higher (n_{tot}=0.098±0.008 mmol g^{-1}) than the loading of samples E-F (n_{tot}=0.06-0.07 mmol g^{-1}). The UV-Vis spectrophotometric analysis of titanium content of liquid phase did not revealed presence of desorbed $TiCl_4$.

3.3.2.2 Enthalpy of adsorption

Calorimetric titrations of sample J with DEP were run by TAM III as performed for binary DEP-$MgCl_2$ systems. In Figure 56 the adsorption isotherm obtained for sample J is illustrated and the results of fit by means of Langmuir model are provided in Table 36, together with the parameters determined in absence of $TiCl_4$ (binary system) for comparison purposes.

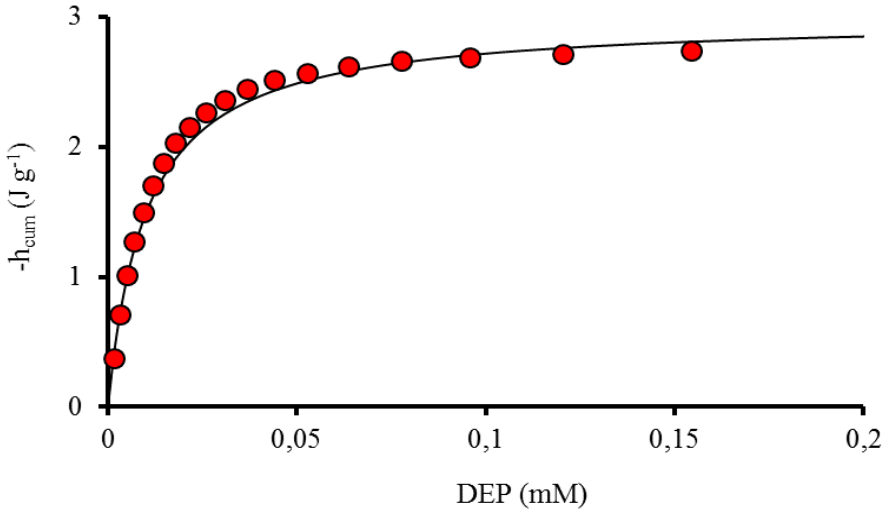

Figure 56: Calorimetric adsorption isotherms of DEP on co-milled $MgCl_2$–$TiCl_4$ (sample J). V_0=0.7mL, $MgCl_2$ = 14 mg, C_{DEP} = 11 mM, 25x10µL additions.

Model	Parameter	J	Binary system*
Langmuir	n_{totL} (mmol g^{-1})	0.04	0.052
	ΔH_{adsL} (kJ mol^{-1})	-83±3	-61.2±2.1
	adj R^2	0.993	-

Table 36: Results of fit from calorimetric adsorption isotherm of DEP on co-milled $MgCl_2$-$TiCl_4$; *average.

The amount of DEP in liquid phase was calculated with n_{totL}=0.04 mmol g^{-1} (Table 36) and logK_{adsL}=4.5 (Table 35). The comparison between binary and ternary systems showed that in presence of $TiCl_4$ the enthalpy of adsorption of DEP on surface was more negative (ΔG_{adsL}= -83±3 kJ mol^{-1}), being favored of about 22 kJ mol^{-1}. Also in this case, no evidence of $TiCl_4$ desorption was found by means of UV-Vis spectroscopy.

3.3.2.3 Entropy of adsorption

The entropy of adsorption of DEP from solution on co-milled $TiCl_4$-$MgCl_2$ sample calculated from values in Table 35 and Table 36 ($\Delta G_{ads(sol \rightarrow surf)}$=-25.6±1.1 kJ mol^{-1} and $\Delta H_{ads(sol \rightarrow surf)}$=-83±3 kJ mol^{-1}) was $T\Delta S_{ads(sol \rightarrow surf)}$=-57.4 kJ mol^{-1}. The entropic change upon adsorption well agree with the expected negative value for an adsorption process.

3.3.3 Interaction $TiCl_4$-DEP in solution

Binding constant (logK_{compl}), Gibbs free energy (ΔG_{compl}) and enthalpy (ΔH_{compl}) of complexation of $TiCl_4$ and DEP in solution were determined simultaneously by calorimetry by means of a single continuous addition of $TiCl_4$ to donors solutions. Figure 57 shows an exemplificative titration; the total molar enthalpy change per mole of metal is plotted against the DEP/$TiCl_4$ ratio.

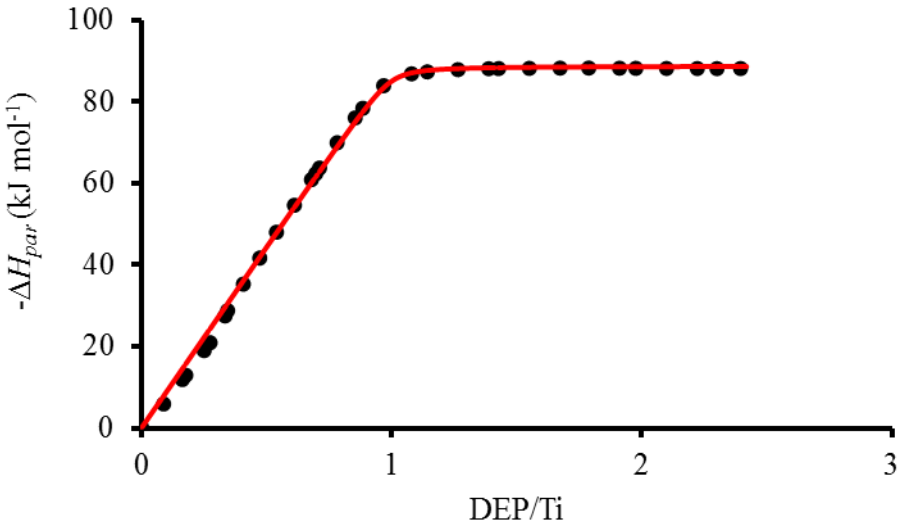

Figure 57: Total molar enthalpy change per mole of metal, as a function of the DEP/Ti in *n*-heptane at 25°; $C°_{TiCl4}$=9.5mM; C_{DEP} =97mM

Titanium tetrachloride formed only one complex with stoichiometry 1:1 with DEP, clearly showed by the change of slope in correspondence of DEP/$TiCl_4$ ratio=1. The analysis of calorimetric data by means of HypDeltaH[109] tool led to the determination of the thermodynamic parameters inserted in Table 37.

	Stoichiometry	logK_{compl} (kJ mol^{-1})	ΔG_{compl} (kJ mol^{-1})	ΔH_{compl} (kJ mol^{-1})	$T\Delta S_{compl}$ (kJ mol^{-1})
$TiCl_4$-DEP	1:1	4.8±0.1	-27.4±0.6	-85.7±1.4	+58.3

Table 37: Thermodynamic parameters for the interaction DEP-$TiCl_4$ in *n*-heptane.

Diethylphthalate exhibits a relatively high affinity for $TiCl_4$ (log$K_{compl=}$ 4.8±0.1) in hydrocarbon, accompanied by a largely negative enthalpy change (ΔH_c= -85.7±1.4 kJ mol^{-1}); the parameters obtained were close to those previously determined in tetrachloroethane[121,122].

Both Gibbs free energy and enthalpy of formation of titanium-DEP complex were found to be close to those relative to adsorption of DEP on $TiCl_4$-$MgCl_2$ co-milled sample (ΔG_{ads}=-5.6±1.1 kJ mol^{-1} and ΔH_{ads}= -83±3 kJ mol^{-1}, Table 35 and Table 36), suggesting a direct interaction between DEP and the $TiCl_4$ adsorbed on the surface.

3.3.4 Possible scenarios for the binding of DEP

Different scenarios exist for the binding of DEP on $MgCl_2$ in presence of $TiCl_4$:

- DEP binds directly on the surface of $MgCl_2$ to a site *close* to $TiCl_4$: in this case desorption of $TiCl_4$ does not takes place and the influence of $TiCl_4$ on the thermodynamic parameters of binding is expected to be relatively low (steric hindrance, weak interactions between $TiCl_4$ and donor).

- DEP binds *on* the $TiCl_4$ present on the surface; in this case desorption does not occurs, but the direct interaction $TiCl_4$-donor may led to very different parameters of adsorption respect the binary $MgCl_2$-DEP system.

- DEP and $TiCl_4$ compete for the same site on the surface of $MgCl_2$: this scenario is more complicate because, beside partial desorption of $TiCl_4$ from surface, the formation of $TiCl_4$-DEP complex in solution according with the equilibrium constants of the processes is expected.

$$DEP_{(sol)} \rightleftarrows DEP_{(surf)} \qquad \textit{Adsorption of DEP}$$

$$TiCl_{4(surf)} \rightleftarrows TiCl_{4(sol)} \qquad \textit{Desorption of } TiCl_4$$

$$TiCl_{4(sol)} + DEP_{(sol)} \rightleftarrows Ti(DEP)Cl_{4\,(sol)} \qquad \textit{Complexation}$$

In case of competition for the same site on $MgCl_2$, quantitative determination of desorbed $TiCl_4$ is mandatory for the elaboration of data, especially the calorimetric ones because the calorimetric signal is the sum of the whole heat exchanged.

Based on the experimental results, the hypothesis of competition between the incoming DEP molecule and $TiCl_4$ for the same site on the surface of magnesium chloride was discarded because no desorption of $TiCl_4$ was evidenced by HPM (detection of *total* titanium in liquid phase) in both UV-Vis and calorimetric titrations; in fact the weakly bind molecules of $TiCl_4$ should be almost

completely displaced the DEP, because of its greater affinity for the surface (in binary systems: $\log K_{adsL}$ DEP=5.2, $\log K_{adsL}$ $TiCl_4$=2.9).

The relatively large difference of enthalpies of adsorption of DEP on pure and $TiCl_4$-treated $MgCl_2$ (binary and ternary heterogeneous systems), together with the very close thermodynamic parameters of interaction of DEP with $TiCl_4$ in solution and with $TiCl_4$-treated $MgCl_2$ (binary homogeneous and ternary systems) suggest the possibility of a direct interaction between DEP and the titanium atom. Nevertheless, the experimental results do not fully exclude the other scenarios or a combinations of them and left space for other investigations on these systems.

3.3.5 Adsorption form gas phase

In Table 38 the thermodynamic values relative to the adsorption of DEP from gas-phase are provided. The $\Delta X_{ads(g\rightarrow l)}$ and $\Delta X_{cond\ (l\rightarrow sol)}$ in Table 30 and Table 31 were used for the calculation. DFT results for binding of DEP in presence of titanium tetrachloride on $MgCl_2$ clusters previously described were not available at the moment, but in progress at the University of Naples as performed with binary systems.

		ΔG (kJ mol^{-1})	ΔH (kJ mol^{-1})	$T\Delta S$ (kJ mol^{-1})
DEP	$\Delta X_{ads\ (sol\rightarrow surf)}$	-25.6	-83	-57.4
	$\Delta X_{ads\ (g\rightarrow surf)}$	-67.6	-153	-85.4

Table 38: Thermodynamic cycle for correction of phase applied to adsorption of DEP on co-milled $MgCl_2$-$TiCl_4$. *$\Delta X_{cond(g\rightarrow l)}$ of dimethylphthalate.

4 Conclusions

The thermodynamic parameters of adsorption of titanium tetrachloride, ethyl benzoate and *ortho*-diethylphthalate on anhydrous physically activated magnesium chloride were experimentally determined for the first time ever.

The Langmuir model results as the best to rationalize the adsorption of $TiCl_4$ and donors from hydrocarbon solution. When using other adsorption models (e.g. Langmuir-Freundlich model) there is no significant improvement in the quality of fit and the obtained $\log K_{ads}$ values are nearly the same as those obtained with the Langmuir model.

In general, the Ziegler-Natta pre-catalysts were confirmed to be very delicate systems due to the very high reactivity of both anhydrous $MgCl_2$ and $TiCl_4$ towards Lewis bases in general and in particular water. However, the methodologies and techniques developed during this work set the bases for more in-depth experimental investigations. Conclusions are organized sections relative to: effect of water, adsorption of $TiCl_4$, absorption of donors, adsorption of DEP on co-milled sample and comparison with computational results.

4.1 Effect of water

- Water is highly reactive towards both $TiCl_4$ and the solid support of anhydrous $MgCl_2$. Even traces present inside the titration apparatus are able to affect the experimental determinations, in particular the calorimetric ones. The interaction of water with both $TiCl_4$ and $MgCl_2$ is a very favourite, exothermic process.

- Investigations on water content performed by Karl-Fischer titrations demonstrated that water molecules in magnesium chloride samples can be divided in two groups based on the reactivity with dilute $TiCl_4$ solutions: “accessible” and ”non-accessible”. The “accessible” water (surface) was able to influence both calorimetric and UV-Vis spectrophotometric determinations of adsorption parameters, while “non-accessible” water (bulk) did not affect the process.

- Removal of water is mandatory for determinations, in particular for the calorimetric ones. Experiments of hydrolysis of $TiCl_4$ and hydration of $MgCl_2$ in *n*-heptane allowed the determination of enthalpies of reaction in the order of magnitude of –100 kJ mol^{-1} per mole of water in both cases (-85 kJ mol^{-1} for magnesium chloride and -128 kJ mol^{-1} for $TiCl_4$). As stepwise calorimetric titrations confirm, water "accessible" to $TiCl_4$ can be easily removed also by treatment with $SiCl_4$ lasting several hours at ambient temperature and moderate concentrations (20-200 mM).

- A residual, un-strippable amount of water was present on $MgCl_2$ even after drastic pre-treatments[127]. The residual water, present as both "water" and hydroxide forms, cannot be stripped even with very harsh conditions (flux of inert gas at 523 K) and was surely present during the determinations. However in the experimental conditions no evidence of this residual water was observed. The effect of the un-strippable water on the determinations was not studied and requires more in-depth investigations, but helps to explain some unexpected, almost neutral values of entropies of adsorption that were found.

4.2 Adsorption of $TiCl_4$ on $MgCl_2$

- In the experimental conditions, $TiCl_4$ weakly binds the surface of physically activated $MgCl_2$. Gibbs free energy of adsorption form solution to surface is $\Delta G_{ads(sol \rightarrow surf)}$=–16.8±0.7 kJ mol^{-1}, $\log K_{ads(sol \rightarrow surf)}$ =2.94±0.13, while the adsorption process was found to be slightly exothermic, associated to a change of enthalpy of $\Delta H_{ads(sol \rightarrow surf)}$=-12.4±1.8 kJ mol^{-1}.

- Adsorption of $TiCl_4$ from solution is almost entropy-neutral ($T\Delta S_{ads(sol \rightarrow surf)}$ = +4.4 kJ mol^{-1}). The adsorption is affected by the medium in which reaction takes place (slightly decreased entropy in cyclohexane). Reaction of $TiCl_4$ with residual traces of water escaped to $SiCl_4$ pre-treatment may explain the value of entropy: hydrochloric acid molecules may leave the surface upon hydrolysis, compensating the loss of entropy of the adsorbed $TiCl_4$ molecule.

4.3 Adsorption of DEP and EB on $MgCl_2$

- In the experimental conditions, diethylphthalate and ethylbenzoate bond the surface of magnesium chloride more strongly (by at least two orders of magnitude) than $TiCl_4$ does; both donors bind the surface with almost the same binding constants: $\log K_{adsL}$=5.2±0.5 for DEP and $\log K_{adsL}$=5.1±0.1 for EB ($\Delta G_{ads(sol\rightarrow surf)}$ = -29.7±2.9 kJ mol^{-1} and $\Delta G_{ads(sol\rightarrow surf)}$= -29.1±0.6 kJ mol^{-1} respectively). Opposite, the calorimetric behaviour of DEP and EB towards $MgCl_2$ is very different. Molar adsorption enthalpy of DEP is found to be about two times greater than the enthalpy detected with EB, with an interaction quantified in $\Delta H_{ads(sol\rightarrow surf)}$ = -61.2±1.2 kJ mol^{-1} and $\Delta H_{ads(sol\rightarrow surf)}$= -27.5±2.3 kJ mol^{-1} for DEP and EB respectively.

- The entropies of adsorption of donors from solution are very different, pointing towards an almost entropy-neutral process in the case of EB ($T\Delta S_{ads(sol\rightarrow surf)}$ = +1.7 kJ mol^{-1}) and an unfavourite process for DEP ($T\Delta S_{ads(sol\rightarrow surf)}$ = -31.5 kJ mol^{-1}).

4.4 Adsorption of DEP co-milled $MgCl_2$-$TiCl_4$ sample

- The presence of $TiCl_4$ on $MgCl_2$ affects the adsorption of diethylphthalate. The affinity of DEP for $MgCl_2$–$TiCl_4$ co-milled sample in presence of titanium tetrachloride is slightly lower than the affinity in the binary $MgCl_2$-DEP system, with a binding constant of process of $\log K_{ads}$=4.5±0.2 ($\Delta\log K_{ads(sol\rightarrow surf)binary\text{-}ternary}$=0.7), correspondent to $\Delta G_{ads(sol\rightarrow surf)}$=-25.6±1.1 kJ mol^{-1}. The molar adsorption enthalpy of DEP in presence of $TiCl_4$ on the surface is $\Delta H_{ads(sol\rightarrow surf)}$=-83±3 kJ mol^{-1}, about 22 kJ mol^{-1} more exothermic than in the binary $MgCl_2$-DEP system.

- No evidence of $TiCl_4$ desorption was found in the experimental conditions by UV-Vis spectrophotometric analysis, and the thermodynamic parameters of adsorption of DEP are close to those relative to the formation of $TiCl_4$-DEP complex in *n*-heptane solution (ΔG_{compl}=-27.4±0.6 kJ mol^{-1}, ΔH_{compl}=-85.7±1.4 kJ mol^{-1}). This evidences points toward a direct interaction of DEP with $TiCl_4$ bind on the surface, however do not discredit other

scenarios (e.g. binding of DEP on an independent site) and further investigations are necessary.

4.5 Comparison with computational results

- The experimental values of enthalpy ($\Delta H_{ads(g\rightarrow surf)}$) and Gibbs free energy ($\Delta G_{ads(g\rightarrow surf)}$) of adsorption from gas phase (obtained by a thermodynamic cycle which takes into account condensation and mixing of reactants to allow comparison with DFT results) result more negative than those relative to adsorption from solution for both $TiCl_4$ and donors. The experimental entropies of adsorption of $TiCl_4$ and donors from gas phase ($\Delta S_{ads(g\rightarrow surf)}$) are all characterized by negative values.

- Evidence of water on $MgCl_2$ surface has been very recently found even after drastic thermal and chemical pre-treatments[127], suggesting that the real system is much more complicate than that used in DFT simulations; computational calculations were based on the assumption of adsorption taking place on a "naked" surface of $MgCl_2$, while in the real systems another component (water) is likely to be present and should be taken into account during the development of computational models. Nevertheless, the experimental data provide in this work of thesis may be useful to elucidate the behaviour of the "real" industrial Ziegler-Natta pre-catalytic system, where surface water probably exists and play a role on the adsorption of $TiCl_4$ and internal donors.

5 Bibliography

1 G. Natta, **1954**, patent 535712.

2 Montecatini, **1954**, patent 537425.

3 K. Ziegler, H. Breith, H. Martin and E. Holzkamp, **1953**, patent 973626.

4 J. Edward P. Monroe, *Polypropylene Handbook*, Hanser, **1996**.

5 A. Peacock, *Handbook of Polyethylene: Structure, Properties an Applications*, Marce Dekk, **2000**.

6 V. Busico, M. Causa, R. Cipullo, R. Credendino, F. Cutillo, N. Friederichs, R. Lamanna, A. Segre and V. V. A. Castelli, *J. Physi. Chem. C*, **2008**, 112, 1081–1089.

7 M. D'Amore, R. Credendino, P. H. M. Budzelaar, M. Causá and V. Busico, *J. Catal.*, **2012**, 286, 103–110.

8 T. Taniike and M. Terano, *Macromol. Symp.*, **2007**, 260, 98–106.

9 B. Liu, T. Nitta, H. Nakatani and M. Terano, *Macromol. Chem. Phys.*, **2003**, 204, 395–402.

10 T. Taniike and M. Terano, *J. Catal.*, **2012**, 293, 39–50.

11 R. Credendino, J. T. M. Pater, A. Correa, G. Morini and L. Cavallo, *J. Phys. Chem. C*, **2011**, 115, 13322–13328.

12 L. Cavallo, S. Del Piero, J. Duce, G. Morini, F. Piemontesi and M. Tolazzi, *J. Phys. Chem. C*, **2007**, 111, 4412–4419.

13 G. Natta and P. Corradini, *J. Polym. Sci.*, **1956**, 20, 251.

14 T. R. Ingraham, K. W. Downes, P. Marier, Z. Z. Hugus, Jr. and S. Steiger, *Inorganic*

Syntheses, **1960**, vol. 6.

15 M. C. Sacchi, I. Tritto, C. Shan, R. Mendichi and L. Noristi, *Macromolecules*, **1991**, 24, 6823–6826.

16 D. S. Breslow and N. R. Newburg, *J. Am. Chem. Soc.*, **1957**, 79, 5072–5073.

17 D. S. Breslow and N. R. Newburg, *J. Am. Chem. Soc.*, **1959**, 81, 81–86.

18 J. C. W. Chien, *J. Am. Chem. Soc.*, **1959**, 81, 86–92.

19 W. Kaminsky, *J. Polym. Sci. Part A Polym. Chem.*, **2004**, 42, 3911–3921.

20 W. Kaminsky, *Macromolecules*, **2012**, 45, 3289–3297.

21 A. Shamiri, M. Chakrabarti, S. Jahan, M. Hussain, W. Kaminsky, P. Aravind and W. Yehye, *Materials (Basel).*, **2014**, 7, 5069–5108.

22 H. H. Brintzinger, H. H. Fisher, D. Mulhaupt, B. Rieger and R. M. Waymouth, *Angew. Chem.*, **1995**, 34, 1146–1170.

23 G. Fink, B. Steinmetz, J. Zechlin, C. Przybyla and B. Tesche, *Chem. Rev.*, **2000**, 100, 1377–1390.

24 L. Resconi, L. Cavallo, A. Fait and F. Piemontesi, *Chem. Rev.*, **2000**, 100, 1253–1345.

25 J. Ewen, R. L. Jones, M. J. Elder, A. L. Rheingold, L. M. Liable-sands and M. Ferrocenes, **1998**, 6018, 10786–10787.

26 A. Razavi and U. Thewalt, *Coord. Chem. Rev.*, **2006**, 250, 155–169.

27 S. K. W. Chun P.S., *Prog. Polym. Sci.*, **2008**, 33, 797.

28 D. J. Arriola, E. M. Carnahan, P. D. Hustad, R. L. Kuhlman and T. T. Wenzel, *Science*, **2006**, 312, 714–9.

29 Ewen J. A., *J. Mol. Cat.*, **1998**, 128, 103.

30 Gibson V. C., *Science (80-.).*, **2006**, 321, 703.

31 G. Domski, J. Rose, G. Coates, A. Bolig and M. Brookhart, *Prog. Polym. Sci.*, **2007**, 32, 30–92.

32 N. Suzuki, J. Yu, Y. Masubuchi, A. Horiuchi and Y. Wakatsuki, *J. Polym. Sci. Part A Polym. Chem.*, **2003**, 41, 293–302.

33 H. Gao, L. Pei, K. Song and Q. Wu, *Eur. Polym. J.*, **2007**, 43, 908–914.

34 H. Gao, J. Zhang, Y. Chen, F. Zhu and Q. Wu, *J. Mol. Catal. A Chem.*, **2005**, 240, 178–185.

35 G. W. Coates, P. D. Hustad and S. Reinartz, *Angew. Chem. Int. Ed. Engl.*, **2002**, 41, 2237–57.

36 Phillips, **1954**, U.S. patent 2825721.

37 M. P. McDaniel, *Advances in Catalysis Chapter 3 – A Review of the Phillips Supported Chromium Catalyst and Its Commercial Use for Ethylene Polymerization*, **2010**, vol. 53.

38 P. Cossee, *J. Catal.*, **1964**, 3, 80–88.

39 E. J. Arlman and P. Cossee, *J. Catal.*, **1964**, 3, 99–104.

40 Andoni, *A flat model approach to Ziegler-Natta olefin polymerization catalysts*, **2009**.

41 E. Saldivar-Guerra, E. Vivaldo-Lima, *Handbook of Polymer Synthesis, Characterization, and Processing*, Wiley, **2013**.

42 K. Matyjaszewski and T. P. Davis, *Handbook of Radical Polymerization* -, .

43 J. S. Wang and K. Matyjaszewski, *Macromolecules*, **1995**, 28, 7572–7573.

44 J. Xia and K. Matyjaszewski, *Macromolecules*, **1997**, 30, 7692–7696.

45 I. Natori and S. Inoue, *Macromolecules*, **1998**, 31, 4687–94.

46 C. Chen, S. Luo and R. F. Jordan, *J. Am. Chem. Soc.*, **2010**, 132, 5273–84.

47 D. L. Thorn and R. Hoffmann, *J. Am. Chem. Soc.*, **1978**, 100, 2079–2090.

48 C. Roger, *Pipelines gas J.*, **2014**, 12, 241.

49 S. Matsuoka, *Polym. Eng. Sci.*, **1965**, 5, 142–147.

50 L. J. Fetters, D. J. Lohse, D. Richter, T. A. Witten and A. Zirkel, *Macromolecules*, **1994**, 27, 4639–4647.

51 P. Horrillo-Martinez, D. C. Leitch, S. A. Ryken, R. K. Thomson, J. D. Beard, B. O. Patrick, L. L. Schafer and G. R. Giesbrecht, *Can. J. Chem.*, **2015**, 93, 775–783.

52 I. Haas, C. Hübner, W. P. Kretschmer and R. Kempe, *Chem. - A Eur. J.*, **2013**, 19, 9132–9136.

53 S. E. Salih, A. F. Hamood and A. H. Abd Alsalam, *Mod. Appl. Sci.*, **2013**, 7, 33–42.

54 G. Talarico, V. Busico and L. Cavallo, *J. Am. Chem. Soc.*, **2003**, 125, 7172–3.

55 V. Busico, R. Cipullo, J. C. Chadwick, J. F. Modder and O. Sudmeijer, *Macromolecules*, **1994**, 27, 7538–7543.

56 L. Almeida and M. D. F. Marques, *Macromol. React. Eng.*, **2012**, 6, 57–64.

57 C. de Santa Maria, *Polymer (Guildf).*, **1995**, 36, 2845–2849.

58 S. Patthamasang, B. Jongsomjit and P. Praserthdam, *Molecules*, **2011**, 16, 8332–8342.

59 P. Pokasermsong and P. Praserthdam, *Eng. J.*, **2009**, 13, 57–64.

60 Shell-Oil, **1979**, US patent 4393182.

61 Shell-oil, **1979**, US patenrt 4414132.

62 C. W. Hock, *J. Polym. Sci.*, **1966**, 4, 3055.

63 G. M. Mackie P., Berger M.N., Lawson D, *J.Pol. Sci.*, **1967**, 5, 493.

64 P. C. Barbè, G. Cecchin and L. Norist, *Adv. Pol. Sci.*, **1986**, 81, 1.

65 G. Giunchi., G. Allegra., *J. Appl. Crystallogr.*, **1984**, 17, 172.

66 M. B. J. Bassi, J.W., Poleto, F., Calceterra, *Crystalloger,* **1982**, 159, 297.

67 K. Costuas and M. Parrinello, *J. Phys. Chem. B,* **2002**, 106, 4477–4481.

68 M. S. Kuklin, A. S. Bazhenov, P. Denifl, T. Leinonen, M. Linnolahti and T. A. Pakkanen, *Surf. Sci.*, **2015**, 635, 5–10.

69 V. Busico, M. Causa, R. Cipullo, R. Credendino, F. Cutillo, N. Friederichs, R. Lamanna, A. Segre, V. Castelli and A. Van, *J. Phys. Chem. C,* **2008**, 112, 1081–1089.

70 G. Natta, *Chim. Ind.*, **1960**, 42, 1207.

71 G. Natta, P. Corradini and G. Allegra, *J. Polym. Sci.*, **1961**, 51, 399–401.

72 G. Natta and I. Pasquoni, *Adv. Catal.*, **1959**, 1, 11.

73 D. V. Stukalov, I. L. Zilberberg and V. a. Zakharov, *Macromolecules*, **2009**, 42, 8165–8171.

74 K. Soga, T. Shiono and Y. Doi, *Makromol. Chem.*, **1988**, 192, 1531 – 1541.

75 T. Taniike and M. Terano, *Macromol. Rapid Commun.*, **2007**, 28, 1918–1922.

76 D. V Stukalov, V. a Zakharov and I. L. Zilberberg, *J. Phys. Chem. C*, **2010**, 114, 429–435.

77 A. Correa, F. Piemontesi, G. Morini and L. Cavallo, *Macromolecules*, 2007, 40, 9181–9189.

78 K. Vanka, G. Singh, D. Iyer and V. K. Gupta, 2010, 15771–15781.

79 H. Mori, K. Hasebe and M. Terano, *J. Mol. Catal. A Chem.*, 1999, 140, 165–172.

80 G. Potapov, G. D. Bukatov and V. Zakharov, *J. Mol. Catal. A Chem.*, **2006**, 246, 248–254.

81 D. V. Stukalov, V. Zakharov, A. G. Potapov and G. D. Bukatov, *J. Catal.*, **2009**, 266, 39–49.

82 D. Liguori, G. Morini and L. Cavallo, **2014**.

83 J. Arlman, *J. Catal.*, **1964**, 98, 89–98.

84 G. G. Corradini P., Busico V., *Compr. Polim. Sci.*, **1988**, 4, 29.

85 D. L. Tuller M., Dani O., *Water Resourse Researce*, **1999**, 35, 1949–1964.

86 W. C. Bray and H. D. Draper, *Proc. Natl. Acad. Sci. U. S. A.*, **1926**, 12, 295–9.

87 K. Morishige, T. Kawai and S. Kittaka, *J. Phys. Chem. C*, **2014**, 118, 4664–4669.

88 X. Peng, Y. Li, Z. Luan, Z. Di, H. Wang, B. Tian and Z. Jia, *Chem. Phys. Lett.*, **2003**, 376, 154–158.

89 O. Hamdaoui and E. Naffrechoux, *J. Hazard. Mater.*, **2007**, 147, 401–411.

90 V. Zelentsov, T. Datsko and E. Dvornikova, **2012**, 1, 209–215.

91 S. Brunauer, P. H. Emmett and E. Teller, *J. Am. Chem. Soc.*, **1938**, 60, 309–319.

92 M. R. Samarghandi, M. Hadi, S. Moayedi and F. B. Askari, *Environ. Heal.*, **2009**, 6, 285–294.

93 K. S. W. Sing, D. H. Everett, R. A. W. Halu, L. Moscou, R. A. Pierotti, J. Rouquerol and T. Siemeniewska, *Pure Appl. Chem.*, **1985**, 57, 603–619.

94 J. Rouquerolt, D. Avnir, C. W. Fairbridge, D. H. Everett, J. H. Haynes, N. Pernicone, J. D. F. Ramsay, K. S. W. Sing and K. K. Unger, *Pure Appl. Chem.*, **1994**, 66, 1739–1758.

95 C. H. Giles, D. Smith and A. Huitson, *J. Colloid Interface Sci.*, **1974**, 47, 755–765.

96 Y. S. Ho, *Carbon N. Y.*, **2004**, 42, 2115–2116.

97 P. Benoit and J. G. Heringt, *Appl. Geochemistry*, **1993**, 8, 127–139.

98 G. P. Jeppu and T. P. Clement, *J. Contam. Hydrol.*, **2012**, 129-130, 46–53.

99 C. Yao, *Sep. Purif. Technol.*, **2000**, 19, 237–242.

100 D. R. Burfield and R. H. Smithers, *J. Org. Chem.*, **1978**, 43, 3966–3968.

101 D. R. Burfield and R. H. Smithers, *J. Org. Chem.*, **1983**, IV, 2420–2422.

102 D. Williams, G. Bradley and M. Lawton, **2010**, 75, 8351–8354.

103 A. S. Meye and C. M. Boyd, *Anal. Chem.*, **1959**, 31, 215–219.

104 E. Scholz, *Karl Fischer titration: determination of water*, Springer, **2012**.

105 J. Clyden, N. Greeves and W. Stuart, *Organic Chemistry*, **2012**.

106 M. B. Smith and J. March, *March's Advanced Organic Chemistry: Reactions, Mechanisms, And Structure*, **2007**.

107 C. Comuzzi, P. Polese, A. Melchior, R. Portanova and M. Tolazzi, *Talanta*, **2003**, 59, 67–80.

108 G. Schwarzenbach, J. Muehlebach and K. Mueller, *Inorg. Chem.*, **1970**, 9, 2381–2390.

109 P. Gans, A. Sabatini and A. Vacca, *J. Solution Chem.*, **2008**, 37, 467–476.

110 S. Kashani-Nejad, K. W. Ng and R. Harris, *Metall. Mater. Trans. B*, **2004**, 35, 405–406.

111 D. Avnir, D. H. Everett, C. Fairbridge, M. Haynes, N. Pernicone and J. D. F. Ramsay, *Stud. Surf. Sci. Catal.*, **1994**, 87, 1–9.

112 C. W. Chronister and R. S. Drago, *J. Am. Chem. Soc.*, **1993**, 115, 4793–4798.

113 MSDS, *Titanium Tetrachloride*, .

114 MSDS, *Anhydrous magnesium Chloride*, .

115 H. Shomate and E. Huffman, *J. Am. Chem. Soc.*, **1943**, 65, 1625–1629.

116 W. H. Johnson, R. A. Nelson and E. Prosen, *J. Res. Natl. Bur. Stand.*, **1959**, 62, 49–52.

117 F. Capone, L. Rongo, M. D'Amore, P. H. M. Budzelaar and V. Busico, *J. Phys. Chem. C*, **2013**, 117, 24345–24353.

118 T. H. Wang, A. M. Navarrete-López, S. Li, D. A. Dixon and J. L. Gole, *J. Phys. Chem. A*, **2010**, 114, 7561–7570.

119 J. A. Duffy and D. E. Macphee, *J. Phys. Chem. B*, **2007**, 111, 8740–5.

120 S. Xia, Z. Fu, B. Huang, J. Xu and Z. Fan, *J. Mol. Catal. A Chem.*, **2012**, 355, 161–167.

121 L. Cavallo, S. Del Piero, J.-M. Ducéré, R. Fedele, A. Melchior, G. Morini, F. Piemontesi, M. Tolazzi and J. M. Ducere, *J.Phys.Chem C*, **2007**, 111, 4412–4419.

122 L. Cavallo, J. M. Ducéré, R. Fedele, a. Melchior, M. C. Mimmi, G. Morini, F. Piemontesi and M. Tolazzi, *J. Therm. Anal. Calorim.*, 2008, 91, 101–106.

123 M. C. Forte and F. M. B. Coutinho, *Eur. Polym. J.*, **1996**, 32, 223–231.

124 J. R. Goates, J. B. Ott, N. F. Mangelson and R. J. Jensen, *J. Phys. Chem.*, **1964**, 68, 2617–2621.

125 C. Dijkgraaf, *J. Phys. Chem.*, **1969**, 65, 660–661.

126 K. Briiggermann, R. S. Czernuszewicz and J. K. Kochi, **1992**, 4405–4414.

127 Unpublished result, *DPI Proect. 931*.

128 D. D. Wagman, *Natl. Bur. Stand.*, **1953**.

129 *http://webbook.nist.gov/cgi/cbook.cgi?ID=C959624*.

130 *http://webbook.nist.gov/cgi/cbook.cgi?ID=C93890*

131 A. G. Potapov, G. D. Bukatov and V. A. Zakharov, *J. Mol. Catal. A Chem.*, **2006**, 246, 248–254.

132 A. G. Potapov, G. D. Bukatov and V. A. Zakharov, *J. Mol. Catal. A Chem.*, **2009**, 316, 95–99.

133 V. Roháč, K. Růžička, V. Růžička, D. H. Zaitsau, G. J. Kabo, V. Diky and K. Aim, *J. Chem. Thermodyn.*, **2004**, 36, 929–937.

134 R. Vladislav, M. E. Jana, R. Květoslav, R. Vlastimil, Z. Milan and A. Karel, *J. Chem. Thermodyn.*, **1999**, 31, 971–986.

135 W. V Steele, R. D. Chirico, a B. Cowell, S. E. Knipmeyer and a Nguyen, *J. Chem. Eng. Data*, **2002**, 47, 667–688.

}

Aknowledgments

I would like to thank all the thermodynamic group of the University of Udine and, in particular, Prof. Marilena Tolazzi for giving me the opportunity to perform my Ph.D. in such an intriguing research field and Dr. Andrea Melchior for the help and the support in the organization and in the development of my thesis project.

A special thanks goes also to my parents, my girlfriend Laura and my friends for the support and colleagues of the department for the nice time spent together in these four years.

I want also to thank the Dutch Polymer Institute (DPI) for giving me this opportunity to work and learn on Ziegler-Natta catalysts and meet intresting people to the meetings and, last but not leats, for the financial support.